Evaluating The Performance Of Ocean Gliders' Technology To Characterize Ship-Radiated Underwater Noise

by

© **Khaled Mohsen Helal**

A thesis submitted to the School of Graduate Studies in partial fulfillment of the requirements for the degree of Doctor of Philosophy.

Ocean and Naval Architectural Engineering

Memorial University of Newfoundland

May 2025

St. John's, Newfoundland and Labrador, Canada

Abstract

This study uses passive acoustic monitoring techniques to investigate the potential of Autonomous Underwater Gliders for assessing and localizing a controlled vessel through underwater radiated noise. The propagation of noise was investigated through an advanced propagation loss model utilizing oceanography data collected by the glider. Comprehensive sea trials were conducted using a Slocum G3 glider equipped with acoustic capabilities. These trials involved capturing the underwater radiated noise from a specific vessel while simultaneously collecting oceanographic data. The first step involved identifying the noise pattern of the target vessel and assessing the individual noise sources in accordance with ISO standards. Subsequent trials involved using a glider, a hydrophone array, and a seabed-moored hydrophone to further analyze vessel noise signatures. The acoustic performance of the glider was compared to that of other conventional stationary platforms. A study was conducted to evaluate the self-noise produced by the glider in order to ensure the precision of the acoustic data. Furthermore, sound propagation loss was studied using the gathered oceanic data. Propagation loss models were developed in two distinct environmental conditions: 1) a shallow coastal inlet 80 m deep and 2) a deep bay up to 200 m deep during summer and winter, both in the presence and absence of strong surface stratification. A range- and depth-dependent sound speed profile map was created to estimate propagation loss inside the area covered by the glider. This led to the testing and improvement of advanced sound propagation models compared to the ISO standard 17208 formulations. The findings demonstrate that the gliders can characterize and measure ship-based URN and locate the direction of the source relative to the glider, thereby improving the understanding of the spatial and temporal variability of ocean sound sources. The study supports the use of AUGs in marine acoustic monitoring, which has implications for environmental policies and the development of quieter vessels.

Acknowledgements

Thanks to my supervisor, Dr. Lorenzo Moro, who made it possible for me to expand my knowledge and grow professionally throughout my doctoral research experience. I would like to express my deepest gratitude to him for their unwavering support and guidance throughout this research journey. Their expertise and insightful feedback have been invaluable in shaping both this thesis and my growth as a researcher. I am particularly thankful for the unique opportunity they provided to conduct research using the Slocum Ocean Glider, which has been a crucial aspect of my PhD.

I would also like to extend my sincere thanks to my colleagues Jacopo Fragasso, Nicolai von Oppeln-Bronikowski, Mark Downy, and Sarik Shaikh Upadhye for their invaluable assistance and for supporting the fieldwork and data collection that enabled this research. Their collaboration, insightful discussions, and willingness to share expertise have enhanced my research. They each contributed to the challenges and successes of the study in their own manner, and I am grateful for their support, drive, and collegial environment.

I extend my deepest gratitude to my wife, Menna, whose unwavering support and encouragement have been instrumental throughout my PhD journey. Her patience, understanding, and belief in my abilities have sustained me during challenging times. I thank her immeasurably for being my rock, my confidante, and my partner in this remarkable endeavor. Thank you, Menna, for sharing this academic adventure with me. Your love and dedication have made all the difference.

Thanks to my family and all my friends for their incredible support, motivation, and closeness during my life back home in Egypt and my whole academic career thereafter—especially through the unprecedented historical period we all experienced in 2020 and 2021.

Statement of contribution

My supervisor, Dr. Lorenzo Moro, provided the main concept of the research of studying the performance of the ocean gliders and their ability to fill knowledge gaps in monitoring and assessing the underwater radiated noise from ships. In addition, he was the principal investigator of the project with the Ocean Frontier Institute (OFI), which provided us with the funds. He carefully reviewed the methodology I designed for the experiments, ensuring its scientific rigor and appropriateness for the research objectives. Additionally, he oversaw the post-processing procedures I developed, helping to ensure that the results obtained were both reasonable and scientifically sound.

I designed the experimental fieldwork plans, performed data management, conducted the data analysis, wrote the first draft of the manuscript and implemented the contribution of the co-authors and external reviewers up to the final publication. During the whole process, I asked for and implemented input and feedback from the other contributors to this study. Furthermore, a deep systematic literature review on the research topic was conducted at the beginning of the study program to highlight the track of the PhD journey.

The research project on the basis of this doctoral thesis was funded by the Ocean Frontier Institute through an award from the Canada First Research Excellence Fund. This work was also supported by the Department of Industry, Energy and Technology (IET) of the Government of Newfoundland and Labrador, Canada.

Table of contents

List of tables

List of figures

List of symbols

α	Depression angle between the horizontal sea surface and the hydrophone in degrees
α_{comp}	Compression absorption coefficient of the seafloor sediment dB/λ
α_{sh}	Shear absorption coefficient of the seafloor sediment dB/λ
β	Hydrophones inclination angle in degrees
τ	Time-delay between the received signals of the two hydrophones in milli-seconds
a	The half-width value between the upper and lower limits of Type B uncertainty
C_{comp}	Compression sound speed in the seabed sediment in metres per second
C_{sh}	Shear sound speed in the seabed sediment in metres per second
C_w	Sound speed in seawater in metres per second
d_s	The source depth (vessel draft) in metres
d_H	The distance between the two hydrophones mounted on the glider in metres
D_{Sl_n}	Slant range (Pythagorean distance) between the sound source and the receiver in metres
H_{dpt}	Hydrophone depth measured from water surface in metres
K	Wavenumber function in frequency in 1/meters
k_c	Re-scaling coverage factor for the combined uncertainty to 95% level of confidence
N	Number of bits of acoustic files
n	Vessel number of runs at individual engine speed
$P[n]$	Raw discrete acoustic data in Pascal
r	Horizontal range between the sound source and receiver in metres
std	Standard deviation of the repeated measurement for Type A uncertainty
u_A	Type A standard uncertainty of the random error in the measurements
u_B	Type B standard uncertainty of the systematic error in the measurements
u_c	Combined standard uncertainty at a confidence level of 66%
u_{GPS}	Standard uncertainty of the geocoordinates measured by the GPS
u_{Tilt}	Standard uncertainty of the hydrophone inclination
U	Total standard uncertainty of the measurement at 95% confidence level
V_{pp}	peak-to-peak voltage of the hydrophone's preamplifier
Z	Water column depth in metres

List of abbreviations

ABS	American Bureau of Shipping (Ship Classification Society)
AIS	Automatic identification system of ships
ANSI	American National Standards Institute
AQV	Average Quadratic Velocity method
AUG	Autonomous Underwater Glider/ Ocean Glider
AUV	Autonomous Underwater Vehicle
BNL	Background Noise Levels dB re 1μPa
BV	Bureau Veritas (Ship Classification Society)
CTD	Conductivity, Temperature and Density sensor
CPA	Closest Point of Approach in metres
DOA	Directional Of Arrival (Azimuth angle) in degrees
DWA	Data Window Angle in degrees
DWL	Data Window Length in metres
DWP	Data Window Period in seconds
ECA	ECHO Certification Alignment method (Sound propagation loss)
ISO	International Organization for Standardization
LR	Lloyd's Register Group Limited (Ship Classification Society)
M-A	The Meyer and Audoly method (Sound propagation loss)
MSL	Monopole Source Levels dB re 1μPa.m at 1 m
PAM	Passive Acoustic Monitoring
PL	Propagation Loss model of sound waves
PRISMA	Preferred Reporting Items for Systematic reviews and Meta-Analyses
RL	Received Noise Levels dB re 1μPa at 1 m
RL_c	Corrected Received Noise Levels dB re 1μPa.m at 1 m
SCA	Seabed Critical Angle method (Sound propagation loss)
SNR	Signal-to-Noise Ratio
SLR	Systematic Literature Review
SSP	Sound Speed Profile in metres per second
SPL	Sound Pressure Level in dB re 1μPa
URN	Underwater Radiated Noise dB re 1μPa.m at 1 m
URN_{Tot}	Averaged Underwater Radiated Noise dB re 1μPa.m at 1 m

Chapter 1

Introduction

Over the last two decades, human activity levels in the ocean have increased significantly, including shipping, fishing, deepwater drilling [Blackwell et al., 2004], and sonar operations [Miller et al., 2012]. Consequently, anthropogenic underwater noise has increased and maritime vessels contribute significantly to this pollution. In particular, the worldwide growth in ocean trade and vessel fleets between 1992 and 2021 [Frisk, 2012; United Nations Conference on Trade and Development (UNCTAD), 2023] have increased the ocean ambient noise levels, especially in the low-frequency range (<150 Hz), as shown through several long-term observations [Andrew et al., 2002; McDonald et al., 2006; Chapman and Price, 2011; Andrew et al., 2011; Williams et al., 2015; McWhinnie et al., 2017]. Increasing noise from humans in the ocean harms marine life, including making them more physically stressed, changing their behavior, and making it harder for them to communicate using sound [Kraus et al., 2005; Rolland et al., 2012; de Soto et al., 2013; Williams et al., 2015; Kraus et al., 2016; Erbe et al., 2019].

In Newfoundland and Labrador (NL), Canada, a wide range of fishing activities take place. Summer is the primary season for fishing vessel traffic. This period overlaps with the migration season of marine mammals, such as humpback, pilot, minke, fin, blue, and killer whales, passing through the St. John's, NL, region [Benjamins et al., 2012]. Noise pollution interferes with essential behaviors such as fish and invertebrates' communication, feeding, and mating processes [Hawkins and Popper, 2016].

Several jurisdictions have started developing new policies and criteria to manage

ships' underwater radiated noise (URN) and address this growing threat. Initiatives have been organized in several countries, for example, the Quiet Vessel Initiative in Canada [Transport Canada, 2020] and IMO, to bring together stakeholders, such as ship designers, shipyards, ship owners, classification societies and government agencies, to develop strategies to mitigate URN emissions. These strategies include proposing design solutions for new vessels, retrofitting existing vessels, and altering ship operations in sensitive areas [North Atlantic Treaty Organization (NATO), 2008; European Union Commission Decision 2017, 2017; United Nations, 2018; Protection of the Arctic Marine Environment (PAME), 2019; Cominelli et al., 2018; Virto et al., 2022]. A key aspect of the success of the proposed strategies is the reliability of the measurement methods and procedures to assess the underwater radiated noise of the vessels, in addition to the quantification of the uncertainty of the reported URNs.

Government regulations and international agreements play a crucial role in addressing the issue of URN from ships, particularly from the perspective of vessel design and operation, to minimize the environmental impact. Government regulations and international agreements rely on the ship classification societies and scientific research to address the problem of URN from ships. The valuation of the URN of the vessel using methods that ensure high accuracy and minimal uncertainty is essential. The vessel's URN assessment is primarily determined by criteria curves in one-third octave bands [American Bureau of Shipping, 2022; DNV GL, 2017; Lloyd's Register Group Limited, 2018; Bureau Veritas, 2014]. These curves categorize the URN according to the purpose of operation, distinguishing between transit, quiet, and research activities. The URN must not exceed the criteria curve, and the uncertainty must be within an acceptable range, such as a maximum of 3 dB, as specified by Lloyd's Register Group Limited [2018]. A vessel may fail to meet the criteria for a specific notation if there is significant uncertainty across multiple frequency bands. Lower uncertainty levels indicate higher trust in the URN assessment, ensuring accurate evaluations without underestimation or overestimation. In order to enable reduced uncertainty evaluations, it has been proposed to apply ocean gliders as moving, untethered passive acoustic monitoring (PAM) observers. Research has shown that these devices are effective in identifying marine mammal presence and behavior, offering essential data for conservation initiatives.

In the following pages, I will share the story of these quiet submarines, the Autonomous Underwater Glider/Ocean Gliders (AUG), and their incredible journeys

to investigate passive acoustic monitoring missions regarding vessel noise signature assessment and detection. AUG(s) extend the knowledge and understanding of how human activities in the ocean can impact remote ocean ambient noise. Anthropogenic activities, especially those of vessels, raise ocean noise pollution and threaten Earth's ecosystems [Williams et al., 2015; Erbe et al., 2019; Lemos et al., 2022]. Therefore, it is challenging to precisely monitor and control the increase in ocean ambient noise levels over a massive space where the sound travels fast and to great distances. AUG(s) reveal the hidden implications of these activities, both in sound recording and in improving our ability to estimate the impact of marine sound sources in the ocean. Accordingly, this research investigates the sound propagation behavior in the oceans, taking advantage of the range- and depth-dependent oceanographic data sampled by the ocean glider.

An acoustic AUG equipped with a hydrophone is a mobile platform for monitoring and sampling the ocean soundscape along the water column and over broad areas. This technology is advantageous due to its silent motion, extended autonomy, low-cost operation in collecting samples from remote areas, and low energy consumption for long-endurance missions [Ferguson et al., 2010; Haxel et al., 2019; Testor et al., 2019; Baumgartner et al., 2020; de Lima et al., 2020]. Their quiet motion and operation enable the study of ocean ambient noise, making them a valuable source of information about the ocean's conditions and processes, either naturally or due to anthropogenic noise [Jiang et al., 2019]. For example, the International Quiet Ocean Experiment (IQOE) is a proposed effort to study acoustic environments and marine life on a large scale, recognizing the challenges of understanding the effects of noise on long-lived, mobile marine species [Williams et al., 2018].

Ocean glider technology, moreover, can support the estimation of the azimuth angle of underwater sound sources to detect and identify biological or anthropogenic sources [Jiang et al., 2019]. When working in parallel with other platforms, gliders can localize cetacean migration. Their accuracy in PAM missions is comparable to traditional acoustic recording platforms, e.g., bottom anchored or support vessel deployed stationary observers [Matsumoto et al., 2011]. Regarding glider navigation, OceanGNS is a cloud-based service that helps ocean gliders tolerate currents and bathymetry, enhancing navigation and operational efficiency. This method calculates the best routes for the glider to achieve its mission targets using current ocean forecast models, historical data, and glider information [von Oppeln-Bronikowski et al., 2021].

Typical fishing vessels were selected for this research study as controlled anthropogenic noise emitters in order to provide a reliable and distinguishable source of underwater noise for the study, which is essential for precise monitoring and analysis. Several sea trials were conducted to investigate the noise output of the selected vessel. A Slocum ocean glider, a surface float-supported hydrophone array, and a bottom-mounted single hydrophone were the three PAM systems used to monitor the vessel's acoustic signature. These initiatives go beyond only evaluating the glider's efficiency in vessel noise monitoring and detection; they seek to comprehend the ecological consequences of fishing vessel noise in the waters of Newfoundland on a broader scale. In addition, the issue of fishing vessels serving as underwater noise sources prompts engineering questions on mitigation strategies to protect marine life.

1.1 Research problem

Marine vessels have multiple sources contributing to their overall noise signatures [Ross and Kuperman, 1989; Jiang et al., 2020]. They are distributed in several locations along the vessel hull structure, generate noise at various frequencies, and have different directivities [Erbe et al., 2019]. Assessing the noise levels caused by ships at sea is a difficult research question because there are many factors that can affect the whole process and make the reported noise levels very uncertain [AQUO, 2014; ISO-17208/1, 2016; Gaggero et al., 2012; Smith and Rigby, 2022]. The uncertainty in determining vessel underwater noise may surge due to variations in several factors: ocean ambient background noise, the determination of range between source and receiver, sound wave propagation loss (PL), vessel operating conditions, and post-processing analysis [AQUO, 2014; Zhang et al., 2020]. For proper and rigorous measures of vessel underwater noise, it is critical to determine and quantify sources of error that could introduce uncertainties in the evaluation.

Fixed PAM stations are the most commonly used system for analyzing ocean sound, as noted by [McKenna et al., 2012; Merchant et al., 2012; Haver et al., 2021]. Surface float structures with cable throughout the water column holding the hydrophones have been widely used in industry and scientific research. Sources of uncertainty related to the structure of the PAM observer might be added on top of the previously mentioned sources. The self-noise of the stationary observer had a

notable impact on the received sound levels. Current-induced vortices caused cable vibrations in low-frequency ranges, leading to increased uncertainty in the measured received sound levels. The mechanical chafing between components, buoy noise, and free surface impact the received sound as well [ANSI/ASA S12.64-2009/Part 1, 2009; AQUO, 2014; Zitterbart et al., 2022]. The depth of each hydrophone can change over time due to the effect of surface waves and ocean current, which can, in turn, affect the recorded sound data. A difference of only a few metres can move the hydrophone into a shadow zone, resulting in variations between 1 and 5 dB in the measured sound levels [AQUO, 2014; Simard et al., 2016].

Bottom-mounted systems are frequently used to assess underwater noise in shallow or deep water [ANSI/ASA S12.64-2009/Part 1, 2009; ISO-17208/1, 2016; DNV GL, 2017]. The system is submerged and consists of an acoustic release, an anchor, and floating buoys [Lin et al., 2019]. However, the seafloor topology profile or sediment type may not be suitable for deploying a moored observer anchored to the seafloor. In this scenario, a drifting surface buoy or a support vessel that holds the hydrophones by attaching a weight to the end of the cable would be a suitable choice. If the weather conditions worsen over time, e.g., an increase in wave height or water currents, the drift angle of the hydrophones would be a problem that leads to a change in the hydrophone depth, increasing the measurement uncertainty [ANSI/ASA S12.64-2009/Part 1, 2009; AQUO, 2014]. Surface buoys provide spatially independent acoustic data for a particular area. They are also expensive and difficult to deploy in deep water, make loud noises, and require mooring ropes that might entangle marine creatures [Kowarski et al., 2020].

Moreover, the sound propagation loss quantity is an essential step in assessing the vessel noise signature level, which estimates the reduction in the sound intensity level between the source and observer. The PL values were calculated based on several parameters: source depth, observer depth, the distance between source and receiver, sound speed profile (SSP), seafloor profile, and seafloor acoustic characteristics. ANSI/ASA S12.64-2009/Part 1; McKenna et al.; ISO-17208/2; Simard et al.; Haxel et al., and MacGillivray et al. have introduced a variety of PL models, from the most direct explicit form to those that solve the sound wave equation numerically. The simplest model may need only the distance between the source and receiver to roughly estimate the PL value; however, the more accurate and reliable the PL model is, the more environmental factors like SSP and the acoustic characteristics and profile

of the seafloor need to be taken into account [Merchant et al., 2012; Ainslie et al., 2022].

The SSP data is usually calculated using a single conductivity, temperature, and density (CTD) sensor cast through the water column. The SSP values may not represent the sound speed a couple of kilometres from the point of measurement. That may lead to unrated PL values [Li et al., 2022]. Additional CTD sensor casts can be performed at different locations to account for variations in sound speed in order to gather more accurate SSP data. By incorporating these additional measurements, the prediction accuracy of the PL values can be improved. Collecting SSP profiles at many points over an area of square kilometres would be cost-effective. However, with just one deployment, AUGs can collect temporal and spatial CTD data for the targeted area.

In addition, the seafloor bathymetry is assumed to be flat in many cases for simplicity, even though the seafloor profiles might change the PL values significantly, specifically in shallow water [Oliveira et al., 2021; MacGillivray et al., 2023]. Combining the actual seafloor bathymetry profile and range/depth-dependent SSP could enhance the PL models.

Therefore, unconstrained by the limitations of stationary platform structures, ocean gliders offer a distinct potential to enhance underwater noise measurement techniques and could be a promising alternative to monitoring ocean sound in that environment. While ocean gliders may have the potential to improve underwater noise measurement techniques, they also come with their own set of limitations and uncertainties that need to be addressed before relying on them as a primary monitoring tool.

1.2 Research aim and objective

The primary aim of this study is to fill the knowledge gap regarding the efficacy and capability of the autonomous underwater Slocum G3 glider as a mobile observation platform for characterizing and detecting underwater radiated noise from marine ships. I also investigated the measurement uncertainty of determining the vessel noise signature based on the acoustic and oceanographic data captured by the glider. To achieve this objective, a comparative analysis was performed, comparing the glider's

performance as a mobile PAM platform in measuring vessels' URN with the standard methodologies using stationary observers as a ground reference through planned and controlled sea trials in the open seas. In addition, sources of measurement uncertainty associated with the glider's observations relative to those of the stationary platforms were investigated.

To further assess the glider's capabilities as a PAM platform, its self-noise during a routine flight in the ocean was investigated and reported, which is crucial in the post-processing of the acoustic files collected by the glider. Moreover, the ability of the glider to detect the direction of a moving vessel in relation to the glider is examined.

The second aim of this research is to analyze the oceanographic data (temperature, salinity, and pressure) collected by the glider to improve the understanding of underwater sound propagation in a particular region. The goal is to demonstrate differences in sound propagation loss models, taking into account the range- and depth-dependent SSP and seabed acoustic characteristics in comparison to the explicit independent forms. This study also included a comparative analysis of two scenarios: assuming a flat bathymetry profile and using actual seafloor profile data. Incorporating range- and depth-dependent SSP into the PL model study facilitates the identification of potential enhancements by using more precise seafloor profile data along the glider's path, as opposed to the previous flat assumption.

In order to reach this goal, the objectives and tasks described in the following sections were completed.

1.2.1 Underwater noise characterization of a small fishing vessel

The average length of a fishing vessel in Newfoundland is between 45 and 62 feet, depending on the fishing activity and type of vessel [DFO, 2022; Burella et al., 2019]. The noise from small vessels typically peaks at a higher frequency than that of large vessels, potentially up to tens of kHz [Hermannsen et al., 2014; Veirs et al., 2016]. Small vessels may be responsible for a significant portion of the high-frequency noise (above 1 kHz) in ocean ambient noise. Small vessels, often operating in shallow-water environments where sound transmission is more efficient above 100 Hz, produce high-frequency noise due to their high-speed engines. The impact of noise emissions from

small vessels has not received enough attention [Erbe et al., 2019; Picciulin et al., 2022; Gaggero et al., 2024].

Noise exposures depend on the vessels' operating conditions. Unlike other commercial vessels, fishing vessels have a wide range of operational states that depend on the type of fishing activity and catch [Burella et al., 2021]. A condition of particular interest is the case of a stationary vessel with the engine running (usual fishing conditions). Therefore, it is crucial to distinguish between the acoustic characterization of the vessel under sailing and stationary operating conditions.

In this work, I tested a typical small fishing vessel from Newfoundland. I used this vessel as a case study to evaluate the ocean glider's performance as a passive acoustic monitoring system, and the analysis also helped me comprehend its noise signature. In particular, the first objective aims to measure and characterize the underwater noise signature. I examine vessel noise using two metrics: underwater radiated noise and monopole source level (MSL). The study aimed to accurately estimate MSL by considering environmental factors that impact sound propagation and assessing the vessel noise signature [Chion et al., 2019; Parsons et al., 2021]. This aspect is not directly considered in URN measurements [ISO-17208/1, 2016]. The scientific community commonly uses the widely accepted ISO-17208/2 standard for MSL estimation, which forms the basis of the proposed MSL method. This standard uses a simplified propagation loss model that may not accurately represent a vessel noise signature, especially in complex maritime conditions [ISO-17208/2, 2019]. The full spectrum of noise characteristics might not be captured accurately, in particular frequencies below 100 Hz, which are related to the machinery and blade passing frequency. Additionally, the standard does not adequately account for influential factors like seafloor reflections and variations in the SSP, which may impact the accuracy of the measurement [MacGillivray et al., 2019, 2023]. Therefore, a numerical propagation loss model was created in this research based on the wave equation solution to simulate PL, particularly at frequencies below 2 kHz, where the vessel noise level is high and dominates at low frequencies.

Finally, the structure-borne noise from the diesel engine and its correlation to the underwater noise were analyzed. I identified the vessel's noise sources and assessed their contribution to the overall noise signature during sailing and when stationary (propeller unclutched). By focusing on this knowledge gap, this work can potentially

contribute to future efforts to improve fishing vessel design and reduce the impact of individual noise sources.

The fishing vessel under investigation is 35 feet in overall length (L_{OA}). The methodology pursued to characterize the vessel's underwater noise is as follows:

- Using the same boat, two sea trials were conducted in August and December 2021 to measure the vessel's URN and MSL.
- A floated surface buoy equipped with an array of three hydrophones, in accordance with the standards set by ISO-17208/1 [ISO-17208/1, 2016] and ANSI 2009 [ANSI/ASA S12.64-2009/Part 1, 2009] was used.
- The vessel operated in two conditions: 1) propeller clutched and 2) propeller unclutched.
- The trial with propeller clutching was performed at three engine speeds: 1400, 1800, and 2200 rpm.
- The trial with propeller unclutching was performed at a 1400 rpm engine speed.
- The structure-borne noise of the vessel hull was measured and correlated with the underwater noise.

1.2.2 Glider self-noise assessment

Self-noise is a significant limitation encountered by gliders, particularly regarding the variability of induced self-noise during the intermittent behavior of the glider's internal mechanisms and sensors [Schofield et al., 2007; Cauchy et al., 2023; von Oppeln-Bronikowski et al., 2023]. Therefore, the second objective was to monitor and assess the glider's self-noise through two missions in different water depths. The following tasks were achieved:

- The first sea trial was in Holyrood, Conception Bay, NL. The water depth was around 70 m. Six complete dives were conducted in decent environmental conditions (Sea conditions with wave heights under 0.5 meters and winds below 1 knots), with no records of an external source of noise onshore or offshore but the glider.

- The second sea trial was in Brigus, Conception Bay, NL. The water depth was around 210 m. Four dives were conducted in environmental conditions similar to those of the first trial. The glider was launched with other two PAM systems.
- The self-noise levels were evaluated and categorized for each source of noise individually.

1.2.3 Passive acoustic monitoring using a glider

Three platforms (acoustic AUG, bottom-mounted hydrophone, and array of three hydrophones) were deployed in the ocean as a group near Brigus, Conception Bay, NL, and they were assigned to measure a fishing vessel noise signature following the ISO-17208 standard. The standard is related to stationary PAM systems. However, I followed the recommended engineering parameters, e.g., closest point of approach and data window time, while controlling and post-processing the glider's data. The objective has been achieved through the following tasks:

- Deployment of the array of the three hydrophones and the bottom-mounted hydrophone following the standards [ANSI/ASA S12.64-2009/Part 1, 2009; ISO-17208/1, 2016]
- The AUG is programmed to fly between two-way points parallel to the vessel's trajectory.
- A comparison between the received levels and background levels in the one-thrid octave band is made to determine the validity of the recordings [Merchant et al., 2014a; Brooker and Humphrey, 2016; ISO-17208/1, 2016].
- The received levels were normalized to the dipole source level at a distance of 1 m from the source using the spherical geometrical equation to represent the URN of the vessel, according to [ISO-17208/1, 2016]. The same method was applied to all three platforms.
- The uncertainty of the vessel noise levels was investigated from the three platforms following the guidelines in [AQUO, 2014].

1.2.4 Sound propagation loss

The second aspect of assessing the glider is sound propagation loss prediction utilizing range- and depth-dependent oceanographic data.

PL is commonly estimated using simple spreading laws for convenience ($PL = N\log_{10}(R)$). R represents the distance from the noise source in metres, while N is a scaling factor. N ranges from 10 to 20, depending on the source and receiver distance. Complex environments limit this approach's ability to construct accurate predictions. It is most effective in scenarios where the environmental properties are range-independent. Spreading law models may result in significant errors when applied to complex coastal and inland water environments [Jensen et al., 2011].

PL models attempt to accurately depict the complex ocean environment by incorporating factors such as the average speed of sound in the ocean, the depth of the noise source, and the way sediments absorb sound on the seafloor [Shaw and Potter, 2015; Ballard and Lee, 2017; Eamer et al., 2020]. Integrating range- and depth-dependent SSP with the actual seafloor bathymetry profile can improve the effectiveness of PL models. The question is, "Does the glider improve the propagation loss model's accuracy in estimating the sound attenuation over distance?"

The following tasks were completed:

- Complex mathematical formulas were investigated, such as the Meyer and Audoly (M-A) method [Meyer and Audoly, 2020], the Seabed critical angle (SCA) method [MacGillivray et al., 2023], and the ECHO certification alignment (ECA) method [Ainslie et al., 2022], which are simplified equations that can estimate the PL better than a simple spreading law.

- A numerical PL model was used in which Parabolic Equation (PE) and Wavenumber Integration (WNI) were used using the AcTup Toolbox [Duncan and Maggi, 2005]. The numerical models allow for the inclusion of the range- and depth-dependent SSP, seafloor bathymetry profile, and acoustic characteristics of the seafloor sediment.

- A comprehensive comparison of the models was performed under different conditions, including scenarios where the SSP and bathymetry were held constant,

situations where either the SSP or bathymetry was range-dependent, and situations where both variables were simultaneously range-dependent.

- Finally, the numerical frequency-dependent PL model was used to simulate how sound travelled in the trial area so that the monopole source of the vessel could be estimated [MacGillivray et al., 2019; Chion et al., 2019]. The comparison of results from both methods allows for the evaluation of numerical models' accuracy and reliability compared to simplified PL models.

Overall, this study contributes to the understanding of the potential advantages of using autonomous underwater gliders for monitoring and assessing vessel noise signatures and provides insights into their efficiency and capability in comparison to conventional monitoring platforms.

1.3 Limitations of the research

The research was carried out with certain limitations. The vessels under measurement during the experiments were two fishing vessels of nearly identical length, beam, and propeller type. Hence, the findings may not be generalizable to other categories of vessels. Vessels of varying types may possess unique attributes and operational circumstances that may impact their acoustic signature, such as tug boats and icebreakers, which may vary depending on the operation and environment.

Regarding the AUG, two hydrophones mounted on the glider's wings were employed. If the hydrophone location is changed to the glider's hull, the results provided in this thesis may change because of the glider's self-noise.

The self-noise assessment of the glider represented the Slocum gliders from the Teledyne Webb Research Corporation. The results might differ for the other types of ocean gliders introduced, such as Seagliders from Kongsberg Underwater Technology Inc. or Petrel-II, developed by Tianjin University in 2012.

The glider's inability to provide a seafloor bathymetry profile during the mission is another limitation. The topology data was collected from previous research using a sonar topology scanner.

1.4 Thesis structure

This thesis integrates materials from five papers by the author [Helal and Moro, 2022; Helal et al., 2024a,b,c]. The research study examines the use of ocean gliders as passive acoustic observers in marine environments, with a specific focus on detecting and assessing vessel noise signatures. Chapter 2 uses materials from Helal et al. [Helal et al., 2024a] and begins with a literature review that examines the use of ocean gliders in detecting vessel noise signatures and the challenges associated with measuring underwater radiated noise from vessels. This review offers a thorough overview of current research and identifies areas that require further investigation. Chapter 3 explains the methodology used for conducting sea trials and experiments with an ocean glider and other PAM platforms, where they are appointed from articles [Helal and Moro, 2022; Helal et al., 2024b,c]. This chapter discusses post-processing methods used to develop propagation loss models and estimate uncertainties across different observational platforms.

Chapter 4 presents the results and discussions of the sea trials, from references [Helal and Moro, 2022; Helal et al., 2024b,c], including a detailed comparison with previous studies. This comparison highlights the advancements and implications of the research. Chapter 5 explores the glider's ability to determine the direction of moving vessels by analyzing received noise levels. The work is based on Helal et al. [Helal et al., 2024c] That research critically examines the limitations and suggests future research directions for optimizing functionality in gliders. Chapter 6 concludes the thesis by summarizing key findings and providing recommendations to improve the performance of gliders as passive acoustic platforms. This chapter outlines the research findings, focusing on their practical implications and potential for future studies in marine acoustic monitoring.

1.5 List of published articles

1. K. Helal and L. Moro. *Assessment of the underwater noise levels from a fishing vessel using passive acoustic monitoring and structure hull vibration.* Canadian Acoustics, Vol.: 50(3), August 2022.

2. K. M. Helal, J. Fragasso, and L. Moro. *Effectiveness of ocean gliders in monitoring ocean acoustics and anthropogenic noise from ships: A systematic review.* Ocean Engineering, Vol.: 295, ISSN: 0029-8018, March 2024

3. K. M. Helal, J. Fragasso, and L. Moro. Underwater noise characterization of a typical fishing vessel from Atlantic Canada. Ocean Engineering, Vol.: 299, ISSN: 0029-8018, May 2024.

4. K. Helal, N. von Oppeln-Bronikowski, and L. Moro. *Advancing Glider-based Measurements of Underwater-Radiated Ship Noise.* The Journal of the Acoustical Society of America, Vol.: 156(4), ISSN: 0001-4966, October 2024.

5. K. Helal and L. Moro. *Measurement Uncertainties of the Underwater Noise Using Slocum Glider* (Draft)

Chapter 2

Literature review

This chapter was adapted from the published article *Effectiveness of ocean gliders in monitoring ocean acoustics and anthropogenic noise from ships: A systematic review*, which is published in *Ocean Engineering Journal*, *Vol.*: 295 and *ISSN*: 0029-8018 [Helal et al., 2024a].

2.1 General overview

Passive acoustic monitoring is a standard method to measure ocean noise. It can be implemented with a single hydrophone or an array of hydrophones that can be moored to the sea floor (stationary deployment) or installed on a moving platform (such as autonomous sailboats, surface drifters, and autonomous underwater vehicles). Stationary deployment systems are the most common method to assess URN from ships, used in conjunction with automatic identification system (AIS) data [McKenna et al., 2012; Merchant et al., 2012, 2014b; Jiang et al., 2020; Haver et al., 2021], marine mammal detection and vocalization [Mellinger et al., 2007; Helble et al., 2013; Charif et al., 2020], and ocean soundscape monitoring [Sánchez-Gendriz and Padovese, 2016; Putland et al., 2021].

However, there is a growing interest in the use of autonomous underwater gliders as a mobile PAM platform in the monitoring of spatial and temporal noise changes in particular marine environments [Klinck et al., 2012; Haxel et al., 2019; Jiang et al., 2019; Cauchy et al., 2023]. Buoyancy-driven AUGs are maturing as a component of

the global ocean observing system as a platform for targeted multi-parameter ocean measurements [Testor et al., 2019]. The gliders are slow (0.25 m/s), but they offer a cost-effective means to measure data across nearshore and open ocean regions, carrying a variety of sensing payloads over time spans approaching a year, depending on configuration [Liu and Xiao, 2017; Wall et al., 2017; Haxel et al., 2019; von Oppeln-Bronikowski et al., 2023]. Furthermore, AUGs can sample the ocean autonomously in a three-dimensional pattern, providing improved tempo-spatial coverage that may be critical in acoustic monitoring. They are often equipped with conductivity, temperature, pressure, and density sensors whose data enhance the accuracy in predicting the ocean sound propagation behavior, consequently decreasing the uncertainty in the estimation of the source sound levels [Cauchy et al., 2023; von Oppeln-Bronikowski et al., 2023].

Increasing the glider's sensor payload capabilities has broadened its applications to include passive acoustic monitoring. In Atlantic Canada in particular, the need for passive acoustic ocean observing monitoring of marine mammals such as North Atlantic Right whales (NARw) has led to the rapid adaptation of underwater gliders to track and detect NARw in their natural habitat without disturbing them [Klinck et al., 2012; Küsel et al., 2017; Gervaise et al., 2021]. Researchers can also use gliders to assess the ocean soundscape, which contains quantifiable information about the sources of sound in the marine environment ([Haxel et al., 2019; Wang and Yuan, 2021a]). With their quiet behavior and ability to sample the ocean autonomously, underwater gliders have become an indispensable tool for oceanographic research and collecting in-situ environmental data in PAM missions [Testor et al., 2019; Cauchy et al., 2023; von Oppeln-Bronikowski et al., 2023]. Therefore, the behavior of the gliders needs to be studied and compared to the traditional fixed PAM platforms when measuring and evaluating the ship's noise patterns. By evaluating the gliders' performance in measuring ship noise, researchers can determine their suitability for long-term monitoring of acoustic pollution in different marine regions. Additionally, the data collected by gliders can help identify areas of high ship noise activity and prioritize conservation efforts in those areas.

Several authors highlighted how different passive acoustic monitoring systems may lead to varying estimations of ships' URN and MSL [McKenna et al., 2012; Simard et al., 2016; Bagočius and Narščius, 2018; Macgillivray and de Jong, 2021]. Between

2009 and 2019, the American Standard Institute (ANSI) and the International Standard Organization (ISO) published standardized procedures to measure ships' URN and MSL [ANSI/ASA S12.64-2009/Part 1, 2009; ISO-17208/1, 2016; ISO-17208/2, 2019; Ainslie et al., 2022]. The proposed procedures establish a measurement methodology for data comparison and reporting. The measurement procedures to assess ships' URN and MSL proposed by the major classification societies build up on the ANSI and ISO Standards. They are used to grant ships special class notations related to URN [Bureau Veritas, 2014; American Bureau of Shipping, 2022; Lloyd's Register Group Limited, 2018]. While these standards significantly improve URN and MSL estimations, they still lack specific methodologies to assess ships' underwater noise in shallow waters [Jiang et al., 2020] and provide simplified methods to estimate the sound propagation intensity loss [ISO-17208/2, 2019; DNV GL, 2017]. In addition, they do not standardize underwater noise measurements performed using autonomous underwater vehicles, including autonomous underwater gliders.

Self-noise is a significant limitation encountered by gliders, particularly regarding the variability of induced self-noise during the intermittent behavior of the glider's internal mechanisms and sensors [Schofield et al., 2007; Cauchy et al., 2023]. Only a few published results on the acoustic assessment of buoyancy-driven gliders are available. Matsumoto et al. excluded recorded data during oil pump operation at turning depth [Matsumoto et al., 2011]. Liu et al. investigated the Petrel II glider's self-noise, and the study revealed that the oil pump produced high noise levels across a broad frequency range (50 Hz to 4 kHz). In contrast, noise from the rudder and hydrodynamics was deemed negligible [Liu et al., 2018]. The self-noise of the Slocum G2 glider was investigated by Haxel et al. in 2019. They determined that the recorded acoustic data must be eliminated during the oil pump operation. The rudder and battery-pack noise could be disregarded due to their short duration of fewer than 0.5 seconds [Haxel et al., 2019]. A study by Jiang et al. aimed to compare the efficiency of gliders and propelled underwater vehicles in detecting sound sources. Due to their low self-noise, the authors posited that the gliders would demonstrate heightened efficiency in detecting target missions [Jiang et al., 2019]. The Petrel-II glider's buoyancy and pitch adjustments generate transient and intense noise interference, which can be mitigated by regulating the operational duration of the acoustic system. In addition, the glider went through modifications applying vibration and noise reduction techniques, resulting in an increased range for vessel detection from 5 to 7.7 km using

the glider [Wang and Yuan, 2021b]. [Kowarski et al., 2020] used the Teledyne Slocum G3 glider equipped with one hydrophone for marine mammal detection in 2020, but no self-noise study was conducted. To conclude, the glider's self-noise should be investigated and clearly reported because it may impact the assessment of the vessel's underwater noise footprint.

This chapter aims to determine the current state of the art on the effectiveness of moving platforms in collecting acoustic data and assessing underwater ships' source levels. The literature review was done by conducting a systematic literature review (SLR) on ocean underwater noise measurements using passive acoustic, unpropelled AUVs. Two research questions (RQs) are introduced as support tools to guide the search. The first research question (RQ_1) provides an overview of the current use of AUGs as platforms for ocean passive acoustic monitoring and the characterization of ocean acoustic sources. The second research question (RQ_2) aims at understanding measurement uncertainties when using AUGs.

2.2 Gathering documents

The review was conducted in accordance with the Preferred Reporting Items for Systematic Review and Meta-Analysis (PRISMA) framework [Torres-Carrión et al., 2018]. This procedure was followed by other authors working in different fields [Kitchenham and Brereton, 2013; Petersen et al., 2015; Shahin et al., 2017; Lenarduzzi et al., 2021]. In particular, the framework was first proposed by Kitchenham and Charters [Kitchenham and Charters, 2007] and consisted of seven components: i. research questions; ii. search strategy; iii. selection criteria; and iv. data extraction. v. quality assessment; vi. data synthesis; and vii. analysis and documentation.

2.2.1 Research questions

The research questions were defined as follows:

- **RQ1:** What is the contribution of autonomous underwater gliders to ocean passive acoustic surveys?
  - RQ1.1: Have AUGs been used to assess the underwater ship noise signature

or other ocean sound sources and/or detect them?

- **RQ2:** What are the uncertainties in estimating underwater sound source levels using both fixed and mobile acoustic observers?

By answering the first research question (RQ_1), an overview of the current use of the AUGs as passive acoustic monitoring (PAM) systems was illustrated. Sub-question $RQ1.1$ was added to see if AUGs have already been used to detect and characterize ocean sources, including ships.

The second research question, RQ_2 provides insights into the uncertainties in the assessment of underwater noise sources.

2.2.2 Search strategy

A rigorous search strategy was developed to identify relevant literature for the systematic search. The digital libraries Scopus and Web of Science were explored using selected keyword strings. Before starting the actual search, I ran a series of trial searches to test the effectiveness of the search strategy. Therefore, the keyword "autonomous underwater vehicle" is added to capture any literature using power-propelled vehicles for PAM missions. This preliminary search also helped adjust the keyword strings. The tuned keyword strings obtained after the trial search and used in the first step of SLR were:

- **RQ1:** keywords that cover RQ1
  - (I) ("underwater radiated noise") OR ("underwater noise") OR ("underwater acoustic*") AND ("glider*" OR "autonomous underwater vehicle") AND (hydrophone* OR "passive acoustic* monitor*")
  - (II) ("underwater radiated noise") OR ("underwater noise") OR ("underwater acoustic*") AND (("glider*") OR ("autonomous underwater vehicle")) AND (hydrophone* OR "passive acoustic* monitor*") AND ("ship*" OR "vessel*" OR "boat*")
  - (III) ((glider) OR ("autonomous underwater vehicle") OR ("Autonomous vehicle") OR ("moving platform") OR ("mobile platform") OR (lagrangian)) AND ((effect) OR (impact)) AND (noise) AND (("marine mammal") OR

("marine fauna") OR (whale) OR (dolphin) OR (cetacean) OR (seal) OR (pinniped) OR (fish))

- **RQ2:** keywords that cover RQ2
  - (I) ("underwater radiated noise" OR "underwater noise" OR "underwater acoustic*") AND (hydrophone* OR "passive acoustic* monitor*" OR "acoustic observ*") AND ("measur* uncertaint*" OR "uncertaint* estimat*" OR "uncertaint*") AND (sea OR ocean)

The strings hereby presented follow Scopus syntactic rules and were subsequently adapted for the search on Web of Science. The strings were tailored for each selected digital library to fit the syntax supported by the library. Some characters were used to increase the search robustness, e.g., double quotes and asterisks, and boolean operators, which helped integrate the keywords to find the most relevant articles.

In addition to searching for relevant scientific literature, I have reviewed technical guidelines and standards on underwater radiated noise from ships issued by international standards and ship classification societies. The selection of the technical report is conducted based on the author's experience and the commonly cited reports by the scientific community in the field. These sources help us understand the current state of practice in underwater radiated ship noise measurements using conventional stationary platforms and assess the passive acoustic AUGs' capabilities to perform similar field measurements.

2.2.3 Selection criteria and data extraction

Initially, the duplicate entries were eliminated from the papers acquired throughout the search process. Then, only peer-reviewed articles from Q1 and Q2 journals were selected. Finally, I reviewed the titles and abstracts of the resulting papers to exclude all papers that did not contribute to answering the RQs.

The remaining articles were subjected to a thorough screening by applying the criteria presented in Table 2.1. Different criteria are used for the two research questions: I1, I2, I4, E1 for RQ1, and I3, E3 for RQ2.

The information extracted from the selected articles and reports was divided into two categories: i) a graphical representation of the number of published articles per

Table 2.1: SLR - Inclusion and exclusion criteria applied to the selected articles, excluding the technical reports

Inclusion criteria	
I1	Underwater vehicles are operated as passive acoustic monitoring systems.
I2	Underwater radiated noise from ships is measured by AUGs.
I3	Investigation on underwater noise measurement uncertainties.
I4	Discussion regarding AUGs' performance in measuring and detecting underwater sound sources.
Exclusion criteria	
E1	Underwater vehicles are used only for oceanography purposes.
E2	Free-ranging underwater sound sources.
E3	There is not a clear discussion regarding the measurement uncertainties.

year to show how the topic's interest has risen over time, and ii) the relevant data extracted to answer and investigate the RQs. With regard to ii), the gathered information includes qualitative and quantitative data on methodology, tools, limitations, and findings from each article. Table 2.2 shows the template followed for the data extraction.

To conclude, the extracted information is going to be a critical point in investigating the interpretation of the RQs in how the moving PAM is helpful for underwater acoustic data collection and assessment, as well as giving us a clear picture of the uncertainties of the entire assessment process either using stationary or movable PAM systems. The pinpointed data will assist in extracting data from multidisciplinary research areas that use the same AUG platform. Moreover, the recommendations and guidelines by the international organizations and classification societies will complete the picture between the findings of the research articles and the requirement to update and start conducting standards for the moving PAM systems.

Table 2.2: SLR - Data extraction features from selected articles

Data item	**Explanation**
Measurement aim	Underwater sound source assessment, detection or monitoring/mapping ocean ambient noise
Observer	Specifications of the PAM system
Sound level representation	Quantitative and graphical representations in Narrowband, 1/3 Octave bands or broadband levels
Frequency ranges	Frequency bands of interest
Sound wave propagation	Propagation loss model types and discussions related to the features used in developing the model
Measurement limitations or uncertainties	What was discussed from the point of view of variability and discrepancies in measurement?

2.3 Number of selected articles

The preliminary search resulted in 2,249 publications. This initial selection was progressively narrowed down to 21 articles following the process mentioned in Section 2.2.3.

Section 2.3 shows the yearly distribution of the papers found with the keyword search discussed in Section 2.2.2. The figure shows that there is a growing interest in the study of underwater noise utilizing AUG and in the analysis of the uncertainties in the identification of the underwater source sound levels (from 1 article, 1979, to more than 280, 2021). The search provided no articles using power-propelled autonomous underwater vehicles (AUV) for measuring ship noise. In contrast, some researchers have used AUGs, which are unpropelled AUVs, as PAM platforms. Thus, the figure shows an increase in interest in using the AUG for PAM purposes.

Section 2.3 presents the yearly distribution of the 29 papers that were selected (reduced to 21 based on PRIMSA chart), subdivided into the topics discussed in Section 2.1. The graph presents the same positive trend. The papers were classified into three groups based on the RQs, as shown in Section 2.3. Firstly, 7 articles are selected under the topic of monitoring ocean ambient noise using AUGs. Finally, the underwater water noise measurement uncertainties include 8 articles to clarify the

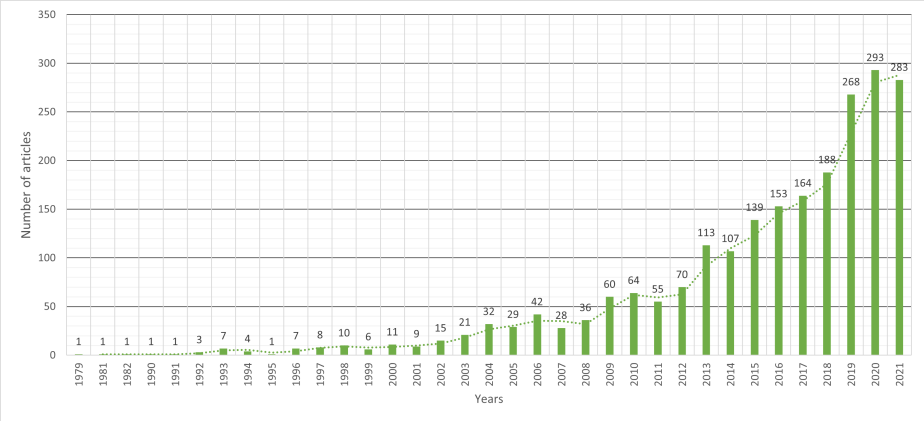

Figure 2.1: Year distribution chart represents the number of unfiltered preliminary searches in the systematic literature review

topic under RQ_2.

The PRISMA flowchart is presented in Section 2.3, providing a concise summary of the outcomes derived from the search technique that was employed. Firstly, the identification process resulted in 1,725 and 524 articles in Scopus and Web of Science, respectively. The screening step started with getting 328 duplicates, which were, therefore, removed from the search. Applying the inclusion/exclusion criteria further, 1,868 articles were excluded: 726 were not peer-reviewed, and 1,119 articles did not comply with the inclusion/exclusion criteria. In the eligibility stage, 53 articles went through the quality assessment process using the data extracted. 24 of these articles were then excluded as they did not meet at least 6 criteria from Table 2.3, leaving 29 articles for deep reading and analysis.

A final screening on this list of 29 papers is performed, following the criteria presented in Table 2.3. Detailed information on this phase of the work is illustrated in Appendix A. Finally, I added to the list of results 6 standards and guidelines from international organizations and classification societies that were considered relevant to this research.

2.4 Literature findings

This section is developed as a narrative discussion of the findings from the selected documents following the SLR criteria, in addition to technical guidelines and reports. The

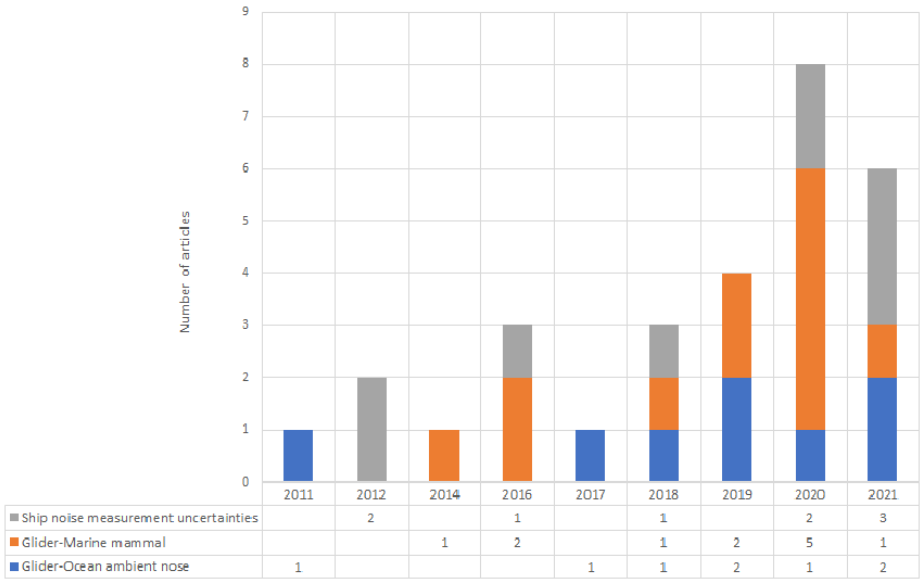

Figure 2.2: Years distribution for the selected articles to be reviewed

Table 2.3: SLR - Quality assessment criteria

Quality assessment	**Criteria**
QA_1	Are the paper objectives clear?
QA_2	Does the study critically present and contextualize the results?
QA_3	Is there a clear statement of the findings?
QA_4	Is the study conducted from an actual data set? the study?
QA_5	A clear description of the environment where the measurement was conducted
QA_6	A clear description of the methodology of measurement and used tools
QA_7	Is data discussed prominently and adequately?

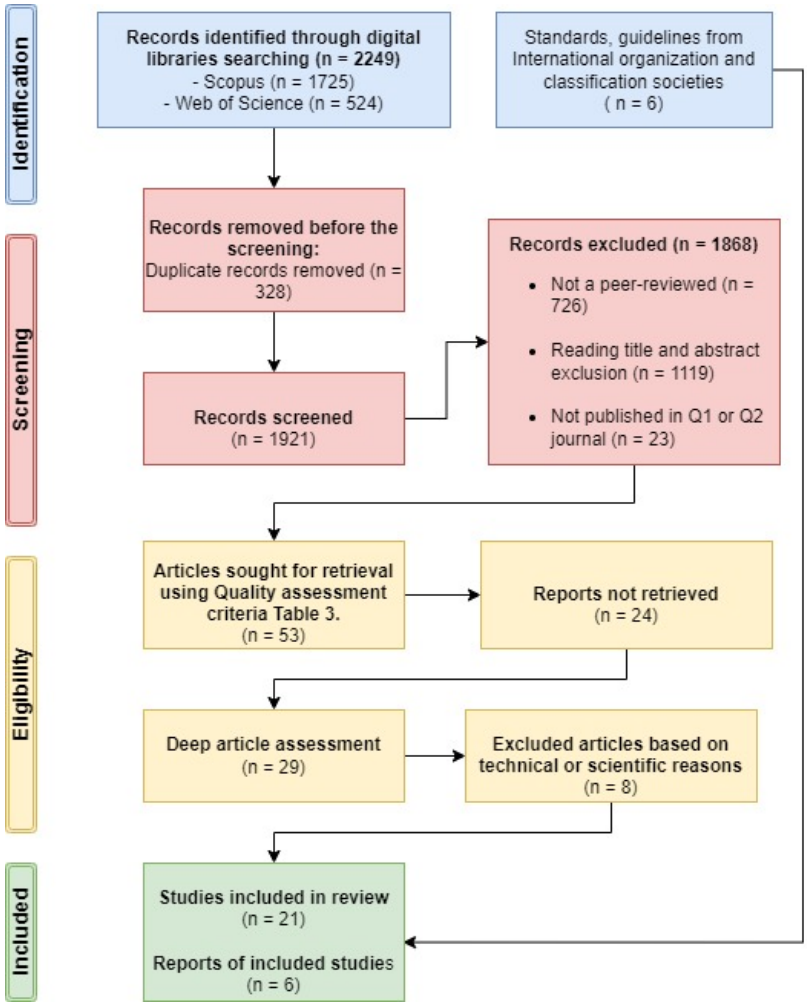

Figure 2.3: PRISMA flowchart

discussion is divided into two main parts, following the research questions. To answer RQ_1, I explore the use of AUGs as PAM systems in the assessment of ocean ambient noise, including the detection and characterization of biological sources, specifically marine mammal detection and shipping radiated noise. Then, to answer RQ_2, I look at the parameters impacting underwater noise measurements, such as types of instruments, vessel operation conditions, and environmental effects. Each parameter contributes a quantity of uncertainty to represent a range of variability in the measured URN levels. The significance of each parameter will be investigated in relation to the overall measured sound levels of a target source.

Over the last two decades, the scientific community's interest in the characterization of the ocean soundscape has significantly increased, as shown by the growth in the number of publications over the years in Section 2.3 and Section 2.3. Underwater noise sources can be categorized into two categories: (1) natural sources and (2) anthropogenic sources [Hildebrand, 2009; Radford et al., 2008; Putland et al., 2017]. Natural sounds include marina fauna vocals, wind-surface interaction, internal wave motion, and geophony. Anthropogenic sources are all linked to human activities, such as shipping, fishing, and ocean exploration and exploitation.

By comparing Section 2.3 and Section 2.3 with Section 2.4, It was evident that the number of publications has risen with the growth in international maritime traffic, fishing, and ocean exploration. This indicates the growing concern about the impact of URN on marine ecosystems, exacerbated by the ever-increasing size of marine traffic. All categories, with the exception of general cargo carriers, have seen significant increases in tonnage in recent years. In particular, bulk carriers saw a very quick rise (41 to 43% of the overall carrying capacity in the last 10 years). At the same time, oil tankers decreased from 31% to 29%, and general cargo saw a slight decline (5% to 4%) [United Nations Conference on Trade and Development (UNCTAD), 2023].

PAM is a proven methodology employed to survey the ocean soundscape. Given the complexity of ocean sound, PAM has been used in many applications, including studying faunal communication and the impact of anthropogenic activities on the ocean soundscape.

Fixed observatory stations are the most common setup for the analysis of ocean sound [McKenna et al., 2012; Merchant et al., 2012; Haver et al., 2021]. PAM systems have been proven to be reliable platforms that allow for long-term recordings that help

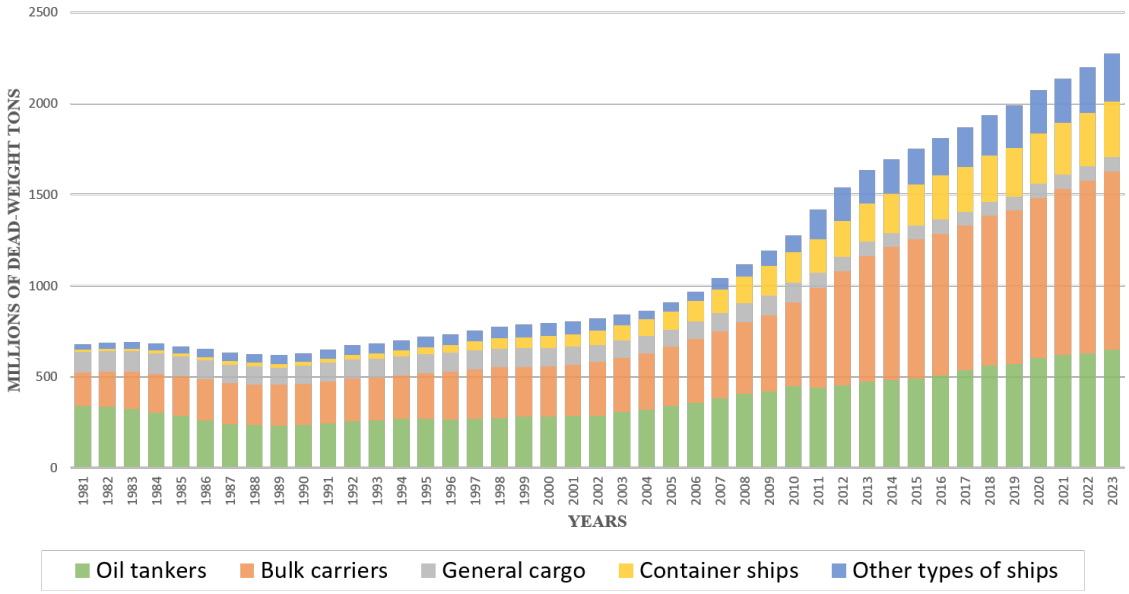

Figure 2.4: World fleet by principal vessel type [United Nations Conference on Trade and Development (UNCTAD), 2023]

understand the change in ocean soundscapes over time. They consist of hydrophones moored to the bottom of the ocean or drifting floating stations [ANSI/ASA S12.64-2009/Part 1, 2009; ISO-17208/1, 2016; American Bureau of Shipping, 2022]. The key aspects in the selection of the most appropriate system arrangement are i) environmental conditions, ii) bathymetry, iii) seafloor topography, and iv) the duration of the recording. In the bottom-anchored arrangement, the hydrophone is installed close to the seafloor, mitigating the waves and weather-induced noise. While this configuration prevents the hydrophone from moving with the ocean currents, the mooring cable may vibrate at low frequencies ($\leq$ 10 Hz) because of the current-induced vortices, increasing the system's self-noise. The moored hydrophone can be deployed in relatively shallow waters as well as in deep water [Lin et al., 2019], but the seafloor topography plays an essential role in the selection of the most appropriate anchoring system and may prevent the use of this configuration. An advantage of the moored hydrophone is its ease of use for extended periods of time. At the same time, the main drawback of this arrangement is the self-noise coming from components of the system: the mechanical chafing between the components, which impacts the frequency range of the measurement [AQUO, 2014; Zitterbart et al., 2022], and the free surface and buoy noise [ANSI/ASA S12.64-2009/Part 1, 2009; AQUO, 2014; Erbe et al., 2019].

Moreover, the depth of each hydrophone may change over time due to the effect of surface waves and the ocean current, and this may, in turn, affect the recorded sound data. A difference of only a few metres can move the hydrophone in a shadow zone, meaning variations between 1 and 5 dB in the measured sound levels [AQUO, 2014; Simard et al., 2016].

Autonomous underwater vehicles (AUVs) have been introduced as passive acoustic monitoring systems in order to overcome the limitations of moored hydrophone setups. Moreover, they allow the researchers to gain additional information on the properties of the ocean environment with the use of additional sensors, e.g., a CTD device, that can provide a 3D representation of the water column. The main drawbacks of traditional AUVs are the effect of the vehicle's self-noise on the quality of the measurements and the limited autonomy.

AUGs are a subclass of AUVs that have recently been employed in PAM activities because they can mitigate some of the drawbacks of traditional AUV systems. For instance, sampling the ocean vertically and horizontally in order to achieve range- and depth-dependent acoustic and environmental parameters, in addition to the cost-effectiveness of monitoring remote oceans with the ability of off-shore real-time communication. However, the literature on the use of AUGs in PAM is still sparse.

2.4.1 Underwater sound measurement using AUG

This section answers the research question (RQ_1): What is the contribution of autonomous underwater gliders to ocean passive acoustic surveys?

PAM can provide information on the ocean soundscape, marine fauna's acoustic footprint, and anthropogenic noise sources. These data can be used to assess the variation of noise levels over time, identify ocean wildlife in the marine ecosystem, and estimate the impact of anthropogenic noise sources on the behavior of the fauna [Cafaro et al., 2018; Soares et al., 2020; De Clippele and Risch, 2021].

When ocean noise measurements are used to characterize anthropogenic noise sources, more information is gained through the use of additional data: sound PL models can be used to assess noise levels at the source, and ships' AIS provides information on the detected vessel.

When noise levels measured in the ocean environment are the object of the analysis, ocean noise measurements can be used to assess how noise radiated from ships contributes to and affects the marine ecosystem [Zhu et al., 2022; ZoBell et al., 2021; Magnier and Gervaise, 2020; MacGillivray et al., 2019; McKenna et al., 2012].

In conclusion, ambient noise levels are an indicator of acoustic pollution, and they are significantly affected by variations in space, time, and sound propagation characteristics, which require an extended and widespread mapping of the ocean soundscape [Wenz, 1962; Merchant et al., 2012; Farrokhrooz et al., 2017; Kinda et al., 2017].

Measurement of ocean ambient noise using AUGs

Ocean ambient noise is measured to understand the ecosystem and characterize natural noise sources. As the selected papers show, AUGs can provide an accurate and extended characterization of the ocean soundscape. The following paragraphs and Table A.2 present the information provided by the selected papers to answer RQ_1.

- Wang and Yuan (2021) used a Petrel-II glider equipped with an array of acoustic sensors to monitor the ambient noise levels in the South China Sea. The results showed the effectiveness of the glider in mapping the ambient noise levels of the area covered by the glider. The changes in the ambient noise levels were dependent on frequency and water depth. In addition, the authors showed the contamination of the ocean noise from a transit vessel passing near the AUG, which consisted of an increase in the recorded levels in the 63 and 125 Hz 1/3 octave bands. The type of vessel is not identified, nor are the vessels' speeds [Wang and Yuan, 2021a].

- Jiang et al. (2019) measured the ambient noise levels in the same location as Wang and Yuan (2021). The measurements were performed using the same glider used by Wang and Yuan (2021). They concluded that the glider recordings show the variation of the noise levels with depth and frequency. Then, they compared the glider's self-noise with an AUV's self-noise. The results show that the AUG provides better recordings due to the higher signal-to-noise ratio. The paper also demonstrated the benefits of the glider in detecting underwater targets compared to the autonomous underwater vehicle. Using sonar equations at different source depths and over a broad range of frequencies, the authors used

broadband and multitone signals to determine the propagation loss between a known source and the glider. The objective was to determine the deployed sources' azimuth angles. The findings show that a glider with two hydrophones on its wings is capable of determining a ship's direction of motion. The authors mentioned that additional research is needed to determine the effectiveness of extending detection using more than one glider in the form of a sensor network. [Jiang et al., 2019].

- In 2019, a Slocum G2 glider was equipped with a single hydrophone and deployed on the U.S. Pacific Northwest coast for a short-term mission to assess the spatial and temporal changes of the underwater ambient noise [Haxel et al., 2019]. The analysis of the recordings showed significant changes in the ambient noise levels throughout the whole mission, where biological, vessel-transit, wind-surface and air-gun noises were detected in different time series.

- Liu et al. (2018) launched another mission in the China Sea using a Petrel-II glider. The mission was 33 hours long, and the glider performed 16 dives, covering 26 km of horizontal distance and 1 km of depth. The ambient noise levels were presented as a function of depth in one-third octave bands and showed the dependency of depth and frequency in assessing the noise level [Liu et al., 2018].

- Matsumoto et al. (2011) used a Slocum G2 glider as a passive acoustic platform with a hydrophone mounted near the rudder to monitor the activity of the submarine West Mata volcano in the northern Lau basin. A two-day mission of 13 dives collected sound data from the active volcano and a spatial map grid of the average spectral levels. The spatial map was created with 50 m and 1 km resolution for depth and range, respectively. A comparison was performed with a fixed observer near the volcano. The results show a high correlation between the data recorded by the glider and a moored hydrophone. [Matsumoto et al., 2011].

The presented works show that acoustic AUGs have significant advantages in sampling the ocean sound of the water column. AUGs have been used as a mobile platform to monitor the ocean soundscape because of their quietness, extended autonomy, and low-cost operation [Ferguson et al., 2010; Haxel et al., 2019; Baumgartner et al., 2020;

de Lima et al., 2020]. AUGs add the advantage of providing an acoustic sampling of the water column in a 3D pattern.

The glider's self-noise is the most considerable limitation highlighted by all the articles. The glider's internal mechanism involves moving mechanical parts that generate sound noise during operations. For example, the self-noise of a Slocum G2 glider includes three components: (A) the glider's rudder noise, (B) the moving battery packs, and (C) the buoyancy engine [Teledyne Webb Research, 2017; Liu et al., 2018; Haxel et al., 2019; Jiang et al., 2019; Lee et al., 2019]. The noise generated by (B) and (C) is intermittent since these sources operate only when the glider varies its trim to switch from diving to climbing and vice-versa. Therefore, the data recorded when (B) and (C) operate should be discarded [Liu et al., 2018; Wang and Yuan, 2021a]. An electronic servo motor controls the glider's rudder for directional adjustments, which produces a broad-band noise signal at various times and for different durations. The rudder noise is mainly present at the top of the dives—approximately in the first 10 metres of the glider dive or climbing—because of the frequent course corrections due to the stronger currents [Haxel et al., 2019; Jiang et al., 2019].

Acoustic measurement of biological sound sources using AUGs

AUVs have played an important role in monitoring ocean wildlife [Baumgartner et al., 2020]. In particular, AUGs have been used to explore the marine environment, detect vocalizations of marine mammals, and investigate oceanographic properties beneficial for underwater sound propagation modeling [Aniceto et al., 2020].

- Aniceto et al. (2020) investigated the arctic ecosystem along the southern part of the Lofoten-Vesterålen region using a Seaglider™and a JASCO Autonomous Multichannel Acoustic Recorder (AMAR) G4. The article concludes that ocean gliders are valuable tools for investigating fauna bioacoustics and background noise while simultaneously recording seawater's physical properties. The authors did not use the acoustic data to localize the detected cetaceans, as it was beyond their scope of work. They mentioned that this task would require either triangulation or data on the species' source levels and calculations of sound propagation [Aniceto et al., 2020].

- Using previously developed tools [Ryan et al., 2014] to record, detect, and classify the presence of humpback, fin, sei, and North Atlantic right whales, Baumgartner et al. (2020) set out to investigate the performance of a Slocum G2 glider in detecting whales from two deployments in spring 2015 and 2016 in the Gulf of Maine. The glider was used as a tool to perform near real-time investigations and help estimate the presence of whales using species-specific calls as proxies [Baumgartner et al., 2020]. Near real-time detections of whales' vocalizations recorded by the glider were compared against acoustic data recorded by a moored DMON/LFDCS buoy deployed in the same area. The comparison showed a lower false detection from the glider's data than the moored hydrophone.

- Fregosi et al. (2020) deployed a Seaglider™model SG607 and two profiling floats to monitor 20 Hz fin whale calls in the Southern California Bight and to compare the results to fixed bottom-mounted recorders [Fregosi et al., 2020]. The authors used the Marine Mammal Monitoring on Navy Ranges system as a fixed array of 178 cabled, bottom-mounted hydrophones operated by the U.S. Navy [Jarvis et al., 2014]. Due to adverse weather during the deployment, all instruments recorded high background noise levels. Flow noise between 12 and 40 Hz was found, and fin whales' vocalizations were masked. The authors stated that the flow noise was due to the glider's speeds during descents and ascents. The authors did not highlight any other source of self-noise induced by the glider.

- Burnham et al. (2019) investigated the distributions of cetaceans and their migration using recordings from three platforms: an Autonomous Multichannel Acoustic Recorders (AMAR) moored system, a cabled icListen AF hydrophone controlled from offshore, and a Slocum ocean glider equipped with a DMON system. The instruments were deployed in the Clayoquot Canyon and detected sei, sperm, fin, humpback, and blue whales. From their analysis, the authors showed that the glider is able to detect cetaceans with the same accuracy as the stationary platforms. They concluded that underwater gliders are promising acoustic platforms to extend the knowledge of detecting marine mammals' behavior, but their capability in localizing the cetaceans is limited due to the small distance between the installed hydrophones [Burnham et al., 2019].

In conclusion, ocean-glider technology can be used to detect cetaceans and identify different species. Their accuracy is comparable to that of traditional acoustic recording systems, with the advantage of scanning larger areas. The latter allows researchers to extend their studies on cetacean migration. The papers also suggest that AUGs can be used to localize biological sources when working in parallel with other platforms. This can be done using an AUG, moored hydrophones, or multiple AUGs to form a network sensor. A drawback of the glider is its self-noise.

Detection and assessment of the underwater ship noise signature and other anthropogenic sources using AUGs

This section answers the research questions ($RQ_1.1$): Have AUGs been used to assess the acoustical power levels of ships or other ocean sound sources and/or detect them?

Ship-radiated noise can be measured for several reasons, including the detection of marine vessels or their impact on the ecosystem. More recently, researchers have developed procedures to measure URN or estimate the MSL of ships. [McKenna et al., 2012; Reis et al., 2019; Jiang et al., 2020]. In 2016, international standards were published to set procedures to measure vessel radiated noise levels using moored or floating systems with three or more hydrophones deployed in the water column [ISO-17208/1, 2016; ISO-17208/2, 2019]. The standards aim to characterize a single vessel as a noise source rather than monitor the impact of URN in the ecosystem. High-cost equipment and environmental marine conditions are limitations in applying the standard's procedures [Jiang et al., 2020; Virto et al., 2022]. Recently, some authors have performed exploratory studies on the use of AUGs to record ship noise:

- Wall et al. (2017) studied the soundscape of shelf-edge Atlantic waters in the southeastern USA using passive acoustic and ocean gliders. The study showed that AUG is effective for passive acoustic monitoring of marine environments. The glider's 29-day mission recorded 8,331 files. The study revealed a significant increase in boat noise in 25 % of the files recorded during the mission, compared to only 1.5 % in previous research conducted by the same author in 2013 [Wall et al., 2013]. They also highlighted that vessel traffic generates high-amplitude broadband noise that can significantly decrease the range at which biological sounds can be detected by the glider.

- Haxel et al. (2019) used a Slocum glider to measure spatial and temporal patterns in underwater ambient noise. They focused on studying sound levels between 50 and 100 Hz, which are greatly affected by sounds produced by ships. The study observed persistently high spectral energy in the ship noise frequency range during a seismic airgun survey conducted in the area. They presented a high level of variability in detecting ship noise levels. However, the increased variability in ship band noise was not accompanied by corresponding changes in the daily ship track length parameter derived from AIS data. The median noise levels at 100 Hz are typically around 85 dB re 1 $\mu Pa^2/Hz$ estimated using a propagation loss model (RAM) and the glider-measured sound speed profiles, local bathymetry, and AIS vessel track information. Therefore, the largest and loudest vessel can contribute to the noise at distances greater than 10 km. Noise from smaller vessels is reduced outside this range and has minimal impact on ambient conditions.

- Stinco et al. (2021) also used a Slocum G2 glider to detect the direction of motion of known sound sources. One experiment used a workboat and a fishing vessel as noise sources. Using a new detection technique, the authors utilized the cavitation noise of the propeller to estimate the azimuth angle of the sound source at each instant of time. The glider recorded the received levels from sources of noise different from the two target vessels. The data led to high accuracy in detecting azimuth angles.

- Wang and Yuan (2021) developed an underwater acoustic glider platform capable of detecting target direction and observing ambient noise. During a regular soundscape measurement mission, a Petrel II glider detected a 42-meter-long vessel travelling at a speed of 8.4 knots. Vessels have a more substantial impact on ambient noise levels at high-frequency bands above 100 Hz. They highlighted that the ambient noise levels decrease by -4 dB to -7 dB per octave at high-frequency bands above 100 Hz, except for the timing point affected by the vessel.

The presented papers show that AUGs can be equipped with an acoustic observer system of one or more hydrophones. AUGs can be used to monitor the global impact of vessel traffic on the ocean soundscape, as they are able to detect multiple noise sources simultaneously [Jiang et al., 2019]. Moreover, by focusing on a single ship,

they can estimate the URN and MSL of that noise source. Still, for this purpose, further studies are required to understand the effect of different PL models on the uncertainty of the calculated vessel sound signature levels. The three-dimensional motion of the glider in collecting the acoustic and oceanographic data can increase the accuracy of PL models and decrease the uncertainties in estimating the source sound levels of a target [Silva et al., 2013; Haxel et al., 2019]. In addition, AUGs can perform long-term missions (six months or more), allowing us to monitor temporal changes over an extended area. As reported in Section 2.4.1, the gliders' self-noise may be a limiting factor when the signal-to-noise ratio is low. Ocean gliders produce noise during manoeuvres, interactions with the environment, and from collecting scientific data. This noise may interfere with ambient noise and ship noise measurements [Cauchy et al., 2023].

2.4.2 Potential sources of error in PAM

This section answers the research questions (RQ_2): What are the uncertainties in estimating underwater sound source levels using fixed and mobile acoustic observers?

A key aspect of mitigating shipping noise is estimating the ships' source levels (URN or MSL) with high accuracy and identifying the measurement uncertainties. This estimation uses passive acoustic data of a vessel's radiated noise and propagation loss models. The variation in quantifying the ship noise levels has to be clearly stated. It is not only affected by the vessel itself, but geographical and environmental aspects also need to be considered. Therefore, it is crucial to evaluate the measurement uncertainties for obtaining highly accurate data on ship noise and implementing effective shipping noise reduction strategies. To answer the research question RQ_2, I have reviewed the selected articles and international standards and guidelines for assessing ship noise. The review includes the uncertainties that may impact ship noise assessment using traditional (fixed) passive acoustic monitoring systems and from AUGs' (mobile platform) measurements. Additionally, the investigation will involve an analysis of the quantification of measurement uncertainties. This will highlight the difficulties in obtaining precise and reliable estimates of ship source levels.

Selected articles

The selected articles from the RQ_2 search discuss the sources of uncertainties in measuring ship noise levels. I have identified 8 relevant articles (Table A.3), highlighting the importance of understanding and managing these parameters. The review examined the factors contributing to the development of uncertainties in estimating ship noise levels and the methods used to mitigate such uncertainties. The quantification of measurement uncertainties will also be investigated to highlight the difficulties of obtaining reliable estimates of ship source levels.

- McKenna et al. (2012) conducted a study where they measured the underwater radiated noise produced by seven different types of modern commercial ships under normal operating conditions. The study indicates that the source level estimates presented in this research were dependent on precise characterizations of the acoustic environment. It was anticipated that there would be some degree of variability due to variations in water column properties observed during each passage of the ship. In order to mitigate potential sources of error in the measurements, a standardized approach was employed, whereby all ships were measured during a consistent time of year and with the use of identical instrumentation. The variations in CPA distances exhibited minimal differences using, for example, AIS, leading to negligible fluctuations in transmission loss, measuring less than 3 decibels. The authors propose that implementing standardized measurement protocols and data reporting may mitigate this problem and enhance the comparability of ship noise data [McKenna et al., 2012].

- Merchant et al. (2012) proposed a methodology for characterizing sound exposure resulting from shipping activities by integrating continuous PAM with AIS shipping data. They highlighted the importance of measuring the background noise in the area of interest, where the sound pressure levels in the study were affected by the presence of both intermittent noises from small local vessels and ambient noise from distant shipping. They also showed high variability in estimating the source level in shallow water ($\leq 150m$) due to high attenuation of sound at both high and low frequencies, as noted by [Jensen et al., 2011]. The authors pointed out that the reflections from the seabed need to be corrected, similar to the sea surface, as also discussed by Magnier and Gervaise in 2020 [Magnier and Gervaise, 2020]. The study only uses a single hydrophone, which

may not provide a comprehensive picture of the acoustic environment in the study area. [Merchant et al., 2012].

- Simard et al. (2016) presented an analysis and modeling of ship source levels (SSLs) of 255 merchant ships measured along the St. Lawrence Seaway in eastern Canada. The study examined the SSLs variability of ships from a diverse merchant fleet based on source characteristics and estimated multivariate the SSLs models. The authors suggested that the variability in estimated SSLs arises from both source characteristics and measurement errors. The paper illustrated statistically that the SSLs did not show a strong correlation with any of these ship characteristics. This suggests that other factors, such as environmental conditions and measurement setups, may have a greater impact on SSL variability. In addition, the estimated SSLs were sensitive to the propagation loss model, which depends on geographic and geoacoustic characteristics. Also, they mentioned that the geometrical spreading would overestimate the radiated noise levels and suggested that a more representative propagation loss model, e.g., RAM or Wavenumber, is required to estimate SSLs accurately [Simard et al., 2016].

- Peng et al. (2018) proposed a model that utilizes the Finite Element Method and Ray Tracing to predict the URN of a fishing boat. This model takes into account realistic environmental parameters in situ. This study emphasized the significance of accounting for various factors, such as sea surface, bottom reflections, source depth, and seabed sediment type, when analyzing propagation loss in shallow water environments (87 m). This consideration is particularly crucial for low frequencies below 100 Hz. To conclude, the paper mentions several factors or parameters that can affect the measurement of boat or ship noise, including water depth, sea surface and bottom reflections, the vessel speed and length, the type of noise, e.g., non-cavitation and cavitation propellers, and mechanical noise (engines and generators) [Peng et al., 2018].

- Jaing et al. (2020) highlighted the parameters that may increase the uncertainty of ship noise measurement. The experiments were conducted in shallow water ($\leq$ 150 m). The authors mentioned that the distance between the hydrophone and the ship may impact the accuracy of the measurement. Also, they suggested that to mitigate the impact of uncertainties in source depth on the propagation

loss model's sensitivity, a vertical distribution of sources was implemented as an alternative to a single-point source. Finally, the author also pointed out the importance of accurately measuring the background noise to increase the confidence level of the ship noise measurement [Jiang et al., 2020].

- In 2021, ZoBell et al. and Haver et al. discussed the factors affecting source level estimation during long-term missions. The seasonal differences, averaging data, and propagation loss model were the significant parameters that should be considered carefully. In addition, the uncertainty in determining the source depth, Lloyd's mirror, and distance from the source to the receiver at the closest point of approach significantly impacted the assessment of the vessel noise signature and its uncertainty [ZoBell et al., 2021; Haver et al., 2021].

Therefore, uncertainty quantification must be explicitly reported as a combined standard error for the significant factors affecting the ship noise level estimation. The measurement repeatability and uncertainty can be minimized based on what was introduced in the literature. High-quality and precision devices will drive high measurement accuracy and a lower standard error. The sea trial should be conducted in good weather conditions (less than sea state 2); the better the weather window selected, the less uncertain it is to evaluate the source noise levels. The significant problems with the environment's impact on sound propagation between the acoustic source and the detection equipment [Merchant et al., 2012; ISO-17208/1, 2016; AQUO, 2014]. The propagation loss model has to be accurate by increasing the certainty of parameters used in developing the model, e.g., source depth, seabed characteristics, and sound speed profile. Other environmental factors, like currents, wind, etc., will interfere with the equipment's deployment and cause self-noise in the hydrophones, adding error in the actual distance between the acoustic source and the detection devices [AQUO, 2014]. The vessel itself is a considerable source of uncertainty; the measured URN is varied with vessel speed, type, length, and operating condition [McKenna et al., 2012; Veirs et al., 2016; ZoBell et al., 2021; McIntyre et al., 2021; Virto et al., 2022].

In the post-processing procedures, the received level averaged over a number of the hydrophones through the water column decreases the uncertainty of the interference patterns [ANSI/ASA S12.64-2009/Part 1, 2009; ISO-17208/1, 2016]. ISO-17208/1 defines deep water as the most efficient measurement environment for monitoring

sound sources compared to shallow water. The shallow water limits the frequencies below the cut-off frequency, which can be adjusted by increasing the ratio between range and water depth [Council, 2003; AQUO, 2014; Hermannsen et al., 2019]. In addition, more runs for the same operating condition will decrease the estimated source level uncertainty [ANSI/ASA S12.64-2009/Part 1, 2009; AQUO, 2014; Brooker and Humphrey, 2016]. Furthermore, the source can be represented as a single-point source instead of a dipole source when the closest point of approach is far from the observer compared to the water depth or the ratio between the vessel's overall length, and water depth is significantly small [AQUO, 2014]. However, this assumption is a loose approximation because of the contribution to the underwater noise signature of multiple complex sources. This methodology is valid only for far-field measurements (when the directivity of the source is not significant) or in the assessment of retrofit-induced changes and noise reduction studies [Chion et al., 2019; ZoBell et al., 2023].

International standards and classification societies

As stated by classification societies, international standards, and guidelines, the uncertainty in the measurement process of a vessel radiated noise has to be quantified and reported. The standard error in the measurement is categorized into two types: measurement uncertainty and measurement repeatability (see, for example, [ANSI/ASA S12.64-2009/Part 1, 2009], [ISO-17208/1, 2016], [AQUO, 2014], [Bureau Veritas, 2014], and [Bosschers, 2017]). Repeatability analysis is the study of the systematic error in measuring sound levels from the same vessel under the same ship operation and environment conditions within a set confidence interval [AQUO, 2014; ISO-17208/1, 2016]. For instance, Humphrey et al., in 2015, investigated the repeatability of noise level measurement from a single hydrophone over several runs with a repeatability of 1 and 2 dB [Humphrey et al., 2015]. At the same time, the assessment of general uncertainty means identifying and quantifying the random error in the source levels based on the uncertainty of the used devices, environment, vessel, and post-processing. The uncertainty in URN assessment under the American National Standard [ANSI/ASA S12.64-2009/Part 1, 2009] and International Standard Organization [ISO-17208/1, 2016] procedures was quantified as combined standard error values and varied based on either the frequency range or measurement grade. A collective summary in Table A.4 of what was presented in the standards and classification

societies is as follows:

- ANSI/ASA addressed the sound pressure level uncertainty derived from errors in calibration, sensitivity, data processing, and amplifier gains of the measuring devices. The total combined uncertainty is 1.3 dB. The URN level variability was about 1.5 to 2 dB, including an error in the horizontal range and depth between source and receiver, acoustic center and sound speed profile gradient. They introduced three grades of measurement (A, B, and C). The uncertainty in grade B is less than in grade C but higher than in grade A. For example, Lloyd's mirror effect affects grade C more highly than grades A and B. For the grades, the average over the runs minimizes the repeatability and uncertainty of SPL.

- In 2016 and 2019, ISO-17208/1 and ISO-17208/2 were published. As shown in Table A.4, combined values of uncertainty in measuring URN levels were 5 dB for frequencies below 100 Hz, 3 dB for 125 to 16000 Hz, and 4 dB above 20000 Hz. The vessel condition and sea state control the levels of measurement repeatability, which are estimated by 3 dB for frequencies below 100 Hz and 1 dB for high frequencies. At the same time, the uncertainty in the sound pressure level is affected by the hydrophone characteristics uncertainties, post-processing frequency domain conversion, and averaging SPL over time. The uncertainty is counted by 1.5 dB and 3.5 dB for low and high frequencies. Lastly, the conversion to received noise level (RL) adds uncertainty because of the variability in the ship-to-hydrophone horizontal distance calculation (e.g., GPS) and the hydrophone depth (e.g., title angle in the cable). Furthermore, the interference patterns from the multipath sound waves developed by the direct and the water-air surface reflections lead to increased RL uncertainty that is frequency-dependent. However, the average SPL over the data window length and the three hydrophones minimize Lloyd's mirror effect.

Table A.4 illustrates the requirements to measure underwater radiated noise from ships and the measurement uncertainties prescribed by four of the leading classification societies. The table compares the classification societies' requirements with the ISO and ANSI/ASA standards and highlights similarities and differences. There is an explicit agreement between the published scientific articles and the standards and

classification societies in assessing vessel noise levels. For instance, BV recommended following ANSI/ASA and ISO-17208/1 to grant silence notation. However, modifications in the BV report reduce the measurement uncertainty compared to ISO-17208/1 [Bureau Veritas, 2014]. ABS published guidelines to measure ship noise levels regarding commercial and research vessels to approve a class notation. The measurement requirements follow the ANSI/ASA and ISO-17208/1 as well [American Bureau of Shipping, 2022]. Lloyd's Register (LR) recommends ANSI/ASA and ISO-17208/1 in all the measurement and post-processing procedures to approve the class notation, for example, transit or quiet notation. However, they added some calculations for the monopole source in shallow water that were not mentioned by the standard. The calculation minimizes the uncertainty of the interference patterns developed by the mirror effect [Lloyd's Register Group Limited, 2018]. DNV GL published measurement procedures for classed vessels to be approved for silent notation. The procedures almost drifted from the previous standards and guidelines without uncertainty quantification, as shown in Table A.4 [DNV GL, 2017].

Sources of uncertainty based on the platform type

In general, any type of PAM observer is impacted by the sources of uncertainty. Firstly, the propagation loss model estimates the intensity level losses caused by the sound waves between the source and receiver. The uncertainty of determining the propagation loss is crucial to consider. The model may consist of the following components: source depth, receiver depth, the distance between source and receiver, seafloor characteristics, and sound speed profile. The model might be developed using different methods. Using the spherical spreading model to estimate the drop in sound wave intensity to the range [ANSI/ASA S12.64-2009/Part 1, 2009; ISO-17208/1, 2016; Simard et al., 2016; Haxel et al., 2019], in contrast, a numerical model can be created associated with environmental factors instead of the range for precise propagation loss prediction [Merchant et al., 2012; Ainslie et al., 2022]. For both methods, the overall uncertainty of the propagation loss model depends on the uncertainty in estimating each parameter.

Background noise is the second element to consider in the assessment of underwater sound sources, and it depends on the frequency of interest. The background noise can be defined as the sounds that are not interesting to the measurement objective. It

should be recorded in the absence of the target ship by at least 2 km from the observer [ISO-17208/1, 2016]. Finally, the vessel speed, length, and directionality contributed to the total uncertainty assessment.

The multipath of sound due to the sea surface and seabed reflection is important to consider. The interference of sound waves may cause overestimating or underestimating the source levels as a function of frequency. It is crucial to correct the RSL: ISO 17028-1 recommended that the power average between the three hydrophone readings might decrease the mirror effect phenomenon [ISO-17208/1, 2016; American Bureau of Shipping, 2022; Lloyd's Register Group Limited, 2018]. The water depth also plays a key role in the frequency range of the measurement. There is a cutoff frequency where the sound waves at specific water depths can be propagated [Urick, 1983; Jensen et al., 2011].

Based on the selected PAM observer, some parameters may add more uncertainty to the measurement of the ship noise and are discussed as follows:

Fixed platform uncertainties The self-noise of the PAM system adds more energy to the received sound. Cable vibrations and mechanical chafing between components induce self-noise. The hydrophone movement either tilts or, with depth due to the internal current, changes the slant range between the noise source and the hydrophone, which increases the propagation loss uncertainty [AQUO, 2014].

Mobile platform uncertainties The use of AUGs instead of conventional PAM systems decreases the factors that may negatively impact the uncertainties of recorded ship noise levels, such as no cables or mechanical chafing. However, the AUG may introduce uncertainties due to its motion. The flow noise caused by glider motion can be ignored due to its low speed of less than 0.25 knots [Aniceto et al., 2020; Cauchy et al., 2023]. However, it may affect the received sound levels for frequencies below 20 Hz. Additionally, gliders generate noise during manoeuvres, which can interfere with the measurements of underwater noise [Dassatti et al., 2011].

The brushless DC motor of the oil pump is the dominant source of self-noise for the glider. The pump has intermittent behavior and operates for 20 to 26 seconds at the maximum water depth the glider reaches and then turns off [Schofield et al., 2007; Cauchy et al., 2023]. Therefore, gliders are capable of acquiring acoustic data

with a high signal-to-noise ratio during their descent and ascent while simultaneously discarding data that has been contaminated by the noise emitted from the oil pump. The noise levels of the rudder and fin remained consistent and had a minimal impact on the overall background noise. They could be disregarded due to their short duration of fewer than 0.5 seconds [Haxel et al., 2019].

Lastly, the accuracy of determining the AUG position underwater impacts the propagation loss between the glider and the noise source. The glider tracking position is uncertain and can be calculated based on the glider flight data and environmental measurements. AUGs primarily estimate their position by assuming velocities using a flight model. Using a model-based approach is essential for tracking the subsurface position of the glider. Challenges arise in energetic tidal basins due to unresolved depth-dependent flow, which can lead to the accumulation of position errors on top of an assumed depth-averaged current. Recent studies have utilized high-resolution acoustic tracking ranges to enhance accuracy by limiting positional inaccuracies and minimizing uncertainties associated with the flight-model approach [Bennett et al., 2021; Cauchy et al., 2023].

2.5 Summary

The use of AUGs for passive acoustic monitoring missions presents various advantages and prospects for enhancing the awareness of the propagation of ship noise in the ocean environment. Acoustic AUGs are versatile tools that can conduct various PAM missions, including monitoring ocean soundscapes, detecting and characterizing marine species, and measuring underwater noise from vessels. The understanding of oceanographic characteristics and underwater noise levels can also be expanded by deploying AUGs, which allows us to collect helpful information autonomously on temporal and spatial changes in large areas of the ocean.

AUGs, unlike conventional fixed PAM systems, operate as quiet platforms, thereby reducing disruptions to aquatic life. This facilitates the acquisition of detailed and extensive data regarding marine mammal populations and behavior. Moreover, AUGs can work simultaneously with other PAM systems to create a network of sensors to localize and track marine mammals.

Additionally, AUGs have the ability to collect oceanography samples from the

surface to the seafloor autonomously. This enables us to investigate the changes in sound speed across distances, both horizontally and throughout the water column. If the acoustic properties and topography of the seafloor were combined with the range- and water column-dependent oceanography data gathered by the glider, the impact of the sea surface and seafloor reflections on sound propagation would be noticeable. This would be advantageous, especially in shallow water environments with a depth of 150 metres, where the impact of reflections is substantial. The understanding of the behavior of sound propagation in remote areas can be improved after integrating the oceanography and PAM data collected by the glider in order to not overestimate or underestimate marine sound levels, for example, ship noise signature levels.

In order to use AUGs for PAM missions, it is necessary to estimate the measurement uncertainties of the data acquired with the AUG and compare them with the uncertainties of the reference platform. This is currently an open problem, and further studies are needed to develop a procedure to quantify measurement uncertainties in PAM systems. A comprehensive method for the assessment of measurement uncertainties would make it possible to compare and generalize the results of existing studies on passive acoustic monitoring in the ocean environment.

Currently, a comprehensive methodology to estimate and report uncertainties in passive acoustic monitoring of underwater noise is still missing. This methodology needs to consider the contribution of a large number of sources of error. This requires a broader body of data that includes measurements performed with different PAM systems, analyzed comparatively, a wide range of water depths, and several weather and environmental conditions. Due to the large number of factors to consider, it is not feasible to extend the existing procedures for the assessment of measurement uncertainties presented in different ISO standards and classification societies' guidelines to a more general situation.

Chapter 3

Methodology

This chapter outlines the methodology used to address the research questions stated in the previous chapters. This section aims to provide a comprehensive description of the research methodology, including the justification for the selection and implementation of particular investigative methods and analytical instruments. A quantitative approach was employed to evaluate the performance of ocean gliders as a passive acoustic monitoring platform, particularly in measuring and characterizing underwater ship noise signatures. This approach allows for a reliable and reproducible data collection and analysis framework.

This chapter organizes the methodology based on the two main sites used in the research. The first site is Petty Harbour-Maddox Cove, where only a fixed buoy is utilized to characterize ship underwater noise. Conception Bay is the second main site where the ocean glider was deployed to complete the research.

The contents of this chapter are based on three published articles:

- *Assessment of the underwater noise levels from a fishing vessel using passive acoustic monitoring and structure hull vibration*, which is published in *Canadian Acoustics*, *Vol.*: 50(3) [Helal and Moro, 2022].
- *Underwater noise characterization of a typical fishing vessel from Atlantic Canada*, which is published in *Ocean Engineering Journal*, *Vol.*: 299 and *ISSN*: 0029-8018 [Helal et al., 2024b].
- *Advancing Glider-based Measurements of Underwater-Radiated Ship Noise*, which

is under review in *The Journal of the Acoustical Society of America*, *Vol.*: 156(4) and *ISSN*: 0001-4966 [Helal et al., 2024c].

3.1 Vessel operations

This section discusses the operational conditions of the vessels, such as specifications and sailing speeds, used to achieve the research objectives.

3.1.1 Petty Harbour-Maddox Cove

In 2021, two sea trials were performed in August and December to thoroughly assess and document the noise characteristics of the fishing vessel. The trials focused on isolating and analyzing the sources of noise contributing to the vessel's acoustic footprint. The sea trials aimed to identify the noise sources in the fishing vessel and measure the extent to which each source contributes to the vessel's acoustic footprint. They took place off the coast of Petty Harbour-Maddox Cove, Newfoundland and Labrador (NL), Canada.

The vessel used in this research trial is a small fishing vessel (see Figure 3.1), and the propulsion system is a diesel engine. The vessel features a 4-blade fixed-pitch propeller. Table 3.1 summarizes the main characteristics of the vessel.

Figure 3.1: Fishing vessel under testing in Petty Harbour-Maddox Cove trials

The tested fishing vessel was set up to operate at prescribed engine speeds (RPM)

and propeller clutch scenarios. Two testing scenarios were recorded for the aforementioned fishing vessel. Scenario 1 involves recording underwater radiated noise and onboard vibration at different RPMs. Scenario 2 records the same measurements while the propeller is unclutched.

Table 3.1: Main specifications of the fishing vessel under testing in Petty Harbour-Maddox Cove trials

Parameter	**Value**	**Unit**
Length OA	10.3	[m]
Beam	3.3	[m]
Maximum ground speed	$9-10$	[knots]
Maximum engine speed	2400	[RPM]
Propeller blade number	4	[−]
Engine cylinders	6	[−]
Gearbox ratio	2.4	[−]

In scenario 1, the vessel was running at three distinct engine RPMs: 1400, 1800, and 2200. The vessel noise signature at each RPM was measured and recorded following [ANSI/ASA S12.64-2009/Part 1, 2009; ISO-17208/1, 2016]. The vessel ran between two waypoints parallel to the PAM observer. Following the completion of these measurements, we conducted measurements for scenario 2. In the second scenario, the vessel was positioned at the closest point of approach (CPA), ensuring it was at least 100 m away from the observer. The propeller-driven shaft was disconnected from the engine, and the engine kept running at 1400 rpm; this trial was titled the "unclutched-propeller" scenario in stationary mode. Table 3.3 illustrates the trial time sequence, where the two scenarios were performed twice in August and December. Each single-speed experiment was repeated two times to capture vessel noise from the port and starboard sides.

The vessel's geocoordinates were recorded relative to the observer using a built-in GPS device. The vessel's engine speed was monitored manually through analogue gauges on the dashboard.

3.1.2 Conception Bay

In 2022 and 2023, I conducted two experiments in Conception Bay, NL, using a glider with wing-mounted hydrophones in order to characterize the underwater sound

signatures of a moving vessel. The experiment followed procedures according to [ISO-17208/1, 2016], except for standard use of a fixed station of an array of three hydrophones, which was replaced with a glider.

The first experiment was performed to assess the acoustic self-noise signature of the Slocum glider. It was conducted in relatively shallow water (60–90 m) (Figure 3.5a). In the second experiment, the glider was used to measure the underwater ship noise of the target vessel in the form of a URN value and compared against fixed PAM observers (see Figure 3.4). It was conducted at depths of around 120–300 m, 14 km away from the first experiment. Assessing the glider's performance as an alternative to fixed platforms would be beneficial in determining its suitability as a PAM observer. In the following text, these sites will be referred to as the shallow and deep water experiments, respectively, noting that the reference to shallow and deep is relative to the selected sites.

Figure 3.2: Fishing vessel under testing in Conception Bay trials

Table 3.2: Main specifications of the fishing vessel under testing in Conception Bay trials

Parameter	**Value**	**Unit**
Length OA	11.9	[m]
Beam	4.57	[m]
Maximum ground speed	$11 - 12$	[knots]
Maximum engine speed	2800	[RPM]
Propeller blade number	4	[−]
Engine cylinders	6	[−]
Gearbox ratio	2.98	[−]

At the deep-water site, a fibreglass vessel (Figure 3.2) measuring 11.9 x 4.57 m, powered by a six-cylinder diesel engine and featuring a four-blade propeller system, was employed as a moving noise source. The vessel was set up to navigate between two waypoints, back and forth, parallel to the PAM platforms' locations (see Figure 3.4). At engine speeds of 1500 and 2000 rpm, four runs each were conducted, with a constant vessel velocity for each engine speed throughout their 4 runs [ISO-17208/1, 2016]. Maintaining a consistent distance between the vessel's path and all platforms was challenging due to operational constraints such as currents, drift, and human error in piloting the vessel.

3.2 Sites and trials information

In this section, the site information regarding the geolocation, water depths, and weather conditions is discussed. In addition, a detailed illustration of the experimental set-up of the sea trials is presented.

3.2.1 Petty Harbour-Maddox Cove

The August trials focused on two main experiments, as described in Table 3.3. One experiment involved maintaining a constant vessel speed at an engine speed of 2200 rpm, while the other examined engine noise at 1400 rpm without the propeller engaged. The December trials extended the scope of the study by conducting four comprehensive experiments at different operational speeds.

Figure 3.3 shows the experimental site location, located approximately 8 km away from the coastline. This area was chosen for the study because it provides ideal conditions for acquiring underwater acoustic data and is far from any shipping traffic. The water depth in the region varies between 120 and 140 metres. The seafloor displays considerable variation in terms of thickness and composition of glacial till, cohesive clay, and gravel, indicating a rocky seabed composition mixed with sand and mud [Shaw and Potter, 2015].

The site area was carefully chosen within a 10 km^2 area across Petty Harbour-Maddox Cove, focusing on seafloor topology with minimum variance. The buoy observer's location was at 47°27'14.28''N and 52°36'7.5''W.

Table 3.3: Operating conditions and sequence of the fishing vessel in Petty Harbour-Maddox Cove trials

#	**Experiment sequence**
Sea trial 1 (August)	
1	Sailing at an engine speed of 2200 rpm
2	Stationary vessel "unclutched-propeller" and engine run at 1400 rpm
Sea trial 1 (December)	
1	Sailing at an engine speed of 1400 rpm
2	Sailing at an engine speed of 1800 rpm
3	Sailing at an engine speed of 2200 rpm
4	Stationary vessel "unclutched-propeller" and engine run at 1400 rpm

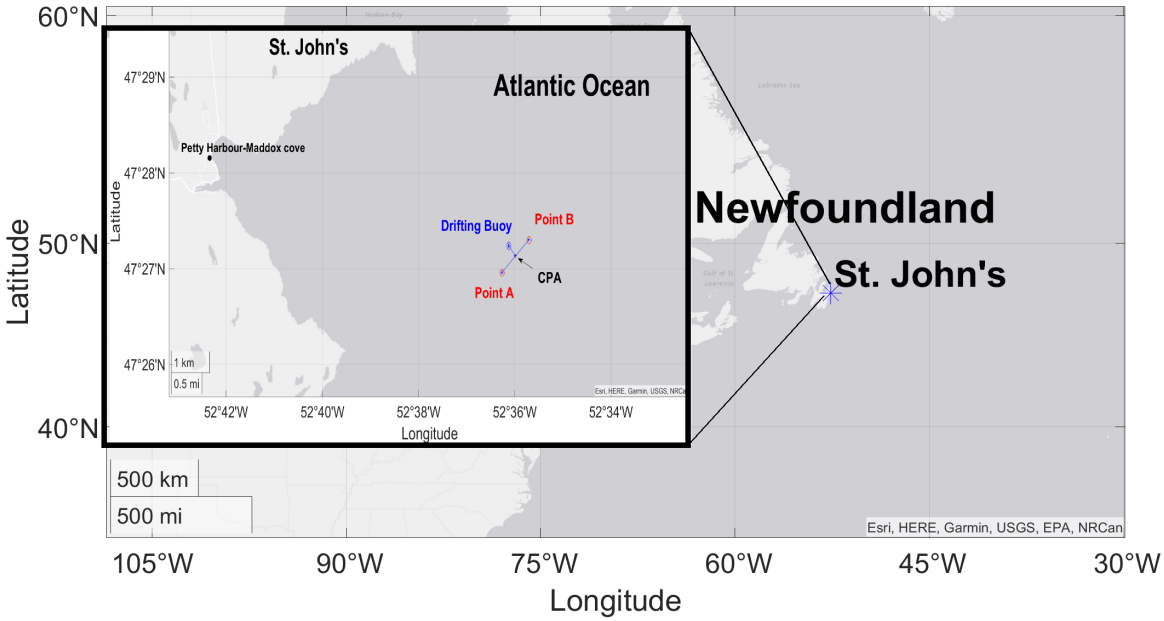

Figure 3.3: Petty Harbour-Maddox Cove site map and deployment area

Environmental conditions were carefully monitored prior to the trials. The weather conditions were aligned on both dates with the standard recommendations for conducting the experiments [ISO-17208/1, 2016]. Table 3.4 presents the parameters of wind speed, current speed, and wave height. The environmental parameters are publicly available on the Smart Atlantic website [The Fisheries and Marine Institute of Memorial University of Newfoundland's Centre for Applied Ocean Technology (CTec) and the Centre for Ocean Ventures and Entrepreneurship (COVE) of Halifax, 2021].

Table 3.4: Weather conditions during the Petty Harbour-Maddox Cove trials

Parameter	August	December
Wind speed [m/s]	3.6 ± 1.2	6 ± 1
Wave height [m]	0.41 ± 0.1	3.5 ± 0.7
Current speed [mm/s]	24 ± 15	152 ± 70

3.2.2 Conception Bay

As described in Section 3.1.2, the Conception Bay experiments were related to the ocean glider acting as a PAM observer to measure and characterize vessel noise signatures. The glider followed a prescribed route between programmed waypoints and performed several dives and climbs at regular intervals. Holyrood Bay, at the head of Conception Bay, hosted the glider's initial tests on July 22, 2022, near 47.4156 N and 53.1331 W. The glider completed six dive and climb cycles (1 dive and climb cycle = 1 yo) profiles at this shallow water location at a water depth of 60 m (Figure 3.5a). In the subsequent deployment in Conception Bay on January 13, 2023 (47.5333 N and 53.1583 W), the glider completed 4 additional yos, diving to 190-200 m. The glider inflection dive depth changed with bathymetry (10 m above the seafloor) between yos, see Figure 3.5b.

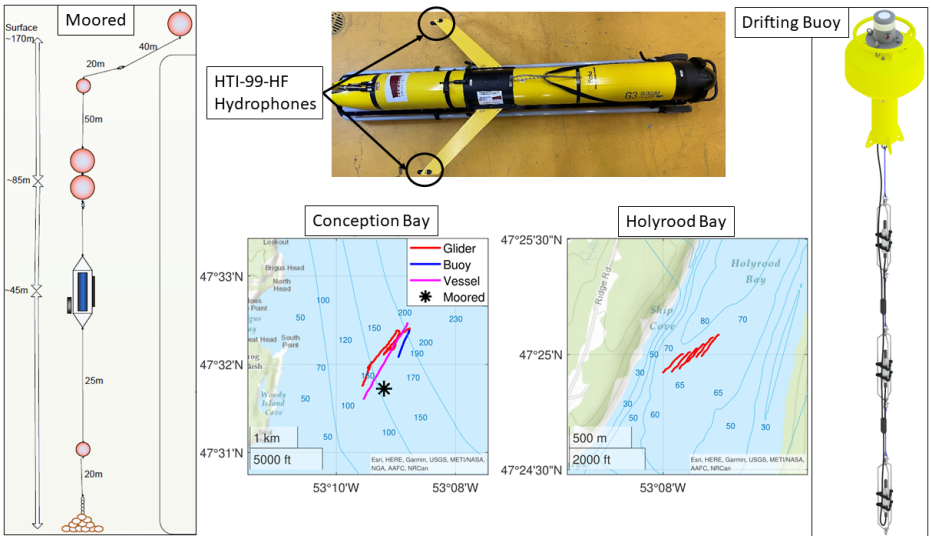

Figure 3.4: Map of the site where the two sea trials were conducted. A drifting buoy and moored systems were used in Conception Bay with the glider. In Holyrood Bay, there was an additional trial by the glider in shallow water

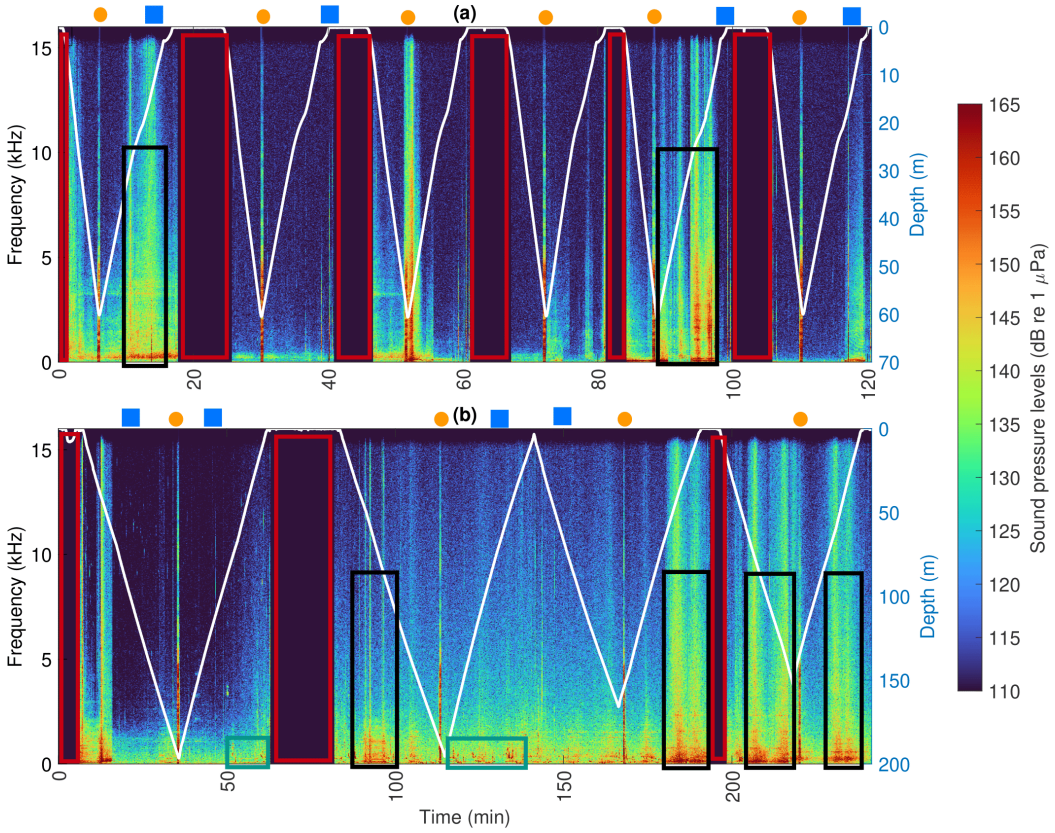

Figure 3.5: At both the shallow (a-Holyrood) and deep experiment sites (b-Conception Bay), the glider's observer's sound spectrogram overlapped with the glider depth. Red boxes indicate periods when the observer did not log data. The black box displays underwater sounds from the vessel being tested. In the green box, dolphins' biological sounds near sea paths are displayed. Orange circles indicate the glider's oil pump at its maximum depth. When the rudder was moving, the blue square box indicated radiated noise.

The glider dive and climb angles were set to 26° for the shallow water trial and 20° for the trials in deep water. In both missions, the glider dynamically adjusted the battery pitch pack position to maintain even climb and dive angles, as well as the automatic buoyancy pump trim (auto ballast) to maintain even vertical speeds of around 10–12 cm/s. In shallow water, the glider surfaced after every single dive and climb cycle, while in the Conception Bay sites, the glider performed several dives and climbs between surfacings, as in the 2^{nd} and 3^{rd} yo's presented in Figure 3.5(b). Due to the currents in Holyrood, the glider was pushed backwards between subsequent

Table 3.5: Weather conditions in both Holyrood Bay on July 29^{th}, 2022, and Conception Bay on January 13^{th}, 2023

Parameter	**Shallow-water site**	**Deep-water site**
wind speed [m/s]	2.1 ± 0.5	2.6 ± 0.8
wave height [m]	$< 0.5 \pm 0.1$	$< 1 \pm 0.1$
current speed [mm/s]	77.1 ± 12	102.9 ± 56

surfacings, leading to an adjacent set of glider profiles oriented alongside the central axis of the bay.

The weather conditions on both days were calm, with states below Sea State 2 observed throughout the duration of the trials [ANSI/ASA S12.64-2009/Part 1, 2009; ISO-17208/1, 2016]. Table 3.5 provides approximate oceanic and atmospheric conditions during the tests based on data provided by a Smart Atlantic buoy near the entrance to the Holyrood Bay area [The Fisheries and Marine Institute of Memorial University of Newfoundland's Centre for Applied Ocean Technology (CTec) and the Centre for Ocean Ventures and Entrepreneurship (COVE) of Halifax, 2021].

3.3 Passive acoustic platforms

This section presents the passive acoustic sensor types and their configurations, in addition to the platforms that carry those sensors. Also, the glider's specifications are illustrated.

3.3.1 Petty Harbour-Maddox Cove

The experiment employed a three-hydrophone array supported by a coastal acoustic drifting buoy and a ballast drop weight model BOS-W manufactured by Ocean Sonics [Ocean Sonics, 2021a], as represented in Figure 3.6. The three hydrophones were attached to 100-meter cables at designated depths of "Shallow", "Middle", and "Deep" located at distances of 32, 63, and 94 metres from the sea surface [ANSI/ASA S12.64-2009/Part 1, 2009; ISO-17208/1, 2016]. The buoy included a data control logger,

lithium batteries, a radiofrequency sender, and a GPS module. The GPS module enabled the geolocation of the buoy and synchronized the hydrophones with Coordinated Universal Time (UTC). The buoy facilitated the adjustment of hydrophone settings pre- and post-deployment and provided supplementary power to the hydrophones as needed.

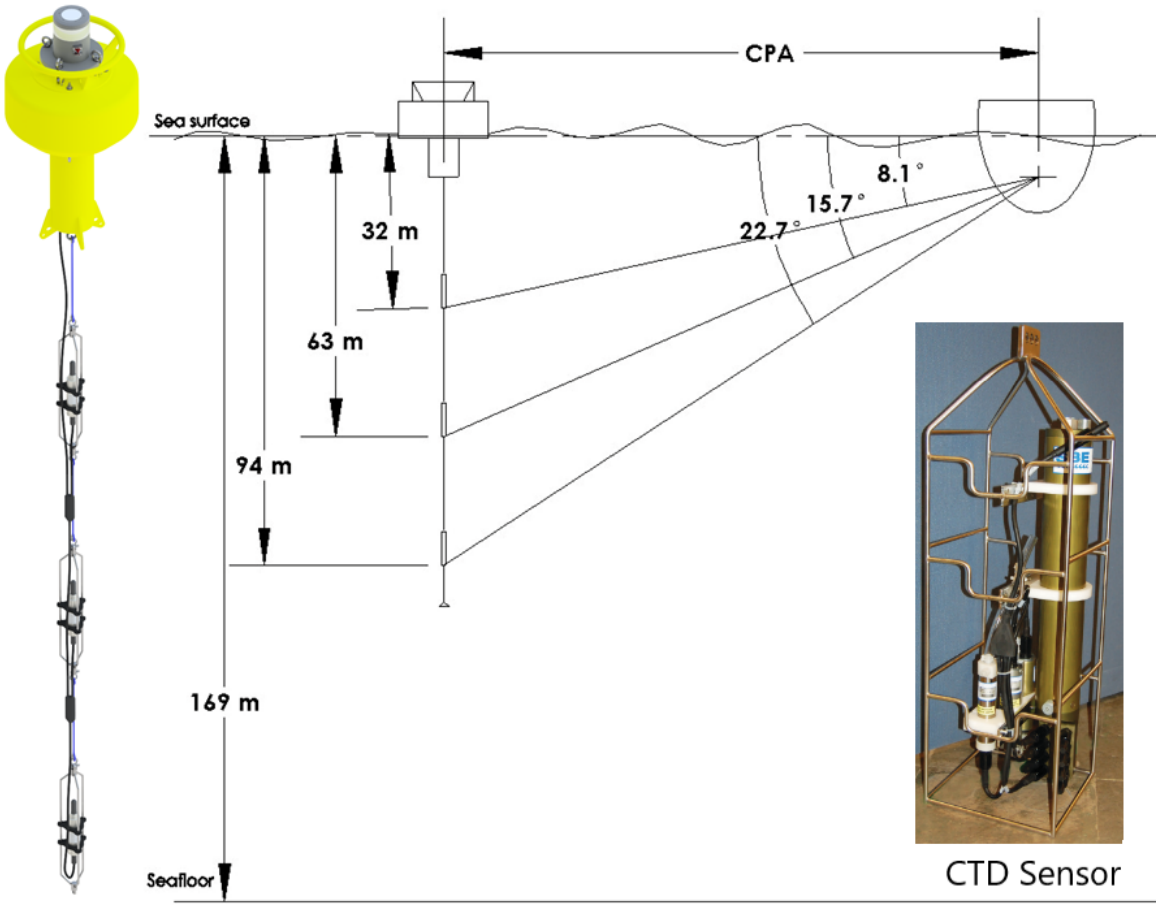

Figure 3.6: Drifting buoy with an array of three icListen hydrophone configurations. The hydrophones' depths are 32, 63, and 94 m from the water surface. In addition, the SBE 25plus CTD profiler was used in the trials.

The hydrophone system is a digital standalone marine acoustic sensor by Ocean Sonics icListen (RB9-HF models) [Ocean Sonics, 2021b]. Each hydrophone includes a data logger, data memory, and an internal lithium battery. The hydrophones were adjusted to sample at a 64 kS/s sampling rate and a 24-bit waveform, enabling the measurement of frequencies up to 25 kHz. The hydrophones are characterized by a flattened sensitivity between 10 Hz and 64 kHz, and their nominal value is equal

to -176.9 dB re V/μPa. They were programmed to record continuously during the mission, and the resulting acoustic files were obtained when retrieving the platform at the end of the experiment.

3.3.2 Conception Bay

The Slocum glider, manufactured by Teledyne Webb Research [Teledyne Webb Research, 2017] is one of the most prolific buoyancy-driven underwater glider platforms in use by the ocean research community. The glider was equipped with an RBR Legato CTD. The tested glider featured a 350 m "high-displacement" (HD) oil pump (450 cm^3). The glider was ballasted and prepared for deployment at the Memorial University glider facility in a large tank, following standard manufacturer recommendations. Baird [2007] provides a basic outline of the procedure.

The glider was equipped with two HTI Ltd. [High Tech, INC., Accessed: 2021] wing-mounted hydrophones, which have consistent sensitivity from 50 to 10,000 Hz with a minimal uncertainty of ± 0.9 dB. An OceanObserver extended payload with 16 acoustic channels up to 8–512 kS/sec by a JASCO Ltd. manufactured OceanObserver multi-channel PAM recording system was attached to the glider where the two hydrophones connected [JASCO Applied Science, 2021]. The OceanObserver was responsible for logging data with 1 TB of internal memory. The glider was configured with an extended energy bay with rechargeable batteries to support the hydrophones and the OceanObserver power consumption. All glider science payload sensor timestamps were synchronized to the glider science data-logging computer.

The port and starboard wing-mounted hydrophones were configured to record acoustic signals at a frequency of 32 kHz using 24-bit quantization, providing a dynamic range of 147 dB between the overload signal and the quantization noise. The hydrophones on the drifting and moored platforms were set to sample at the same rate. The start-up time of the OceanObserver on the glider is around 60–120 s, resulting in the glider recording being restricted to 10 metres below the surface on the first glider dive segment only but continuously thereafter.

The glider served as the primary PAM platform for the shallow water (Holyrood site) trial. This configuration, which did not include the drifting hydrophone array and

bottom-mounted hydrophone that were employed in other trials, enabled the evaluation of the glider's acoustic performance without interference from other measurement systems.

In the deep water tests (Conception Bay), the hydrophone array and the bottom-mounted hydrophone were deployed with the glider (Figure 3.4). The buoy had the full-length hydrophone array set at fixed depths of 32, 63, and 94 m [Ocean Sonics, 2021a], as well as a deep-depth mooring with a single Ocean Sonics icListen RB9-HF hydrophone 45 m above the seafloor [Ocean Sonics, 2021b]. The moored platform was fully immersed in the water and consisted of a float array, battery pack, acoustic release, and an anchor, as shown in Figure 3.4. The noise levels were evaluated and classified from each PAM platform separately as a stand-alone observer for comparison purposes.

Table 3.6 summarises the sea trials information conducted to achieve the research objectives.

Table 3.6: Sea trials summary

	Seat Trial 1	**Sea Trial 2**
Location	Petty Harbour-Maddox Cove	Conception Bay
Water depth	120 m	Shallow: 60 m Deep: 190 m
Weather	<Sea state 2	<Sea state 2
PAM observer	Array of three hydrophones	Glider Array of three hydrophones Bottom-mounted hydrophone
Vessel type	Fishing vessel (LOA 10.3 m)	Fishing vessel (LOA 11.9 m)
Operating speed	1400 rpm 1800 rpm 2200 rpm stationary	1500 rpm 2000 rpm

3.4 Acoustic files data processing

The acoustic files were processed using Equation (3.1) and Matlab® software with full-scale normalized values (x[n]) ranging from -1.00 to 1.00; thus, the number of bits (N) equals 1. When using native values instead of normalized, the N would equal the number of sampling bits. Sensitivity values throughout the dynamic range and an analog-to-digital converter peak-to-peak voltage were then used to apply the conversion to sound pressure values in Pascal units $P[n]$. Finally, the sound pressure levels (SPL) were computed using the Matlab Signal Processing Toolbox and presented in a narrowband with a resolution of 1 Hz and a one-third octave band.

$$P[n] = x[n] \times \frac{V_{pp}}{2} \times \frac{1}{2^{N-1}} \times \frac{1}{10^{\frac{sensitivity}{20}}} \times 10^{-6} \quad [Pa] \tag{3.1}$$

Pre-processing the raw acoustic files required sensitivity, an analog-to-digital converter peak-to-peak voltage, and the dynamic frequency range as illustrated in Table 3.7. These prompted the conversion to sound pressure values in Pascal units P[n] using Equation (3.1). Finally, the Matlab Signal Processing Toolbox was used to figure out the SPL of any desired acoustic window, and the results were presented in two narrowband frequency domains: one with a resolution of 1 Hz and the other with a resolution of one-third of an octave. This style of sound-level presentation was used throughout the thesis results.

Table 3.7: Pre-processing information of each hydrophone type used in the trials

Parameter	**icListen-HF**	**HTI-99**
Sensitivity [dB re 1 V/μPa]	-176.9 ± 1.1	-164.5 ± 0.9
V_{pp} [volts]	6	9
Frequency range [Hz]	$10 - 100k$	$20 - 16k$

3.4.1 Desired acoustic window extraction

Spectral analysis can be used to isolate and determine the relative sound amplitudes of sound sources in acoustic recordings [Jiang et al., 2019; Cauchy et al., 2023]. Figure 3.7 presents the spectrogram of the sea trials conducted in Petty Harbour-Maddox Cove

and is similar to Figure 3.5, which represents the spectrogram of the recorded sound by the glider in the Conception Bay trials. In order to determine the vessel under test noise, the CPA was identified with the aid of the mission time stamp of each trial. Figure 3.7 is an example of the CPA location, labeled with a dotted black line. The acoustic data was cropped to a window size of 30 to 45 seconds, where the CPA centred the extracted windowed acoustic file for the post-processing analysis.

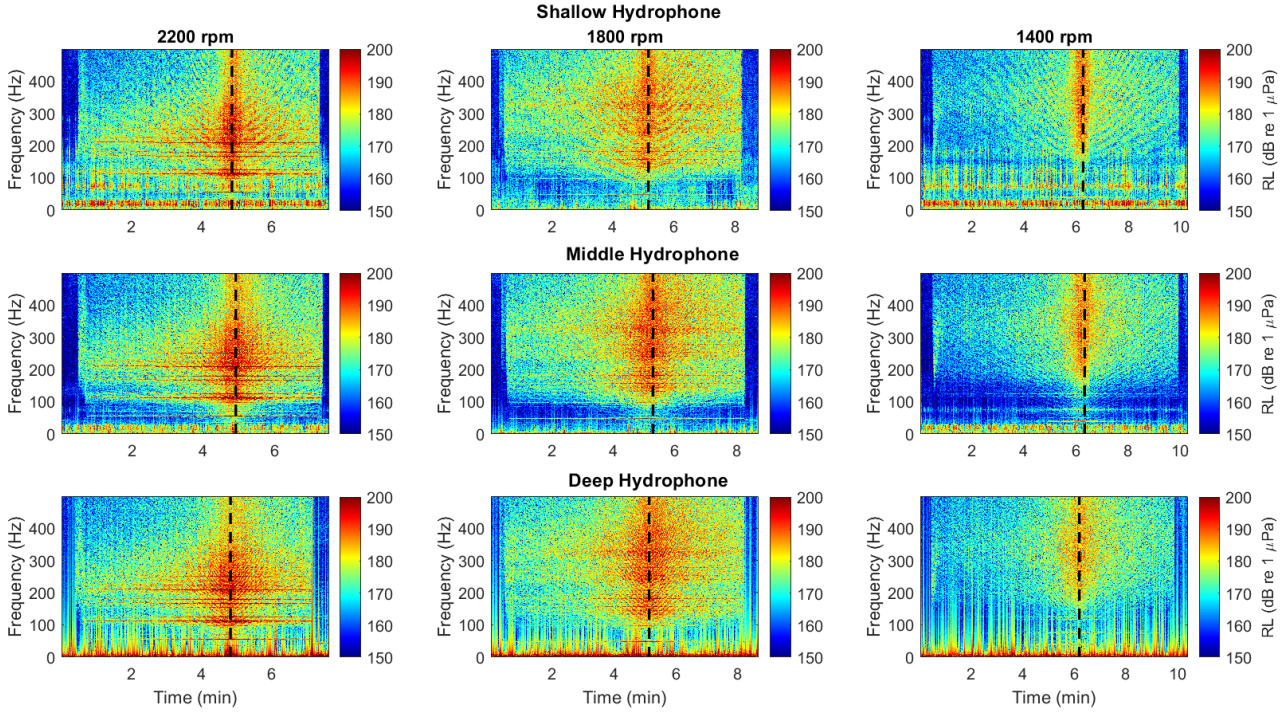

Figure 3.7: Spectrogram of the RL by the fishing vessel at 1400, 1800, and 2200 RPM trials in Petty Harbour-Maddox Cove trials

In Conception Bay, the spectrogram (Figure 3.5) of the hydrophones, notes from the field tests, and the glider flight data help us figure out when noise sources like vessel noise or biological sounds are present. Moreover, by carefully reviewing the glider flight record, it is possible to determine the timing and noise levels of specific glider moving components in preparation for subsequent analysis. Also, acoustic windows with low noise intensity were used to calculate the background noise, which occurred when the vessel was 2 km away from the observers. The data logging paused either when the glider approached or reached the surface, as indicated by the red boxes on the spectrogram (Figure 3.5). Orange dots illustrate the noise levels produced by the glider's buoyancy engine and battery pack. Blue squares indicate noise levels due

to the use of the rudder. Also, marine mammals (dolphins and minke whales) were sighted and identified during the deep experiment (highlighted with green boxes).

3.5 Glider self-noise

The glider was placed in the shallow-water site to assess its self-noise in a sheltered and quiet environment and in the absence of any externally controlled sound sources.

Several methods of self-noise assessment exist. Tesei et al. used a single hydrophone to measure the self-noise of the Slocum glider in a water tank. The water tank may overestimate the self-noise levels because of wall reflections, as noted by [Tesei et al., 2019]. [Cauchy et al., 2023; Haxel et al., 2019; Jiang et al., 2019] also used mounted hydrophones, which were attached to the glider at the front and/or tail in the open-field ocean. The mission flight data files were used to identify dive phases, transitions, and the duration of each phase. Time-frequency analysis is used to characterize different types of self-noise, specifically ambient noise, rudder noise, and pump motor noise. These characteristics are measured during an ordinary dive [Cauchy et al., 2023; Haxel et al., 2019; Jiang et al., 2019]. I followed the same procedures to determine the self-noise of the Slocum glider.

The glider continuously records acoustic data during its flight, from the surface to the deepest point. By superimposing the flight data with the corresponding acoustic files, I can derive time-series signal windows that effectively represent the occurrence of each noise source, such as buoyancy pumps, rudders, and the pitch motor. Using the same time windows, the acoustic file segments were analyzed to estimate the acoustic signature for every state of the different motors in the glider. An analysis was performed on the port and starboard hydrophones to take into account the directional characteristics of the self-noise. A comparative analysis, in narrowband and one-third octave bands, was conducted between the resultant noise levels and the ambient noise of the ocean. Spectral analysis techniques are used to identify the characteristic frequencies and intensity of noise each moving component produces.

In shallow water trials, the ocean was subject to contamination from diverse sources of acoustic interference. Thus, the sixth dive was selected for the purpose of analyzing the acoustic signature of different motors. Figure 3.5b shows that the first dive in the deep water trial had less background noise than the others, making

it the practical choice for investigating the self-noise signature.

3.6 Vessel noise signature

This section outlines the methodology used to analyze the underwater noise signature of the vessels under test. In Sections 3.1 and 3.2, the experimental framework was implemented in two separate locations, where a series of comprehensive sea trials were conducted. Three PAM observation systems were utilized to gather acoustic data, with variations in their deployment across different sites. The methodology for identifying the vessel's noise signature was consistent in all experiments. However, the analysis methods varied based on the observation system and operational conditions under examination, such as CPA and sound propagation loss, as discussed in the following section 3.7. This methodology facilitated a comprehensive evaluation of the ship's acoustic emissions, enabling a comprehensive understanding of its noise characteristics in different environmental and operational conditions.

The fishing vessel noise signature assessment is a combination of sequential processes. The ISO and the ANSI have rules and guidelines for reporting a ship's underwater radiated noise in certain situations, such as the depth of the water, how the measurement equipment is set up, how the ship is being used, and how the data is processed afterwards [ANSI/ASA S12.64-2009/Part 1, 2009; ISO-17208/1, 2016; ISO-17208/2, 2019]. ANSI presents three measurement grades, which control the uncertainties and variability of the measurement. This study followed Grade B to measure and assess the fishing boat URN, which is similar to ISO-17208/1. The limitation of the water depth led to the use of Grade B, whereas Grade A needs at least 300 m of water depth.

3.6.1 Closest point of approach

If you do a normal vessel transect, as discussed in Section 3.1, the fishing vessel noise levels would be highest where the observed hydrophone was the CPA. That assumption may not work with large vessels, where the highest noise can be captured after the vessel passes the CPA.

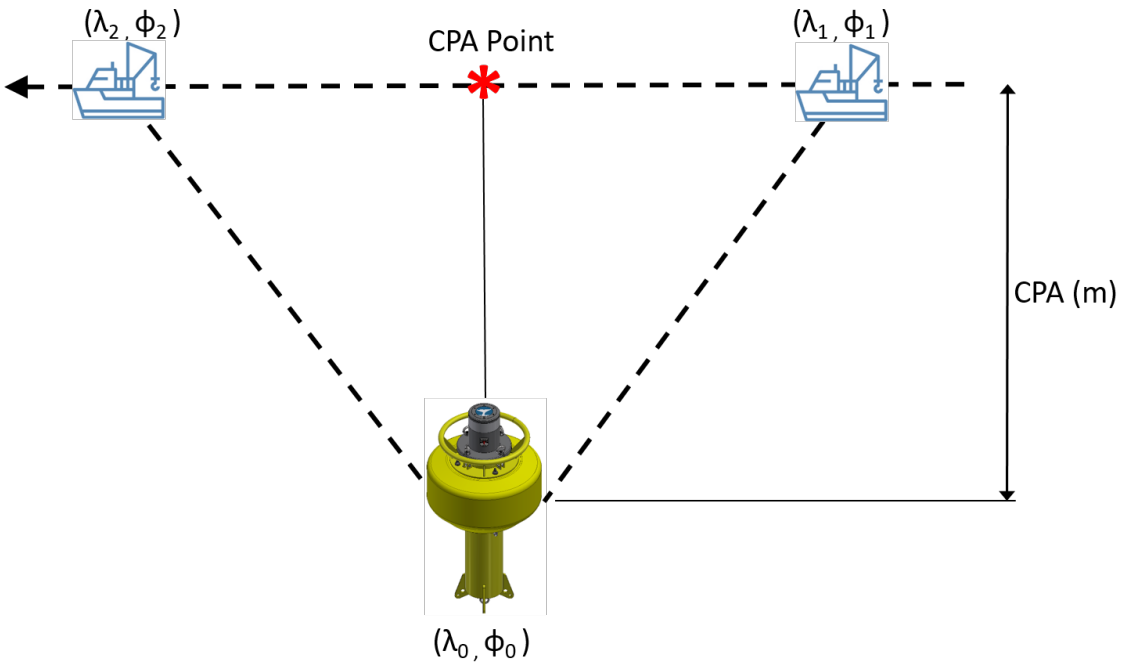

Figure 3.8: CPA measurement layout

The CPA, in metres, between the vessel and the hydrophone array was calculated directly based on the actual latitudes (λ) and longitudes (ϕ) recorded from an attached GPS device in the vessel and the PAM observer for each trial using Equation (3.2) [Jiang et al., 2020]. Then, the actual slant range (D_{Sl_n}) between the fishing boat and each hydrophone was computed by considering the CPA and the depth of each hydrophone, using Pythagoras' theorem. Figure 3.6 shows the CPA and each hydrophone depth with the slant range in the hypotenuse of the right-angle triangle. This method is followed for all PAM platforms' hydrophones, utilizing the actual distances.

$$CPA = \frac{1852 \times 60 \times \cos(\phi_0) \mid (\lambda_2 - \lambda_1)(\phi_1 - \phi_0) - (\lambda_1 - \lambda_0)(\phi_1 - \phi_2) \mid}{\sqrt{(\lambda_2 - \lambda_1)^2 \cos^2(\phi_0) + (\phi_1 - \phi_2)^2}} \quad (3.2)$$

where λ_0 and ϕ_0 are the latitudes and longitudes of the surface buoy, and λ_1, ϕ_1 and λ_2, ϕ_2 are the latitudes and longitudes of two points on the vessel's trajectory as shown in Figure 3.8. During the tests, the vessel maintained a constant velocity; thus, the two points were equidistant from the CPA point for the same time period.

The glider's GPS coordinates were determined using the glider's flight computer. This system compensates for glider drift by providing GPS coordinates projected onto the water surface during its motion. Thus, CPA was calculated using the corrected GPS from the glider and the vessel. Then, the slant range between the glider and the vessel was calculated by integrating depth readings obtained from the altimeter.

3.6.2 Background noise assessment

During the sea trials, background noise sources were carefully considered to ensure precise measurements of the vessel under testing. The selected sites were more than 10 km away from the nearest primary route for commercial ships, providing an environment with minimal direct sound source contamination. No offshore operations were observed during the missions. Therefore, the anticipated ocean ambient noise levels were mainly impacted by the vessel being tested, environmental noise, and marine fauna.

Our approach consisted of assessing the background noise levels (BNL) of all the PAM observers used during any sea trial simultaneously at the beginning of the experiment. Afterwards, the sound received by a particular platform is adjusted using the BNL measured by the same platform.

For each sea trial, I systematically recorded background noise levels over a total interval of four minutes, capturing two minutes before and after the planned experiments. The BNL measurements were made when the vessel under testing was at a distance of approximately 2 km from the acoustic observer and its diesel engine was turned off [ISO-17208/1, 2016]. All other sound sources, except the vessel that was under testing, were considered background noise sources. This ensured an accurate representation of the ocean ambient noise for each sea trial through background noise recordings, which allowed for a reliable assessment of the vessel noise signature from different PAM observers, as in our case.

The received sound level (RL) captured by each hydrophone is recorded for a duration of t_{DW}, which is a function of the vessel speed and CPA, and calculated using Equation (3.3) [ANSI/ASA S12.64-2009/Part 1, 2009; ISO-17208/1, 2016]:

$$t_{DW} = \frac{2 \times CPA \tan(30)}{v} \tag{3.3}$$

where v is the advance speed of the vessel for a particular trial. Table 3.8 shows the vessel speeds recorded using the GPS attached to the vessel. The variation is calculated based on the differences in speeds when the engine speed remains constant. Figures 3.5 and 3.7 illustrate the RL by each hydrophone, and the CPA location can be recognized.

Table 3.8: The vessel advanced speed during the Petty Harbour-Maddox Cove sea trials

Trials	#	**Nominal engine speed** [RPM]	**Advanced speed at CPA** [konts]	**Averaged speed** [konts]	**Speed variation** [konts]
August	1	2200	9.40	9.25	±0.77
December	1	1400	6.00	6.30	±0.35
	2	1800	7.80	7.60	±0.48
	3	2200	9.30	9.10	±0.68

A comparison between the RL and BNL in One-Third Octave Band (OTOB) is made for each hydrophone individually according to its depth to determine the validity of the recordings [Merchant et al., 2014a; Brooker and Humphrey, 2016] as shown below:

- No background correction is needed if the difference between the RL and BNL is greater than 10 dB.
- If the difference ranges between 3 and 10 dB, the BNL must be subtracted from the RL.
- If the difference is less than 3 dB, the recorded data will be discarded in that frequency band.

If the correction is needed, Equation (3.4) (L_n)is used to subtract the background noise levels at specific frequency bands (f_i).

$$RL_c = 10 \times \log_{10}(10^{\frac{RL(f)}{10}} - 10^{\frac{BNL_n(f)}{10}}) \quad [\text{dB } re\ 1\mu Pa] \tag{3.4}$$

In the ocean glider trials, as detailed in Section 3.5, there was a potential for ambient noise contamination by the glider's internal mechanisms. An acoustic window

was carefully selected for BNL analysis to prevent interference from the glider's motors or the vessel under testing. The Conception Bay trials identified the glider's final ascent in shallow waters and initial descent in deeper waters as optimal segments for evaluating ocean background noise without interference from glider self-noise. The glider's BNL data was averaged across these segments, beginning with the initial dive post-oil pump deactivation and concluding prior to the pump reactivation for ascent. During these recording intervals, the research vessel stopped engine operation and kept a distance of around 2 km from the glider to further decrease noise interference.

3.6.3 Underwater radiated noise

The URN parameter plays a crucial role in achieving the paper's first objective because it is widely acknowledged and utilized by classification societies and scientific committees. The calculation of URN is facilitated by applying the geometric spreading law, which is primarily dependent on the spatial separation between the vessel and the hydrophone, thus simplifying the acoustic propagation model [ISO-17208/1, 2016; ANSI/ASA S12.64-2009/Part 1, 2009]. The calculation process begins with the processing of the received sound levels by each hydrophone with the background noise.

To derive the corrected received noise level (RL_c), I first applied a BNL correction. To find the vessel dipole source level, or URN, at a distance of 1 m from the source, the geometrical spreading of sound loss was used to make a normalized distance correction. For each vessel operation, this correction was applied using the CPA measured during that particular run, ensuring consistent URN measurements. Consequently, the geometrical spreading loss correction was applied for every measurement taken on each PAM platform, referencing the actual latitudes and longitudes recorded from the vessel and the respective platform [Jiang et al., 2020]. This process is detailed in Equation (3.5). To comprehensively evaluate the URN, it was averaged across all frequency bands for the n number of hydrophones, as outlined in Equation (3.6).

$$URN(n) = RL_c \; + \; 20 \times \log_{10}(D_{Sl_n}) \quad \text{dB re } 1\mu\text{Pa at 1m} \tag{3.5}$$

$$URN_{TOT} = 10 \times \log_{10}\left(10^{\frac{URN_1(f_i)}{10}} + 10^{\frac{URN_2(f_i)}{10}} + 10^{\frac{URN_3(f_i)}{10}}\right) \quad \text{dB re } 1\mu\text{Pa at 1m} \tag{3.6}$$

If a frequency band is disregarded after BNL comparison, the URN can be computed from one or both of the remaining hydrophones; if not, the band level will be NaN. This method ensures that the mean URN values are obtained from a comprehensive dataset, considering any discrepancies in data availability between the hydrophones.

Following the procedures outlined in Section 3.2, the vessel under testing conducted each experiment at a specific speed for two to four runs. In order to gain a precise understanding of the URN emitted by the vessel, a calculation was made to determine the average URN for each speed. This was achieved by taking the arithmetic mean of the URN values obtained from each individual run and subsequently dividing this sum by the total number of runs conducted at that particular speed. The averaging approach in this study complies with the guidelines outlined in the corresponding ISO standard [ISO-17208/1, 2016].

3.7 Sound propagation loss models

The empirical PL values, which describe how the sound intensity attenuates due to traveling through the water, are not available in this study to precisely characterize the vessel noise signature. Therefore, the article also aims to show the help of using range-dependent oceanography data (temperature, salinity, and density) of the ocean in characterizing the propagation loss of sound compared to use of range-independent parameters. How can the changes in SSP get different PL values, particularly in shallow water? It is well known that there is no standardized method of determining the propagation loss that accounts for the environment uncertainty. Because of that, we used several existing models from previous studies for our comparison.

Propagation loss is commonly estimated using simple spreading laws, see Equation (3.7), as utilized in the previous section, to correct the measured received sound level of a sound source due to the sound intensity attenuation with distance. R represents the distance to the noise source in metres, while N is a scaling factor. N

ranges from 10 to 20, depending on the distance between the sound source and the observer. This approach is limited in constructing accurate predictions in complex environments. It is most effective in scenarios where the environment's properties are range-independent. Spreading law models may result in significant errors when applied to complex coastal and inland water environments [Jensen et al., 2011]. Therefore, the study focused on frequency-dependent numerical PL models that can include marine environmental parameters.

$$PL = N \log_{10}(R) \quad \text{dB re } 1\mu\text{Pa} \tag{3.7}$$

The goal of numerical PL models is to accurately show the complex ocean environment. These models depend on many factors, including the average sound speed in the ocean, the depth of the sound source, and the characteristics of sediment absorption on the seafloor [Ballard and Lee, 2017; Yang et al., 2018]. However, integrating sound speed profiles (SSPs) throughout the water column, in addition to the seafloor topology profile, can improve the effectiveness of PL models in predicting sound attenuation. Wavenumber integration (WNI) and the parabolic equation approach (PE) are two numerical methods that use SSPs to accurately model how sound travels through the ocean layers horizontally and vertically [MacGillivray et al., 2023; Jensen et al., 2011]. Some limitations were reported for wavenumber integration, which is typically frequency-dependent, which means they may not accurately represent the behavior of sound at different frequencies and may not be suitable for more complex environments, such as those with strong bottom interaction or in-homogeneous media [Liu et al., 2021]. The parabolic equation approach is based on the assumption of a slowly varying sound field in the horizontal direction. This assumption may not hold in some situations, leading to inaccurate results [Oliveira et al., 2021]. However, these techniques can represent the sound propagation behavior in the complex ocean environment compared to the explicit equations.

Alternatively, previous research has presented modified simple techniques applicable to shallow and deep waters. These methods do not require extensive numerical computation. Among these techniques are the ISO-17208/2 standard [ISO-17208/2, 2019], the Meyer and Audoly (M-A) method [Meyer and Audoly, 2020], the Seabed Critical Angle (SCA) method [MacGillivray et al., 2023], and the ECHO Certification Alignment (ECA) method [Ainslie et al., 2022], which are simplified equations that

can estimate the PL better than a simple spreading law. The ECA and ISO-17208/2 methods primarily focus on surface reflection, whereas the SCA and M-A approaches take into account both surface and seafloor reflections. They are sensitive to the accuracy of seabed properties. These models require less computation effort compared to the numerical PL models.

3.7.1 Petty Harbour-Maddox Cove

An SBE 25plus Sealogger CTD profiler was used in these sea trials (August and December trials) to collect oceanographic data, specifically temperature, salinity, and pressure. The profiling began on the ocean surface and extended to the seabed, which represents range-independent oceanography data. Data processing took place after the completion of all planned experimental trials. The CTD profiler collected data with a resolution of 50 samples per meter, allowing for precise vertical profiles of the water column. The Gibbs-SeaWater (GSW) Oceanographic Toolbox, a well-known tool in marine science for precise thermodynamic calculations, obtained the SSP, which is necessary for accurate estimates of underwater source levels [MacGillivray et al., 2023]. Figure 3.9 displays the changes in temperature, salinity, density, and sound speed observed during the two trials. These changes provide important information about the current oceanographic conditions at those times.

ISO 17208-2

After collecting SSP in the area of experiments, two methodologies were used for estimating the MSL, which differed from each other for the implemented PL models. First, I used the formulation presented in [ISO-17208/2, 2019], which considers the impact of reflections from the sea surface. The model estimates a propagation loss correction factor (PL_{ISO}) using Equation (3.8). The calculation is based on the source's depth and the depression angle between the noise source and the hydrophone's depth. It is evident that the sound speed does not contribute to the PL correction.

The PL_{ISO} is calculated thusly:

$$PL_{ISO} = 10 \times \log_{10}\left(\frac{1}{2} + \frac{1}{4K^2 d_s^2 \sin\alpha^2}\right) \tag{3.8}$$

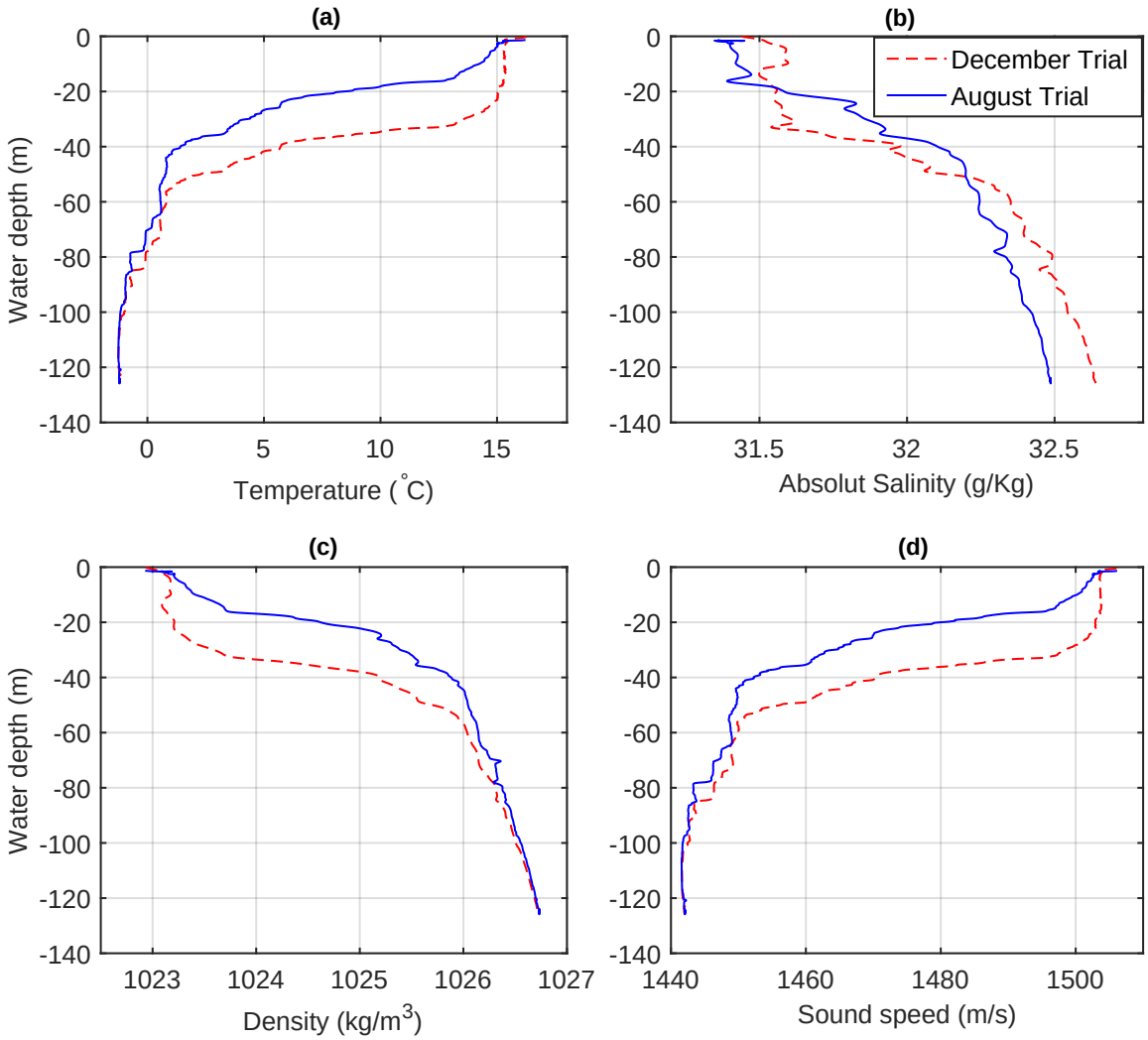

Figure 3.9: Temperature, salinity, density profiles and the calculated sound speed profile in August and December trials in Petty Harbour-Maddox Cove

where K is the wavenumber, d_s is the source depth, and α is the angle between the horizontal surface and each hydrophone.

This approach does not account for diverse environmental parameters, such as the sound velocity profile and seabed interaction, which may affect the PL [MacGillivray et al., 2023]. In addition, PL_{ISO} calculated as per Equation (3.8) is valid for deep water, defined in the Standard as 150 m in depth or more.

Numerical propagation loss model

Currently, no benchmarked PL model can sufficiently address the diversity of the ocean environment in modeling sound propagation. This section investigates models that aim to solve the wave equation numerically, specifically those that view the ocean as a deterministic environment where the speed of sound varies based on spatial coordinates. In addition, the models account for the impact of the ocean bottom by assigning a reflection loss based on the grazing angle. There are two main categories of models: range-independent and range-dependent [DiNapoli and Deavenport, 1980; Oliveira et al., 2021].

As specified in the studies [Peng et al., 2018; MacGillivray et al., 2019; Chion et al., 2019; MacGillivray et al., 2023], and in the technical guidelines [Lloyd's Register Group Limited, 2018; Bureau Veritas, 2014], a frequency-dependent PL model that accounts for the ocean's environmental parameters should be implemented to decrease the uncertainty in the MSL estimation when oceanographic data within the area of trials are available. Considering that the water depth during the sea trials ranged between 120 m and 140 m, the collected CTD data along with data of the seabed characteristics (Table 3.9) retrieved from relevant literature [Shaw and Potter, 2015; Ballard and Lee, 2017; Eamer et al., 2020; Dall'Osto and Tang, 2022] were utilized to implement three propagation loss models. Each model is based on a different technique to solve the acoustic wave equation: i) Parabolic Equation (PE), ii) WaveNumber Integration (WNI), and iii) Finite Element Method (FEM).

The PE method simulates propagation loss by solving a reduced Helmholtz equation for ocean sound propagation, which was developed to solve range-dependent problems. The method is particularly suited for frequencies below 1 kHz [Bureau Veritas, 2014; MacGillivray et al., 2019]. It handles complex refraction and diffraction phenomena where the wavelength is comparable to or larger than ocean features [DiNapoli and Deavenport, 1980]. The PE method disregards the effects of backscattered sound, which is considered insignificant by the majority of ocean-acoustic propagation models [Lin, 2019]. At low frequencies, sound waves propagate over longer distances with significant bending due to the speed of sound variations in the water, which the PE method can accurately simulate. However, the PE method's assumptions and approximations become inaccurate at higher frequencies, making it less effective than approaches that handle shorter wavelengths with the environment,

such as the ray tracing method [Collins, 1993].

The WNI techniques have been widely used to simulate sound propagation in stratified media and have been proven effective in simulating sound wave propagation in shallow waters [Erbe et al., 2022]. This approach enables precise modeling of complex environments, capturing the interactions between sound waves and the layered structure of the ocean [Jensen et al., 2011] at frequencies lower than 4 kHz [MacGillivray et al., 2019, 2023]. However, the study [MacGillivray et al., 2023] discussed the lack of the WNI method in estimating consistent source levels below 1 kHz at different CPAs.

Finally, an FE model of a section of the water column was used to estimate the sound PL. The FE method is not widely used in ocean acoustics since the large propagation domain normally investigated results in computationally intensive simulations. On the other hand, when the simulations are focused on short-range low-frequency problems, the FE method has been proven efficient [Jensen et al., 2011]. Given the relatively shallow water problem, the area surrounding the buoy and the ship at the CPA was modeled using unstructured quadrilateral elements of 0.25 m to simulate sound waves up to 2 kHz. The boundary conditions of the model are as follows: the water-air interface is considered a soft boundary with pressure equal to zero (pressure release) to account for the mismatched impedance between the air and water [Gong et al., 2023]. The seabed was modeled as an impedance boundary using density and compressional sound speed in Table 3.9. The two sides of the model were simulated free-field conditions using a perfectly matched layer, which truncates the computational domain of the open region.

Given the wide frequency range investigated in this study, I performed simulations using the discussed methods and a combination of the resulting PL models over the frequency range of interest, similar to an investigation by [MacGillivray et al., 2019, 2023]. This is discussed in the results section of this thesis.

3.7.2 Conception Bay

The glider covered distances of 550 metres at the shallow water site and 1,500 metres at the deep water site. The glider collected conductivity, temperature, and pressure data using an onboard CTD payload. The data was sampled at a rate of 0.5 Hz to

Table 3.9: Environmental parameters used for PL numerical models for Petty Harbour-Maddox Cove sea trials

Parameter	**Value**
Source depth [m]	1.2
Water column depth [m]	160
Model range [m]	500
Sediment density [kg/m^3]	2100
Compressional sound speed [m/s]	1950
Compressional wave absorption [dB/λ]	0.4

calculate the SSP. Figure 3.10 illustrates the SSP for each half-yo motion by the glider and the average value.

The PL of sound was investigated at the two sites. In total, six PL models were created using the ISO, PE, WNI, ECHO, SCA, and M-A methods for both shallow and deep water. A comprehensive comparison and analysis of the discrepancies between the models' outcomes was conducted. The models addressed 100 m and 500 m ranges, including multiple receiver points at various depths: 20, 30, 40, 50, 60, and 70 metres for the shallow-water site, and 30, 60, 90, 120, and 150 metres for the deep-water site. The sound source was consistently positioned at a depth of 2 metres and applied to all the models. This approach allows for a detailed study of propagation loss variations in different water depths with dramatic SSP changes, which is important for precise acoustic modeling and analysis.

In terms of the PE and WNI models, the AcTup toolbox [Duncan and Maggi, 2005] was used to implement both models for a frequency range of 10 Hz to 160 Hz and 200 Hz to 4 kHz. The numerical solution had a boundary condition starting at 1 wavelength to avoid a singularity at the source location. The depth resolution was a function of the frequency and is equal to $0.25 \times wavelength$. The horizontal range resolution was $1m$ step. The vessel draft (source depth), SSP, seafloor bathymetry, and acoustic characteristics of the seafloor sediment were used as inputs to the models. The source depth and the seabed acoustic characteristics are kept the same, while the SSP and seabed bathymetry change by changing the location where the PL was calculated (range-dependent).

Sound waves in shallow water environments often interact with the seafloor because

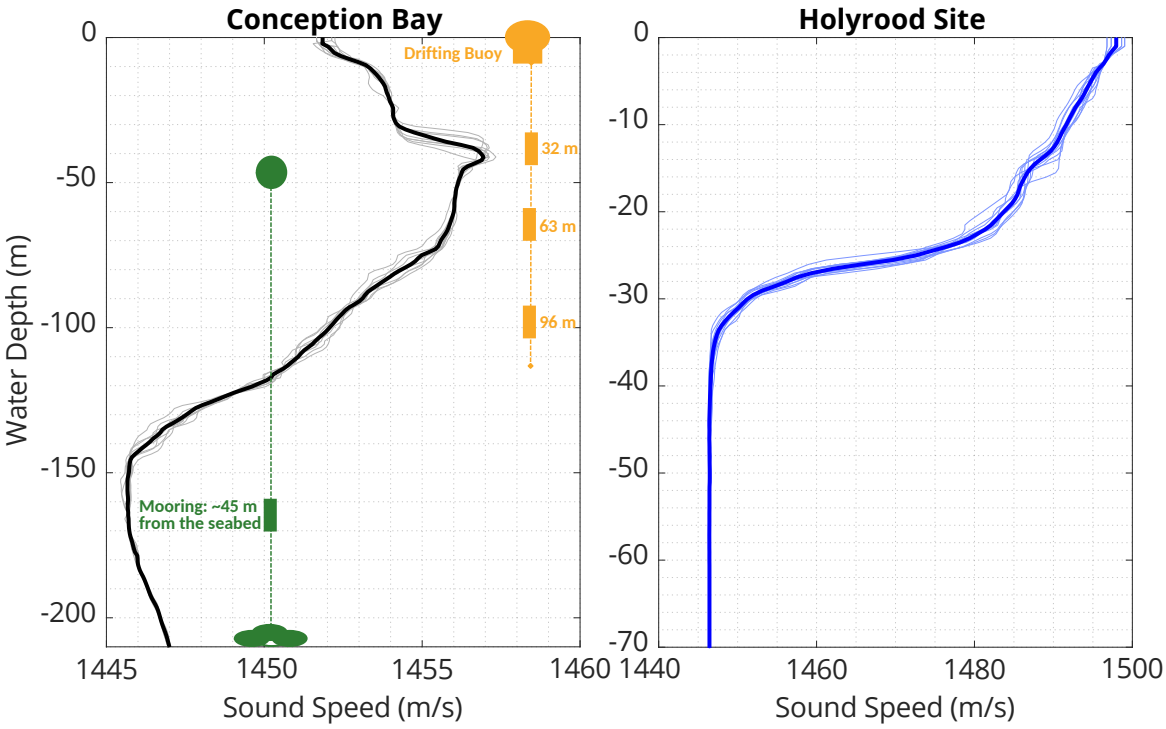

Figure 3.10: Sound speed profiles were calculated from the glider temperature and salinity data. The black line refers to the average sound speed profile at the Brigus site; on the other hand, the blue color is for the Holyrood site. The faded lines are the glider's profiles collected during each single dive.

of the limited depth [MacGillivray et al., 2023]. This interaction results in reflection, refraction, and absorption of the sound waves that are impacted by the composition of the sediment. For example, sandy sediments generally have higher sound speeds than muddy sediments. The speed of sound in sediments varies with frequency, impacting the strength of reflected waves. Furthermore, sediment density is an important factor in determining acoustic impedance and attenuation coefficients Dall'Osto and Tang [2022]. The limitation in the PL calculation was the ability to determine the sediment layer thickness or how many layers were under the seafloor. We treated the seafloor as a halfspace, which is characterized by constant acoustic properties and that might have a negative impact on lower frequencies below 20 Hz in 60 m water depth. In deep water, the interaction of the seabed is less important; however, the sediment acoustic characteristics are used to keep only the SSP as the only changing parameter. As stated in the introduction, the SSP presented in this study is both a range-dependent profile (from the glider) and a range-independent profile. This method helped us

understand how the glider contributes to the performance of the PL models.

Given the challenges in accurately estimating seabed acoustic properties at the selected site from the acoustic data, SSP, and bathymetry profile, I relied on verified data from the scientific community to ensure robust results in the numerical propagation loss models. Table 3.10 displays the acoustic properties of the sediment found on the seabed, containing a central layer of mud and a dispersion of sand and gravel [Shaw and Potter, 2015; Ballard and Lee, 2017; Dall'Osto and Tang, 2022].

Table 3.10: Conception Bay seafloor acoustic characteristics for shallow and deep water

Parameter	**Shallow water**	**Deep water**
Source depth $[m]$	-	2
Water column depth $[m]$	60	205
Model range $[m]$	550	1500
Sediment density $[kg/m^3]$	1600	1600
Compressional sound speed $[m/s]$	1650	1500
Compressional wave absorption $[dB/\lambda]$	0.002	0.0006

3.8 Monopole source levels

This section discusses the methodology used to calculate the MSL of the vessel being tested. The MSL plays an important role in analyzing the vessel's underwater noise signature. This method assumes the vessel is a point source of sound placed in a hypothetical infinite lossless medium, leading us to measure its source level at a standardized distance of 1 m [Chion et al., 2019]. They are also used to quantify the noise generated by ships, particularly in the low-frequency band, and are crucial for evaluating the impact of vessel noise on marine ecosystems [Chion et al., 2019; ZoBell et al., 2023].

The recognition of MSL is crucial for developing procedures to minimize the effects of vessel noise on marine life and for designing ships with reduced noise emissions. A study was conducted to investigate the impact of retrofitting on the radiated noise and MSL of container ships. The results revealed an interesting reduction in MSL in the low-frequency range after retrofitting, suggesting that modifications in vessel design

have the potential to decrease noise levels [ZoBell et al., 2023]. In addition, MSL encompasses the consideration of environmental factors that impact sound propagation in the ocean. The calculated MSL not only offers clarification into the vessel's acoustic impact but also enables a comparative analysis of the variations between the different propagation loss models used. The performance of the glider can be investigated to characterize the vessel noise and its impact on the ambient noise of the ocean.

As discussed in Section 3.7, various propagation loss models have been applied to the dipole source level/URN obtained from Section 3.6.3 to be converted to the MSL of the vessel under testing.

3.8.1 Engine contribution to the vessel noise signature

MSL data acquired from December trials 1 and 4 were used to evaluate the engine's contribution to the overall URN by comparing the spectra obtained when the vessel is stationary at the CPA with engine speed 1400 rpm (propeller unclutched) with the data acquired while the vessel is advancing with engine speed 1400 rpm and propeller clutched.

The overall vessel noise was split into two sources: the engine and the propeller. The energy spectrum for each frequency band is computed under both clutched and unclutched conditions. The clutched propeller scenario was used as a reference, where the noise was higher compared to the unclutched scenario. The energy spectrum is simply the area under each OTOB band, which is calculated as the product of the squaring amplitude and the width of the band [Rao, 2016]. Then, the difference in noise level for each band was used to represent the percentage of the propeller contribution. Accordingly, two noise level values were obtained for the engine and propeller, expressed as percentages of the overall URN. This comparison allowed for a clear understanding of the impact of the propeller on the overall underwater radiated noise. The data obtained provides valuable insights into the noise distribution between the engine and propeller under different operating conditions.

3.9 Structure-borne noise

During the December trials in Petty Harbour-Maddox Cove, structure-borne noise measurements were taken onboard to investigate the structure vibration velocity level corresponding to the underwater radiated noise. The impact of the engine and the propeller on the structure-borne noise of the fishing vessel was analyzed and compared simultaneously with the off-board URN measurement. For safety reasons, the vessel operator refrained from repeating these experiments in the Conception Bay trials. Onboard accelerometer sensors were installed on the engine foundation to capture the engine velocity vibration, as shown in Figure 3.11. A Data Acquisition Hardware multi-channel NI CDAQ chassis with NI-9234 modules was utilized, setting the sampling rate at 8 kHz (Nyquist frequency: 4 kHz).

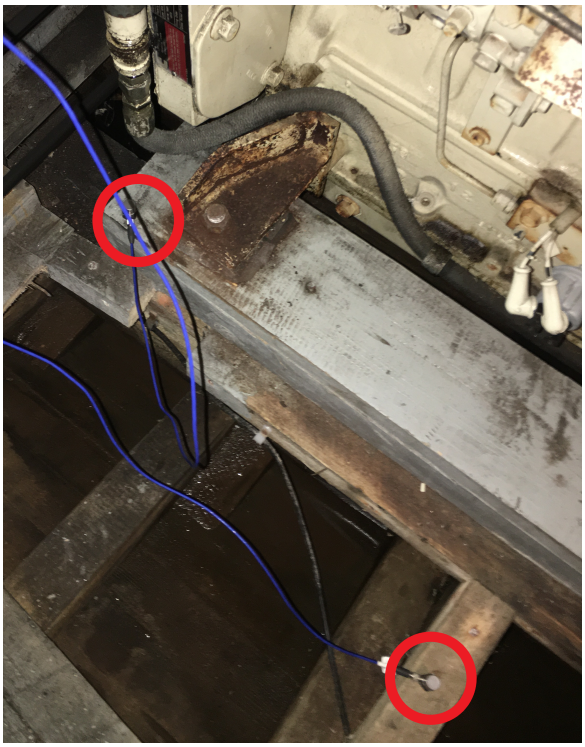

Figure 3.11: Accelerometers location inside the engine room during Petty Harbour-Maddox Cove trials

Acceleration data was recorded for a duration of 300 seconds for each engine speed, for both clutched and unclutched propeller conditions, while the engine speed was 1400 rpm, as discussed in Section 3.1.1. In each scenario, two 60-s window data intervals were selected and averaged to represent the engine vibration. At the same time, URN

measurements were taken off-board, as described in Section 3.6.

The acceleration was converted to velocity in the frequency domain. These measurements were used for a comprehensive comparison between the structure's velocity level and underwater radiated noise levels in narrowband and OTOB. The fundamental frequencies that are present in structure-borne noise were identified. Based on the operational characteristics of the engine and propeller, I proceeded to establish a correlation between these frequencies. The results section also discusses a correlation between underwater noise levels and vibration levels using the average quadratic velocity method (AQV) [Cintosun and Gilroy, 2021].

3.10 Measurement uncertainties

The measurement uncertainties were analyzed to complete the analysis of the effectiveness of ocean gliders in assessing ships' URN. The uncertainty analysis was conducted for Conception Bay trials only, where three PAM platforms—i.e. ocean glider, hydrophone array, and seabed-moored hydrophone—were used at the same time to measure the ship noise, as discussed in Section 3.3.2. Following the steps outlined in Section 3.6, the noise signature of the ship (see Figure 3.2) was determined from the three platforms. Next, the measurement uncertainties were calculated separately for each platform. The lower the uncertainty, the more reliable the measurement results will be.

Based on the literature discussed in Section 2.4.2, the sources of uncertainty were identified and assessed for each platform. This process included computing the standard uncertainty of the mean of the vessel's URN measurements for each platform [AQUO, 2014; Keizer et al., 2022]. The standard uncertainty of the mean is a statistical measure that quantifies the expected variance of measured underwater radiated noise levels [Korean register, 2021; Farrance and Frenkel, 2012]. Therefore, this study introduced an approach for quantifying uncertainties in glider-based assessments of underwater source noise, filling a gap in the existing literature. The outlined approach enables a comparative analysis of uncertainties in the glider system and traditional fixed PAM platforms.

3.10.1 Standard uncertainty

The focus in this part of the study is specifically on measurement uncertainty, which differs from measurement error. Measurement error refers to the difference between measured and true values, which have been adjusted based on the calibration certificates of each instrument used in the measurement process. Measurement uncertainty refers to the built-in doubt surrounding measurement errors, which are unknown and should be minimized in order to improve the measurement quality. This uncertainty is converted to statistical quantities called standard uncertainty, expressed as an interval, and defined by a confidence level following the systematic approach discussed below.

First, the sources of measurement uncertainty need to be identified, which will be shown in the next section. Next, the uncertainty value induced by each parameter involved in calculating the vessel's URN is estimated. This estimation is performed using two different methods: one for estimating Type A (random error) uncertainties and the other for Type B (systemic error) uncertainties [Taylor, Barray N. and Kuyatt, Chris E., 1994; ISO/IEC Guide 98-3, 2008].

The evaluation of Type A standard uncertainty (u_A) relies on statistical techniques, typically derived from repeated measurements, to show the random effect. It includes the mean and the estimated standard deviation (std) under the assumption of normally distributed data. The calculation is conducted for repeated measurements at individual engine speeds and can be calculated using Equation (3.9) [Taylor, Barray N. and Kuyatt, Chris E., 1994; ISO/IEC Guide 98-3, 2008].

$$u_A = \frac{std}{\sqrt{n}} \tag{3.9}$$

where n is the number of measurement sets.

Type B evaluations include multiple sources of information, including past experiences, calibration certificates, manufacturers' specifications, calculations, published data, and common sense. Type B uncertainty (u_B) assumes a rectangular or uniform probability distribution of every estimated measurement outcome. In this case, you may only be able to estimate the upper and lower limits of the uncertainty. Under

such circumstances, it is typically assumed that the value is equally likely to fall anywhere within this range. Equation (3.10) shows the calculation of Type B uncertainty, where a is the half-width between the upper and lower limits [Taylor, Barray N. and Kuyatt, Chris E., 1994; ISO/IEC Guide 98-3, 2008].

$$u_B = \frac{a}{\sqrt{3}} \tag{3.10}$$

The law of the propagation of uncertainty combines the standard uncertainties from Type A and B evaluations with negligible covariance between the standard uncertainty components. The root-sum of squares (RSS) is used, which requires squaring individual standard uncertainties, summing the squared values, and subsequently taking the square root of the sum to determine the combined standard uncertainty (u_C). The RSS consistently provides lower total uncertainty compared to a simple summation. Consider a scenario where one measurement component has a low uncertainty range while another has a high range. These inaccuracies would cancel out each other when combined. Finally, to determine the total uncertainty (U) at a 95% confidence level, the coverage factor (k) is employed. Generally, a value of k is selected for a 95% confidence level, usually using the standard normal distribution. It is expected to use $k = 2$ [Taylor, Barray N. and Kuyatt, Chris E., 1994; ISO/IEC Guide 98-3, 2008].

$$U = ku_c = k\sqrt{\sum u_A^2 + \sum u_B^2} \tag{3.11}$$

3.10.2 Parameters to calculate uncertainties

This study focused on the main sources of error that significantly impact the assessment of vessel noise signatures. They are the distances between the vessel and the observer, hydrophone depth changes due to array line inclination, background noise variation, vessel noise directivity, frequency response, and source depth (vessel draft).

Distance to the CPA

The distance measurement uncertainty is the key parameter in the overall quantification of the uncertainty. It was divided into two items, one associated with the accuracy of the GPS used and the other associated with the uncertainty caused by the

hydrophone line inclination with the fixed PAM platforms. The number of satellites in the measurement area primarily determined the accuracy of the GPS device [Oxley, 2017]. All experiments connected an average of 8 to 12 satellites to the GPS. That leads to accuracy within a 4.9-meter radius under the open sky with a 95% confidence level [van Diggelen and Enge, 2015]. As a result, the GPS uncertainty is classified as Type B uncertainty, which is a systematic error and is normally distributed. The 4.9 m radius was converted to standard uncertainty at the coverage factor ($k = 1$) by dividing by 2 to represent the half-width between the upper limit (4.9 m) and lower limit (0 m) for a normal distribution of 66% confidence level. The average CPA in Conception Bay trials was 180 m; therefore, the GPS standard uncertainty (u_{GPS}) is calculated using Equation (3.12).

$$u_{GPS} = 20\log_{10}(CPA + \frac{4.9}{2}) - 20\log_{10}(CPA) \quad [dB] \tag{3.12}$$

Array line titling

Regarding the hydrophone line angle in the drifting buoy system and seabed-moored hydrophone, the tilt angle (denoted as β) is defined as the angle between the vertical axis and the line created by the cable supporting the hydrophones. The icListen hydrophones, equipped with a magnetometer and accelerometer, provide data on their orientation and heading relative to the positive y-axis. A vertically upward orientation of the hydrophone corresponds to an orientation reading of 0°s. The hydrophones attached to the drifting buoy line are positioned in a downward orientation with a nominal angle of 180°. However, in practice, the measured tilt angles for these hydrophones varied between 167° and 171°.

Conversely, the seabed-moored hydrophone, facing upwards, has a nominal angle of 0°, with actual measurements ranging from 6° to 13°. These variations in tilt angle lead to changes in the slant range (δD) between the hydrophone and the vessel, calculated using Equation (3.13). The standard uncertainty in hydrophone inclination, represented as u_{Tilt}, is treated as a Type B uncertainty with a uniform distribution due to the unknown uncertainty in the magnetometer and accelerometer's readings within the hydrophone.

$$\delta D = \sqrt{(H_{dpt} \sin \beta)^2 + (H_{dpt} - H_{dpt} \cos \beta)^2} \quad [m] \tag{3.13}$$

The hydrophone depth (H_{dpt}) is measured from the water surface for the drifting buoy and from the seabed for the moored platform.

$$u_{Tilt} = 20 \log_{10}(D_{Sl_n} + \frac{\delta D}{\sqrt{3}}) - 20 \log_{10}(D_{Sl_n}) \quad [dB] \tag{3.14}$$

Background noise

The background noise variability during the trials was also included in the uncertainty analysis, which impacts the uncertainty of the vessel noise levels at broadband frequencies. The variation of background noise is estimated as the difference between its level at the beginning and end of the sea trial. The difference between the two measurements is considered the standard deviation in the background noise levels. The standard uncertainty of the background noise is calculated by dividing the variation by 2, assuming a normal distribution.

Vessel directivity

The vessel noise directivity significantly impacts the measurement process of the vessel noise signature. Each transect run assumes that the vessel under testing is a single-point sound source. The sound emissions from the port and starboard sides do not align at the same speed. Therefore, we use the measured URN variation between the port and starboard to illustrate the directivity of the vessel's underwater noise at the same speed and conditions. This variation is called directivity standard uncertainty, and it is frequency-dependent. The undefined process of the vessel manufacturer leads to the classification of the directivity standard uncertainty as Type A uncertainty, which follows a normal distribution to account for the random error resulting from the repeatability of runs at each speed and the number of hydrophones capturing data. The directivity standard uncertainty is calculated from the mean of the available data. The number of available data varies depending on the observed platforms. The drifting buoy has 3 hydrophones. As a result, three times the number of runs are available to be averaged, and there are 12 available data points for each speed. However, the

glider and bottom-mounted systems had fewer hydrophones, resulting in a reduction of the averaged data to 8 and 4 available, respectively.

The analysis of the vessel's directivity includes the uncertainty of the vessel's operational speed, as the vessel did not run at exactly the same speed for each run. The vessel operation speed uncertainty is embedded in the directionality uncertainty values.

Frequency response

The frequency response of the hydrophones has a significant impact on the measured acoustic files, particularly for the high frequencies above 10 kHz [Hayman et al., 2013]. At low frequencies, when the acoustic wavelength is significantly larger than the radius, the frequency response of a hydrophone remains flat, with a slow rise in response as the frequency increases [Cotter et al., 2019]. In Section 3.3.2, the icListen hydrophones used in the drifting buoy and seabed moored system have a frequency response variation between 0.7 and 2.1 dB in the range of 10 Hz to 64 kHz. The HTI-99-HF hydrophone mounted on the glider has 1.1 dB of variability from 1 Hz to 64 kHz. The standard uncertainty is considered Type B and is normally distributed because the information is provided in the calibration certificate of the hydrophones.

Source depth

Finally, the uncertainty of the propagation loss model greatly affects the calculation of the MSL of the vessel. The depth of the source and the variability in the SSP are the two main determinants of the MSL's standard uncertainty. While accurate measurements of the vessel's draft variability were not accessible, it was observed that the wave height on the day of the trial was below 0.3 metres. Therefore, the variation in source depth is assumed to be 0.3 metres. This assumption is considered a Type B standard uncertainty, which follows a uniform distribution, reflecting the lack of direct measurement data and relying on observed environmental conditions to estimate the variation. The sound speed profile was measured using the glider CTD, as discussed in Section 3.7. The difference between estimating the MSL using the average and range-dependent SSP was considered a representation of the uncertainty.

3.11 Conclusion

The methodology used in our study was described in this chapter, with a particular focus on two major open-water sea trials. These experiments collected acoustic data using a glider, a bottom-mounted hydrophone, and an array of three hydrophones. There were two hydrophones mounted on the glider's wings. The main source of noise was a fishing boat, and the underwater noise signature of the vessel was carefully described. I created propagation loss models to estimate source levels using the CTD data collected from the glider. The measurement uncertainty for each PAM observer was estimated, which enabled us to gain a thorough comprehension of the data's reliability and potential variability.

The characterization of vessel noise took place in deep water. The sources of noise in the vessel were evaluated at different operating conditions for clutched and unclutched propeller. This comprehensive analysis allowed us to understand how various operational states of the vessel contribute to its overall acoustic signature, providing valuable insights into the complexity of underwater noise sources.

The glider's self-noise was assessed in shallow and deep dives. The source of the noise has been determined. This evaluation of the glider's acoustic footprint was crucial for distinguishing between ambient noise, vessel noise, and any potential interference from the measurement platform itself. By characterizing the glider's self-noise across different dive profiles, we enhanced our ability to isolate and analyze the target acoustic signals accurately.

In addition, the oceanography data, such as temperature, salinity, and density, was collected from the glider and CTD profiler to be used in developing the PL models. By including environmental variables in our propagation loss models, we were able to get a better sense of how sound waves move through the water column when the SSP changes over range.

Chapter 4

Results & Discussion

This chapter examines experimental data on vessel-generated underwater noise with, a focus on acoustic signatures and the primary sources of noise using an ocean glider. This study's findings contribute to the knowledge of underwater acoustics and have implications for the effectiveness of ocean gliders as platforms for passive acoustic monitoring. The findings could be applied to the observation of ocean ambient noise and the assessment of vessel noise signatures.

The materials in the chapter are based on three published articles:

- *Assessment of the underwater noise levels from a fishing vessel using passive acoustic monitoring and structure hull vibration*, which is published in *Canadian Acoustics*, *Vol.*: 50 (3)[Helal and Moro, 2022].
- *Underwater noise characterization of a typical fishing vessel from Atlantic Canada*, which is published in *Ocean Engineering Journal*, *Vol.*: 299 and *ISSN*: 0029-8018 [Helal et al., 2024b].
- *Advancing Glider-based Measurements of Underwater-Radiated Ship Noise*, which is under review in *The Journal of the Acoustical Society of America*, *Vol.*: 156(4) and *ISSN*: 0001-4966 [Helal et al., 2024c].

4.1 Vessel noise characterization

That section presents the results of Petty Harbour-Maddox Cove sea trials to characterize the underwater noise of a fishing vessel. Only the measurement systems drifting buoy and accelerometers were used, as detailed in Section 3.3.1.

4.1.1 Background noise levels

Before each trial in Petty Harbour-Maddox Cove, assessments of BNL were carried out. Figure 4.1 plots the apparent trends in the frequency and depth-dependent BNL among the three hydrophone receivers using a dotted black line. The deepest hydrophone always had a higher BNL than the mid-depth and shallow hydrophones, especially for frequencies below 250 Hz. There was a noticeable difference of 8 to 10 dB in the BNL measurements before each run. The finding aligns with [Brooker and Humphrey, 2016], where the measured vessel noise was higher at the deepest hydrophone than the shallower ones at low frequencies. Furthermore, in all trials, the deepest hydrophone consistently showed higher background noise levels below 50 Hz. The hydrophone was located near the deep-sound channel and may capture noise from great distances [Merchant et al., 2014a; Erbe et al., 2019]. The deep-sound channel depth is determined from the measured sound speed profile and located at the minimum sound speed value. As shown in Figure 3.9 (d), the deep-sound channel was between 100 m and 110 m deep.

Table 4.1 presents the BNL broadband levels obtained across various frequency ranges. The present study reveals a notable consistency in the BNL across the 10 Hz to 10 kHz frequency range between the August and December trials. The 63 and 125 Hz bands are useful indicators for evaluating potential ship noise contamination far from the experiment site [Merchant et al., 2014a; European Union Commission Decision 2017, 2017; De Clippele and Risch, 2021], and they were also comparable throughout all the experiments. The BNLs at the low-frequency indicators ($\leq$ 1 kHz) were comparable, which led to reliable measurements of the vessel noise characteristics according to the standards. However, the December trial observed more ambient noise between 2 and 8 kHz, potentially due to environmental factors such as wind, wave height, or internal currents. Overall, these fluctuations in the BNL fall within the uncertainty ranges defined in [ISO-17208/1, 2016].

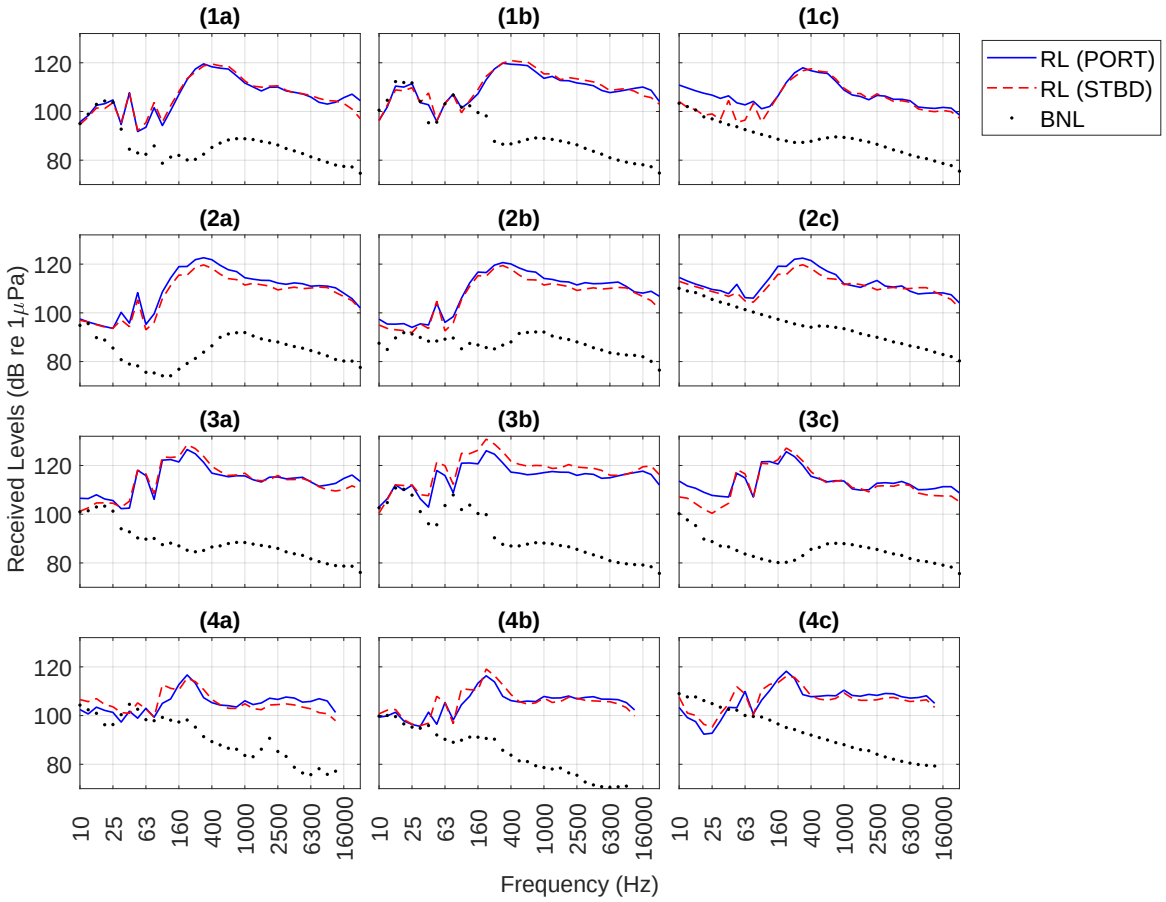

Figure 4.1: The received levels of the port and starboard sides of the fishing vessel were compared to the background noise levels in OTOB. December trials: (1a) shallow-hydrophone at 1400 rpm engine speed, (1b) mid-hydrophone at 1400 rpm engine speed, (1c) deep-hydrophone at 1400 rpm engine speed, (2a) shallow-hydrophone at 1800 rpm engine speed, (2b) mid-hydrophone at 1800 rpm engine speed, (2c) deep-hydrophone at 1800 rpm engine speed, (3a) shallow-hydrophone at 2200 rpm engine speed, (3b) mid-hydrophone at 2200 rpm engine speed, and (3c) deep-hydrophone at 2200 rpm engine speed. August trial: (4a) shallow-hydrophone at 2200 rpm engine speed, (4b) mid-hydrophone at 2200 rpm engine speed, and (4c) deep-hydrophone at 2200 rpm engine speed.

When evaluating underwater radiated noise, the background noise fluctuations at low frequencies (below 2 kHz) remain relatively stable throughout a single day. This stability allows us to take a single measurement at the beginning and end of the measurement process on the same day. Beyond 2 kHz, background noise can fluctuate rapidly due to environmental factors such as wind, current speed, and rain. As a result, it is necessary to conduct repeated measurements for trials that span

multiple days.

Table 4.1: The number of repeated measurements of the background noise levels in broadband representation (dB re 1μPa at 1m). The data were collected on the days of the trials in August and December 2021 at the same location (Petty Harbour-Maddox Cove)

#	**63**	**125**	**250**	**0.5k-1k**	**2k-8k**	**0.01k-10k**	**0.01k-25k**
August							
1	97.77	96.78	93.75	86.33	82.10	98.14	N/A
December							
1	99.00	99.10	86.97	87.51	84.04	98.32	97.80
2	96.84	93.91	91.23	91.84	87.25	97.50	96.98
3	98.77	97.82	86.15	88.40	84.50	99.58	99.05

4.1.2 Received noise levels

Figure 4.1 shows the RL at each hydrophone of the array at the CPA between the vessel and the observed buoy, along with the BNL measured before each trial. RL presents similar patterns for the port or starboard sides. The plots show that RL did not increase during the trials compared to the BNL at frequencies lower than 25 Hz. Additionally, it is evident that the hydrophone with the most extended depth shows higher BNL. This is probably due to the fact that this hydrophone is located in the deep sound channel and may capture sources of noise from a considerable distance (Figure 4.1 1c and 3c).

Figure 4.2 shows the RL_c OTOB spectra calculated as discussed in Section 3.6.2. The discontinuity in RL_c presented in Figure 4.2(d) is because the corresponding RL was less than 3 dB higher than the BNL. The plots show that RL_c generally increases with the vessel's engine speed. Specifically, in the 160, 200, and 250 Hz bands, an 8 dB difference was observed between 1400 and 2200 rpm. The difference between the corrected RL_c values for the same engine speed shown in Figure 4.2(c and d) is because of the variation of CPA between the two trials. Thus, the geometrical spreading was applied for the purpose of reasonable comparison.

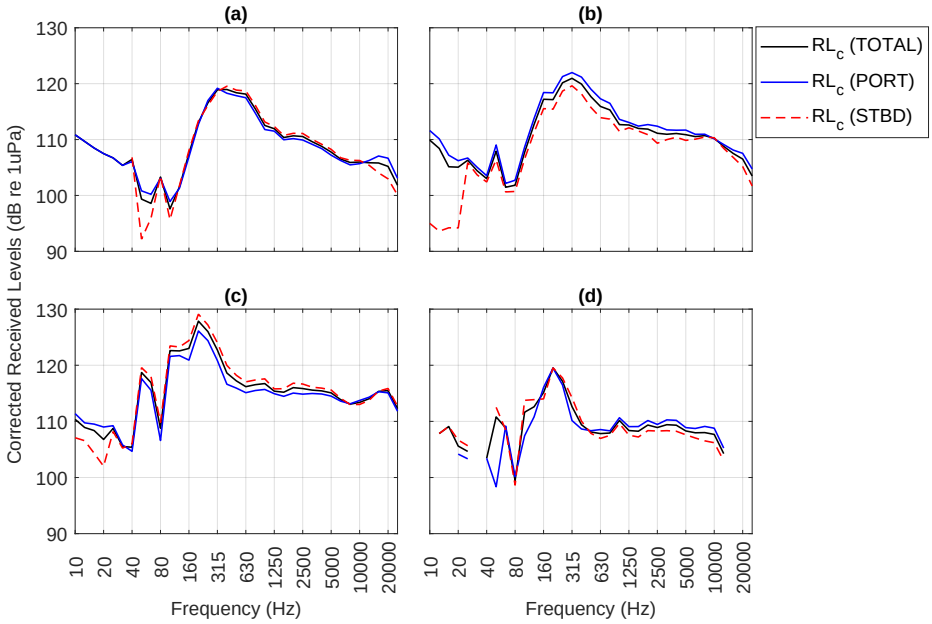

Figure 4.2: Corrected RL_c presented for port and starboard in OTOB (Petty Harbour-Maddox Cove): a) 1400 rpm in December (CPA = 224m), b) 1800 rpm in December (CPA = 137m), c) 2200 rpm in December (CPA = 166m), and d) 2200 rpm in August (CPA = 240m)

The current RL_c data is insufficient for conclusive assessments of underwater radiated noise levels. Until the final step of the analysis, there was no proof that the two sides of the vessel had differing noise levels. Background correction and application of the spherical spreading loss model are essential to modifying the RL_c. Figure 4.2 shows the RL_c following [ISO-17208/1, 2016]. The RL_c values shown in Figure 4.2 are the power-averaged sound pressures from the shallowest, middle-depth, and deepest hydrophones. RL_c bands that were eliminated when the RL_c was less than 3 dB from the BNL are indicated by discontinuities in Figure 4.2(d). The RL_c showed a positive correlation with the vessel's engine speed. Specifically, in the 160, 200, and 250 Hz bands, an 8 dB difference was observed between 1400 and 2200 rpm. Next, the normalized distance between the vessel and buoy at CPA was utilized to estimate the underwater radiated noise of the fishing vessel.

4.1.3 Underwater radiated noise

Maintaining a consistent CPA distance, as prescribed in [ISO-17208/1, 2016], was challenging due to the buoy's drift and the need for manual navigation of the vessel, and some variability in the CPA distance was expected due to the operating conditions [McKenna et al., 2012; MacGillivray et al., 2019]. The measured CPA was 185 metres, with a deviation of less than 30 metres across all runs.

Figure 4.3 shows that the URN levels displayed consistent patterns at various engine speeds, with minor amplitude differences between the port and starboard sides. The noise from the port and starboard sides of the vessel follows the same trend, and the differences between the two sides fall within 3 dB (Figure 4.3). However, some discrepancies are evident at lower frequencies (below 125 Hz), particularly in the 1400 rpm trial, with higher noise on the port side.

The fluctuation of the BNL values causes a noticeable variation in URN below 100 Hz. At low engine speeds (1400 rpm), the URN levels were comparable on both sides above 100 Hz. At 1800 rpm, the port side shows a URN level 3 dB higher than the starboard side above 100 Hz. In contrast, the URN levels were higher on the starboard side than on the port side at 2200 rpm, as shown in Figure 4.3(c). Both the speed and direction of water currents during each trial may have caused URN level variations on both sides. Figure 4.3 provides a comprehensive depiction of the overall URN of the vessel, highlighting its URN signature at various sailing speeds.

The URN of the vessel exhibited a unique noise pattern with tonal peaks ranging from 20 to 315 Hz in OTOB. The article [Picciulin et al., 2022] displays the narrowband and OTOB of small fishing boats, revealing fundamental peaks primarily from the diesel engine below 500 Hz. The low-frequency noise (below 150 Hz) detected in the URN coincides with the fundamental frequencies and harmonics produced by the engine and the blade passing frequency (BPF). Figure 4.3(a) illustrates that the URN levels are lower at low speeds (1400 rpm) above 500 Hz. In Figure 4.3 (b and c), an increase in URN levels is observed with the increase in vessel speed, indicating that the initiation of cavitation is usually related to increased hydrodynamic noise levels.

The broadband URN levels, ranging from 10 Hz to 25 kHz, were examined and presented in Table 4.3. An increase in cruise engine speed led to a corresponding increase in broadband URN levels, except for the frequency range of 500 to 1 kHz.

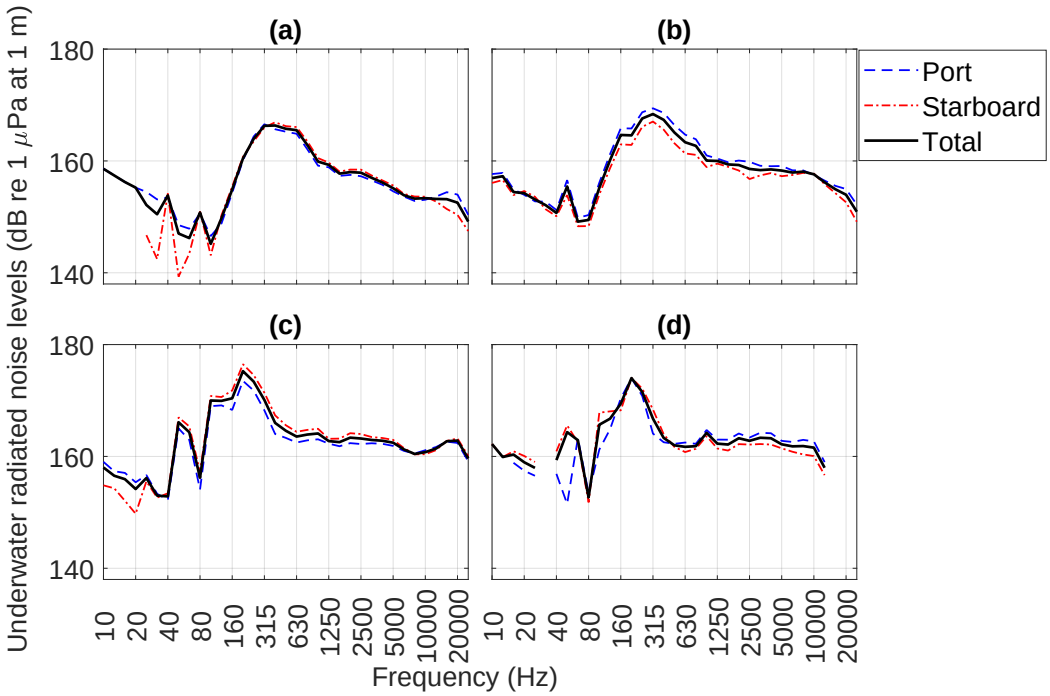

Figure 4.3: Underwater radiated noise levels presented in OTOB port and starboard sides of the vessel: a) 1400 rpm in December, b) 1800 rpm in December, c) 2200 rpm in December, and d) 2200 rpm in August (Petty Harbour-Maddox Cove).

The levels in the low-frequency bands of 63, 125, and 250 Hz experienced significant increases of 18 dB, 20 dB, and 10 dB, respectively. In contrast, the mid-band range of 2 to 8 kHz only doubled between the low and high engine speeds. The fishing vessel noise signature levels are aligned with previous review research [Parsons et al., 2021]; the vessel noise levels ranged from 145 to 195 dB re 1μPa @ 1m. These findings highlight the dependence of URN levels on engine speed and frequency bands, providing valuable insights into the acoustic characteristics of the fishing vessel during its operations.

4.1.4 Propagation loss model

The energy loss of the sound waves was calculated using the PL models described in Section 3.7.1. In Figure 4.4(a), the PE model values matched with ISO 17208-2 below 125 Hz, while the WNI showed agreement in the mid-frequency range of 160 Hz to 2 kHz. The FEM showed a deviation in all bands of about 5 to 6 dB. This was probably because of the computational complexity and sensitivity to mesh quality, and it was

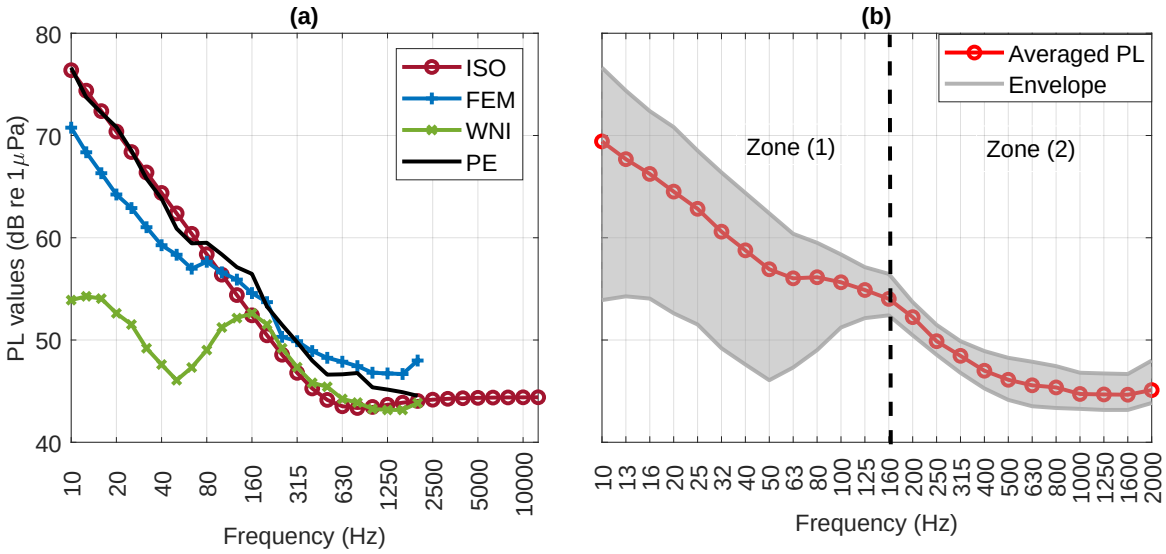

Figure 4.4: (a) Propagation loss values using the ISO 17208-2, Parabolic equation, Wavenumber integration and Finite element method from December trials (b) Envelope around the maximum and minimum value among the 5 PL models for each frequency band

not possible to set accurate boundary conditions, especially for large domains and higher frequencies.

The agreement in the results of the PE and WNI is between 160 Hz and 2 kHz. As discussed in [MacGillivray et al., 2019], the average between PE and WNI is used below 4 kHz, and [Meyer and Audoly, 2020] used WNI for frequencies below 1 kHz and not for higher bands. MacGillivray et al. studied a hybrid PL model between WNI and beam tracing up to 4 kHz. This model produced an accurate representation of the reference levels above 1 kHz; however, the authors found difficulties in estimating source levels below 1 kHz. Accordingly, a fifth PL model based on the average of the PE and WNI between 10 Hz and 2 kHz (PE+WNI) was included in the results [MacGillivray et al., 2023].

A PL model defined as the average of the five models: ISO, PE, WNI, FEM, and PE+WNI from 10 Hz to 2000 kHz is plotted in Figure 4.4(b) (Averaged PL). For each frequency band, the maximum and minimum values are evaluated between all of the 5 PL models (ISO, PE, WNI, FEM, and PE+WNI) and drawn the envelope around the datasets. The envelope width is obviously larger at low frequencies and decreases at higher frequencies.

The frequency range below 2.5 kHz was split into two zones at 160 Hz, where a significant decrease in the envelope area occurred, as seen in the dashed line in Figure 4.4(b). Zone 1 is for the frequency range of 10-125 Hz, while the second zone goes from 160 Hz to 2 kHz. The 2 kHz limit is chosen as the end of zone 2. Beyond this threshold, the wavelength becomes smaller, and numerical models are not efficient to model those frequencies. The ISO standard form can be an acceptable representation of the higher frequencies, as the measurements are conducted at a water depth marginally near the deep water definition.

Returning to the individual results from each PL model, a broadband PL value is computed by the five PL models for each zone, as shown in Table 4.2. The broadband values revealed notable differences in zone (1) among the five models, with envelope area equal to 182.36 [dB re 1 μPa.Hz]. Consequently, the low frequencies (zone 1) are sensitive to the employed PL model and might influence the MSL calculation with significant uncertainty. Therefore, based on the literature, the PE model was selected to represent the PL model in Zone 1, as it aligns with the [MacGillivray et al., 2019] discussion and recommendations by [Bureau Veritas, 2014; Lloyd's Register Group Limited, 2018].

Conversely, the area of the envelope in zone 2 is much smaller (43.30 [dB re 1 μPa.Hz]), indicating that the mid-frequency range can be accurately estimated using any of the models suggested in Table 4.2. However, following the literature, an average of PE and WNI (PE + WNI) was selected to model this area [MacGillivray et al., 2019].

Figure 4.5 shows the hybrid PL model used in the study to estimate the MSL of the vessel under test. The similarity between the results of the hybrid PL model and ISO 17208-2 comes from the fact that the water depth is close to the deep-water threshold defined in the Standard.

4.1.5 Monopole source level

The effectiveness of the hybrid PL model is determined by its thorough consideration of environmental factors, which are critical for accurately understanding the complexity of underwater acoustic propagation. Although useful for comparison, the ISO model has a narrow focus and cannot fully consider the diverse environmental

Table 4.2: Broadband values representing each proposed PL model are used to describe zones (1) and (2).

PL model	**Zone (1)**	**Zone (2)**
ISO[1]	65.40	45.80
PE[1]	65.77	47.75
WNI[1]	50.80	46.05
FEM[1]	61.70	48.72
PE+WNI[1]	58.28	46.90
Envelope Area[2]	182.36	43.30

[1] dB re 1μ Pa
[2] dB re 1μPa*Hz

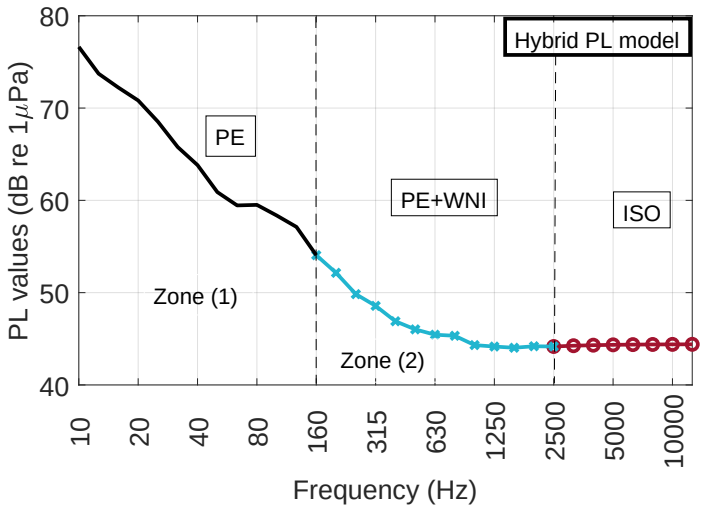

Figure 4.5: The hybrid PL model that was used to estimate the MSL

Table 4.3: The fishing vessel source levels are represented in URN and MSL (dB re 1μPa at 1m) in several frequency bands. The MSL is estimated using two methods: (a) PL_H hybrid PL model of PE and WNI; (b) PL_{ISO} is ISO 17208 form. The levels pertain to the December trial, encompassing three engine speeds of 1400, 1800, and 2200 rpm.

	1400 RPM			**1800 RPM**			**2200 RPM**			
Band [Hz]	**URN**	**MSL**		**URN**	**MSL**		**URN**	**MSL**		**BNL**
		PL_H	**PL_{ISO}**		**PL_H**	**PL_{ISO}**		**PL_H**	**PL_{ISO}**	
63	146	159	158	149	162	161	164	177	177	98
125	149	158	156	160	168	167	170	178	177	97
250	164	163	165	167	167	169	173	172	174	86
500 - 1k	164	161	160	163	161	1597	164	150	160	88
2k - 8k	156	153	152	158	155	155	162	15	159	84
10 - 10k	160	175	175	161	174	174	166	177	176	99
10 - 25k	159	174	174	161	173	173	166	176	176	99

influences on MSL at different frequencies. The differences between the two estimated MSLs, as shown in Figure 4.6 illustrate the environmental impact on some frequency bands that the simplified model might overestimate or underestimate. As a result, the understanding of MSL becomes more representative of the vessel noise signature.

Figure 4.6 illustrates the comparison of MSL and URN at the sailing conditions at the three designated engine speeds. The MSL has been computed using the hybrid PL model and ISO 17208-2 form, where broadband data is presented in Table 4.3. In the frequency range below 315 Hz, the MSL showed a significant difference (approximately 20 dB) compared to the URN, it showed a smaller difference of around 3-4 dB. Detecting low-frequency sound signals with long wavelengths was challenging because of the small distance between the vessel and the observer. However, the PL model can correct the received noise levels with the use of a magnification factor for the energy in the low-frequency bands, as illustrated in Figure 4.6. As a result, the MSL allows the vessel noise signature to be decoupled from the environmental effect on sound propagation.

The engine significantly contributes to the overall induced noise within the fishing vessel. Figure 4.7 displays the MSL and URN of the vessel at 1400 rpm engine speed, considering both clutched and unclutched propeller scenarios. The engine significantly contributes to the ambient noise in the ocean at frequencies below 500 Hz; in particular, Figure 4.7 (b) removes the contribution of the propeller to the URN,

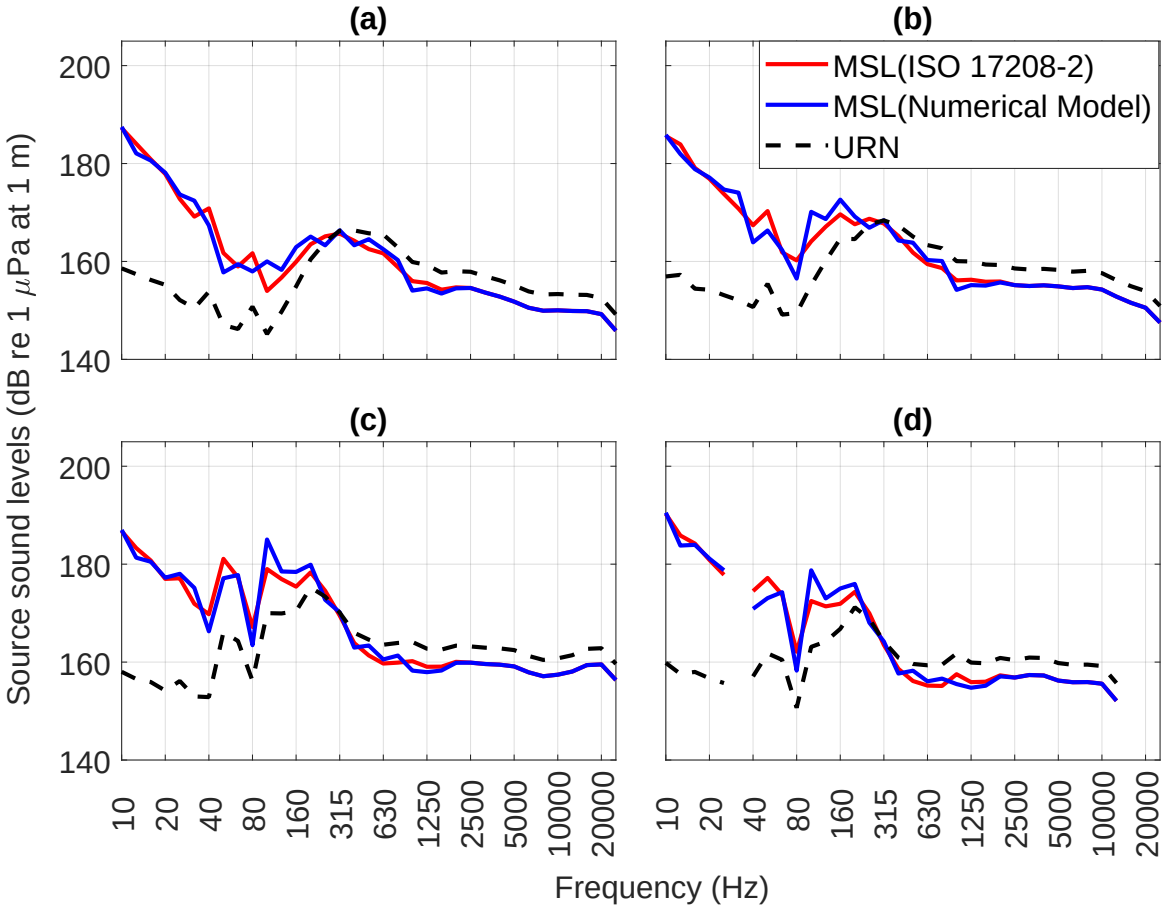

Figure 4.6: Monopole source levels are compared with the dipole source levels. The simple form ISO 17208-2 and the hybrid PE and WNI models are used to estimate the levels of monopole sources. a) 1400 rpm trial in December; b) 1800 rpm trial in December; c) 2200 rpm trial in December; d) 2200 rpm trial in August.

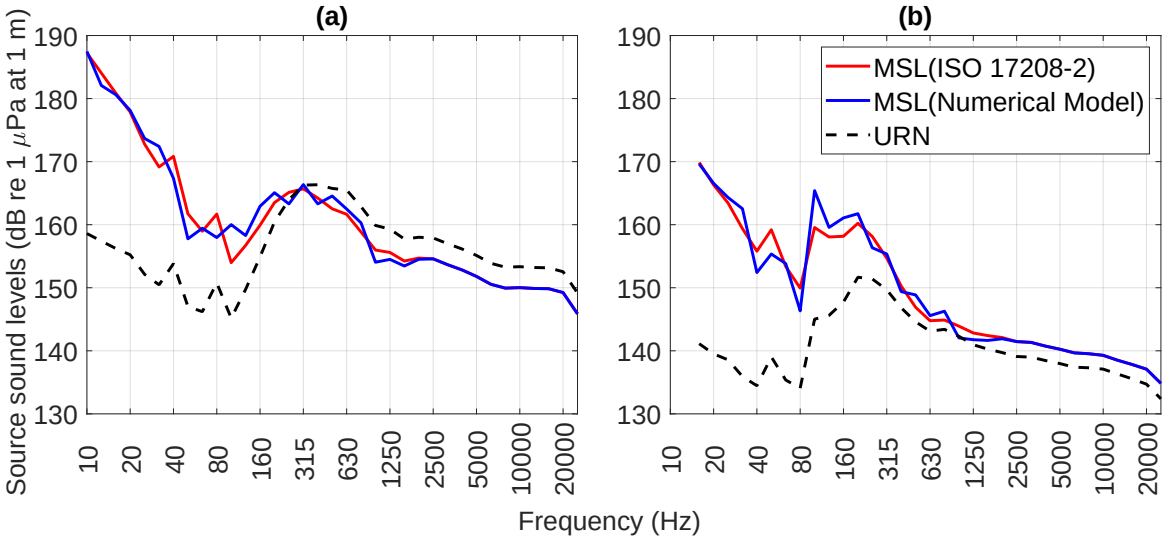

Figure 4.7: Monopole source levels and underwater radiated noise at 1400 rpm. a) Propeller clutched. and b) Propeller unclutched.

highlighting the primary effect of the engine. Table 4.4 presents the broadband levels for both operating conditions. Figure 4.8 shows the vessel noise signature in both operating conditions: clutched and unclutched propeller overlapping for comparison.

The analysis of URN introduces uncertainties in determining the vessel's induced noise, especially at frequencies below 250 Hz, as highlighted by Figure 4.6. A significant difference of approximately 18 dB is observed between the URN and MSL at frequencies of 63 Hz and 125 Hz. The discrepancy may lead to underestimating the vessel noise levels in these particular frequency ranges. Also, there is a significant difference of around 14 to 16 dB between the broadband MSL value and the corresponding URN of the vessel in the frequency range of 10 Hz to 25 kHz. This mismatch emphasizes the need for a precise estimation of the MSL, taking environmental factors into account via robust propagation loss models, in order to thoroughly evaluate the effect of fishing boats on ocean noise levels.

Last but not least, the fishing vessel under testing has a noise signature similar to that of larger vessels. The MSL can be compared with the results of previous studies. [MacGillivray et al., 2023] acquired a total of 12,079 MSL values measured on 1,880 vessels. The MSL levels peaked between 60 and 90 Hz, with an average of 190 dB. URN of 57 merchant ships was measured in the East China Sea by [Peng et al., 2018]. They used the Normal Modes model, combined with geoacoustic parameters,

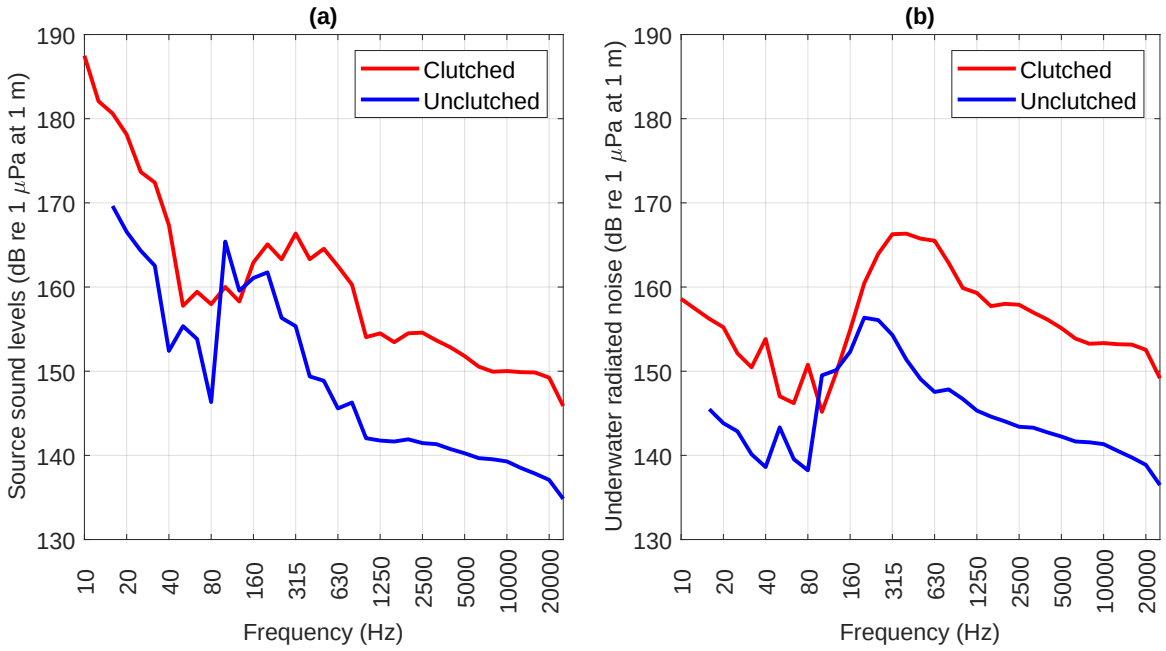

Figure 4.8: The vessel noise signature during clutched and unclutched propeller. a) Monopole source level, b) Underwater radiated noise.

to model the PL of transiting ships. The averaged MSL varied between 172 dB at 50 Hz and 130 dB at 1 kHz. The study [Simard et al., 2016] measured 255 MSL values of merchant ships in the St. Lawrence Seaway. The estimated MSLs showed high variability and were sensitive to the PL model employed. The average MSL of all ships was 197.2 dB in broadband (for comparison, the fishing vessel in this study had a 175 dB broadband MSL).

Engine contribution to the vessel URN

The acoustic data analysis presented in this section highlights the contribution of the engine and the propeller to the total underwater noise signature of the fishing vessel. Figure 4.9 shows how these sources contribute to the overall vessel noise spectrum. The engine contributed more than 60% at low frequencies (below 15 Hz) and in specific bands (63 Hz, 100 Hz, and 250 Hz), with values surpassing 70%. The propeller substantially contributed more to the URN at frequencies ranging from 16 Hz to 50 Hz and mid-frequency between 400 Hz and 4000 Hz. At frequencies above 4000 Hz, similar contributions were detected from the engine and propeller. The engine is the second contributor to the MSL of the vessel behind the propeller, especially in the

Table 4.4: Broadband levels of the monopole source level and underwater radiated noise level (URN) (dB re 1 μPa at 1m) of the fishing vessel are represented at some of the interested frequency bands. The levels in the table are measured at an engine speed of 1400 rpm for both the clutched and the unclutched propeller from the engine. PL_H hybrid PL model of PE and WNI, while PL_{ISO} ISO 17208 form.

	Clutched			**Unclutched**			
Band [Hz]	**URN**	**MSL**		**URN**	**MSL**		**BNL**
		PL_H	**PL_{ISO}**		**PL_H**	**PL_{ISO}**	
63	146	159	158	139	158	158	98
125	149	158	156	150	164	162	97
250	163	163	165	156	161	163	86
500 - 1k	164	161	160	147	151	150	88
2k - 8k	156	153	153	142	145	145	84
10 - 10k	160	175	175	149	165	164	99
10 - 25k	159	174	175	148	164	163	99

63 Hz band. At higher frequencies (above 2 kHz), the propeller's role increases due to cavitation effects, but the engine still contributes significantly to the ambient noise in all frequency bands. This conclusion is consistent with the results of the paper [McKenna et al., 2013] (focused on the noise footprint of container vessels). In that work, the effect of the engine is significantly below 1 kHz. The fact that the fishing vessel under testing is smaller and moves more quickly in this instance justifies the higher threshold (2 kHz).

4.1.6 Diesel engine's structure-borne noise

The measurement of onboard structure-borne velocity accurately captured the engine firing frequency per cylinder (FFPC), the total firing frequency (TFF), and the main shaft speed (RPS). Table 4.5 shows the rotational frequencies of the engine during the sailing experiments at 1400, 1800, and 2200 rpm. The FFPC was the dominant frequency associated with harmonics. The first harmonic was the rotational speed of the driver shaft of the engine (RPS = 2 $\times$ FFPC), and the sixth harmonic was the TFF (6$\times$FFPC).

The OTOB of the structure-borne velocities showed a decreasing pattern with decreasing engine speed. The velocity levels reduced sharply above 2.5 kHz, as illustrated in Figure 4.10, and the MSL values remained consistent at high engine speed,

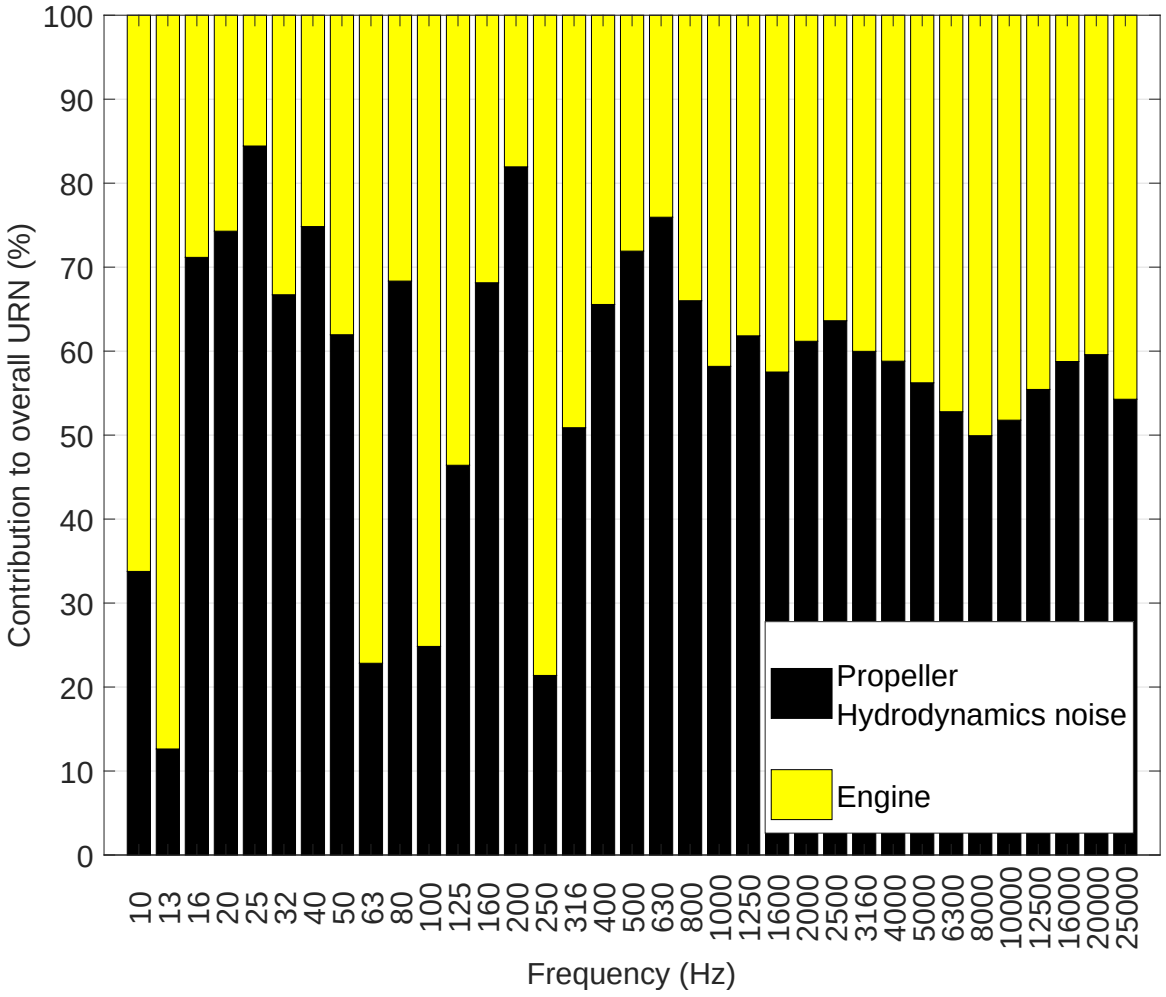

Figure 4.9: Contribution of the propeller and hydrodynamics compared to the engine to the overall underwater radiated noise of the fishing vessel

as in Figure 4.10(b and d). A significant change was noticed when the engine speed was decreased to 1400 rpm; the MSL showed a decreasing trend above 2.5 kHz, as in Figure 4.10(f). At this frequency, the propeller's contribution to the higher frequency ($\geq$ 2.5 kHz) was not discernible in the structure-borne noise data.

By comparing Figure 4.10(f) and (h) at 1400 rpm, the structure velocity patterns were almost similar for both clutched and unclutched propeller conditions. However, a significant reduction in MSL was observed above 315 Hz, attributable to the diminished propeller effect, while at lower frequencies, the levels remained relatively unchanged. In the narrowband analysis, the frequencies were the same in the clutched and unclutched conditions (FFPC = 11.9 Hz, TFF = 71 Hz, and RPS = 23 Hz). In the clutched regime, the propeller frequency was not clearly identified by the structure-borne noise; however, it was recognized by the received sound levels, which peaked at around 39 Hz, as shown in Figure 4.10(g).

Table 4.5: Fishing vessel operating conditions are presented from the linear narrowband analysis of the structure-borne and radiated noise recorded at the same time. (a) is the engine's nominal value. (b) are the engine's actual recorded values. (c) is the propeller frequencies.

Parameter	**1400 RPM**			**1800 RPM**			**2200 RPM**		
	a	b	c	a	b	c	a	b	c
RPM[1]	1400	1435.3	-	1800	1728	-	2200	2022	-
RPS[2]	23.33	23.92	9.71	30	28.8	12.1	36.67	33.7	13.9
FFPC[3]	11.67	11.96	-	15	14.4	-	18.33	16.85	-
TFF[4]	70	71.8	-	90	86.4	-	110	101.1	-
BPF[5]	-	-	39.18	-	-	48.1	-	-	55.6

[1] Engine revolution per minute
[2] Engine shaft revolution per second and first harmonic of the firing frequency per cylinder
[3] Engine firing frequency per cylinder
[4] Engine total firing frequency
[5] Blade passing frequency

The narrowband linear analysis of RL showed apparent tonal frequencies at 9.65 Hz, 19.4 Hz, 29.3 Hz, and 38.7 Hz with the propeller clutched to the engine. The frequencies observed were those of the primary blade frequency and its harmonics. Moreover, the URN highlighted the distinct engine harmonics. The URN showed the contribution of the engine cylinder firing frequency and its harmonics up to 40 times the fundamental frequency in the unclutched state. Overall, the tonal frequencies in

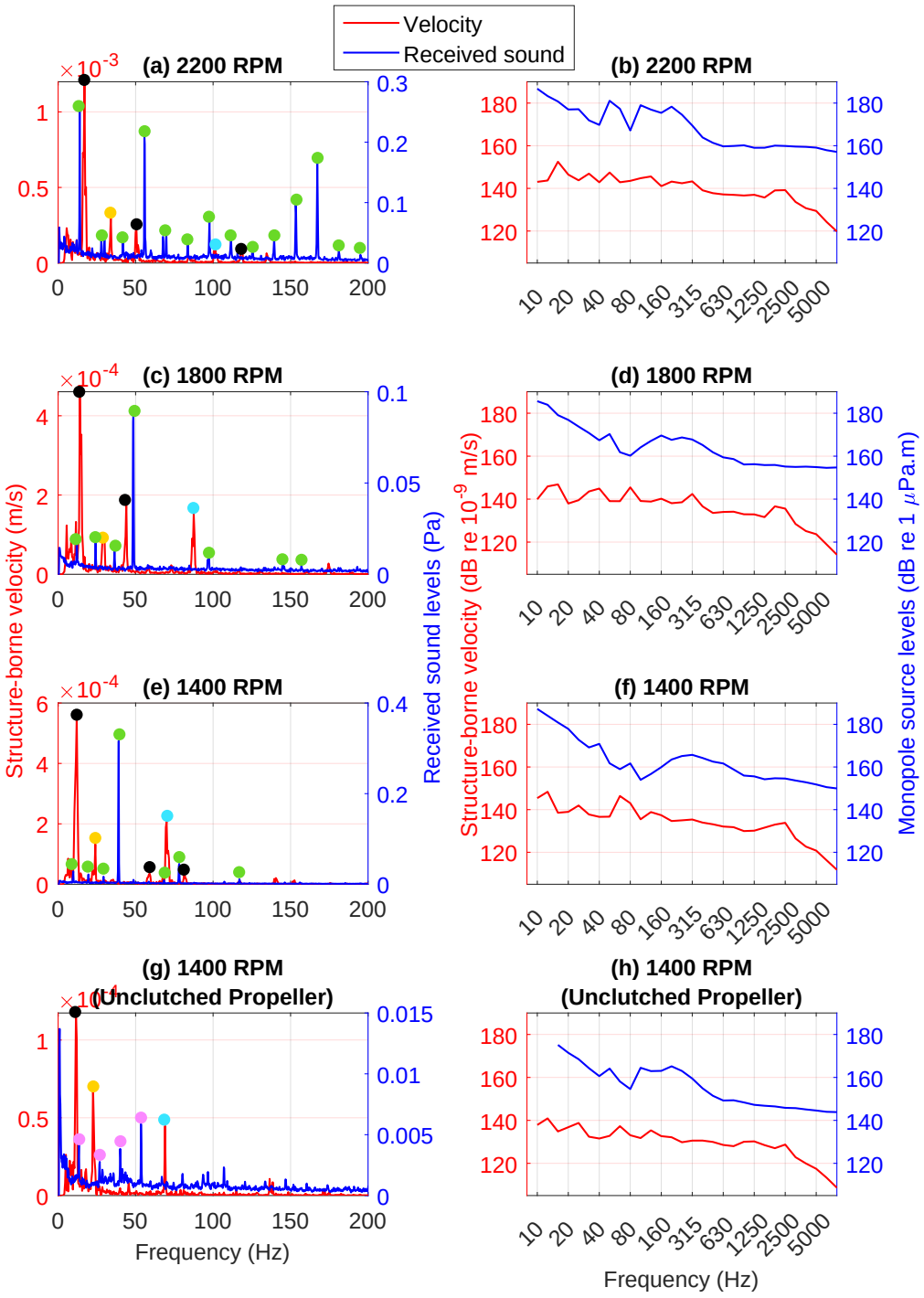

Figure 4.10: Narrowband and OTOB velocity analyses of vessel noise: Black dots indicate cylinder firing and harmonic frequency, yellow for shaft RPS, green for blade passing frequencies, blue for engine's total firing frequency, and purple for peaks from engine and transmission shafts when the propeller is disengaged

the URN and structure-borne noise are matched with slight shifts due to the gearbox ratio.

4.1.7 Correlation of onboard vibration levels with underwater radiated noise

Noise levels measured underwater can be related to onboard vibrations. This yields a frequency-dependent correlation between underwater SPL and structure-borne velocity levels, measured in an array of locations in the engine room.

Analogous to what is presented in [Cintosun and Gilroy, 2021], velocity levels are averaged across the measurement points to calculate the AQV.

Sound pressure levels are plotted against AQV values, with one point for each engine speed. These curves are plotted for each third-octave frequency band in Figure 4.11.

The plotted curves highlight the monotonic relationship between AQV and SPL, which can be used to build a statistical predictive model that relates onboard vibration levels to underwater radiation, similar to what is done in [Cintosun and Gilroy, 2021]. However, the plot doesn't exhibit the linear relationship between velocity levels and acoustic source levels described in [Cintosun and Gilroy, 2021].

More factors should be considered in this correlation: the study [Deeb and Seto, 2022] performed a similar analysis, using a neural network to build a transfer function between onboard vibration levels and underwater sound pressure, with an average error of 6.63 dB re 1 μPa at 1 m. However, the results of the analysis are limited to a small vessel class, a calm sea state, and a small number of operating conditions. The authors note that the sensitivity of the transfer function to a large number of environmental features should be investigated.

To conclude, the potential effects of fishing vessel noise on marine species and the broader ecosystem in Newfoundland still need to be more adequately understood. In addition, the issue of fishing vessels as underwater noise sources prompts engineering questions on mitigation strategies. This problem needs to be addressed starting from the design phase. While larger vessels can rely on advanced design techniques and custom solutions, for smaller fishing vessels, designers and owner-operators need to

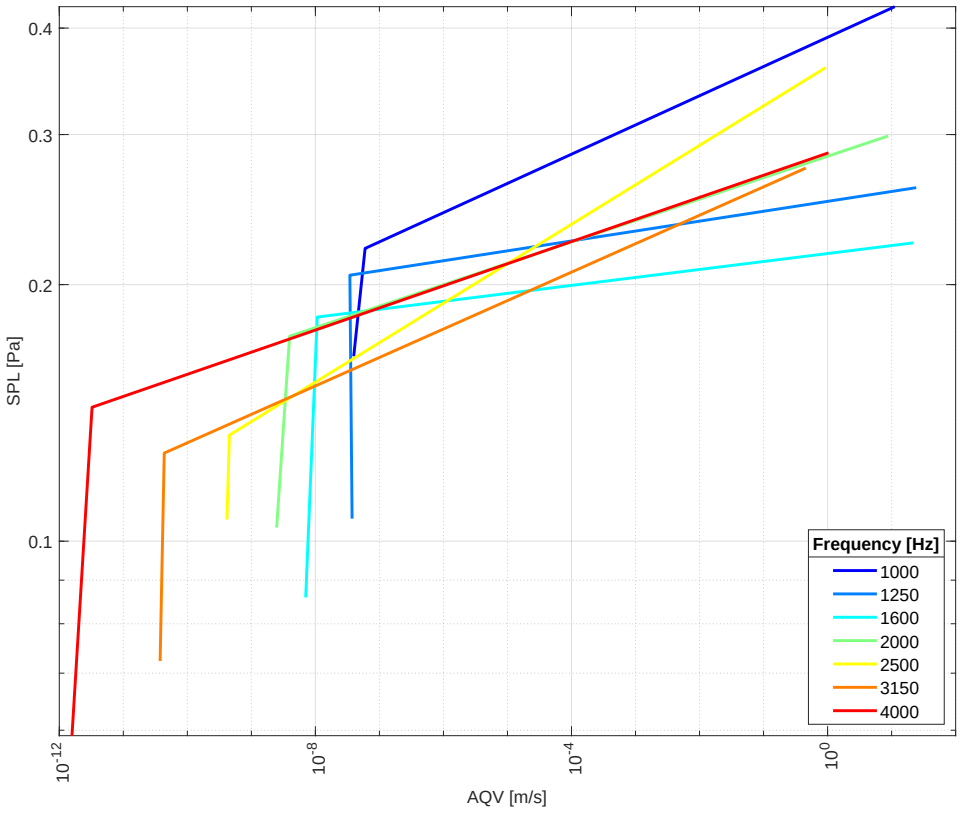

Figure 4.11: Relation between AQV and SPL for different frequency bands

be provided with a set of techniques focused on reducing noise transmission from the most relevant onboard sources. Indeed, a dedicated study to reduce noise from every single vessel would be an unbearable cost for small fishing enterprises, which could instead benefit from guidelines and general mitigation principles on reduction techniques for different fishing vessel categories [Burella and Moro, 2021]. Any study to propose mitigation strategies to control underwater noise from vessels has to start with assessing the underwater radiated noise and characterizing the main sources contributing to it.

4.2 Acoustic glider performance

4.2.1 Glider flight description

Glider flight data was evaluated using the glider onboard flight computer to reconstruct the glider behavior in depth, time, and space. The glider made a series of consistent six V-shaped dives to a maximum depth of 60 metres at the shallow water location (Holyrood Bay). The glider did four dives at the deeper-water site in Conception Bay, and the depth it went to was very variable between dives, as shown in Figure 4.12. The glider made a single V-shaped dive to a depth of around 200 metres during the initial dive. The second and third dives were completed in a continuous flight, with no surface in between, and reached depths of 195 and 170 metres, respectively. During these two dives, the glider's trajectory isolates the recordings from potential noise caused by the hull interacting with the water surface. This approach maintains data integrity and reduces disturbances during dive sequences, which may lead to discarding more windows of the recorded noise. The latest dive was another single V-shaped dive profile, with the glider diving to about 160 metres before returning to the surface.

The oceanography data collected by gliders during sea trials in Holyrood Bay and Conception Bay provides insightful visualizations of temperature and salinity profiles across various water columns, as depicted in Figure 4.13. This figure illustrates significant disparities in temperature gradients from the surface to the seafloor. Notably, there is a stark temperature change of approximately 13 °C in shallow water areas,

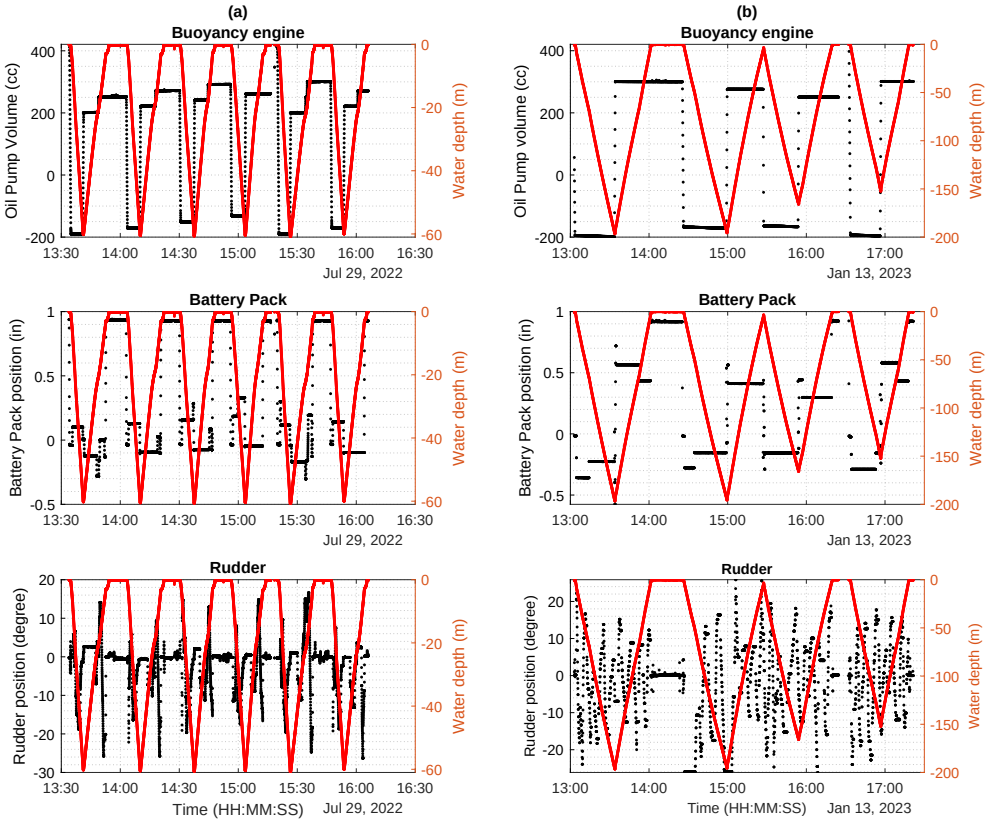

Figure 4.12: The glider's flight depths are illustrated in red for both the shallow and deep water sites, while its internal mechanisms are represented in black and overlapped in a single plot. (a) shows the flight patterns recorded during the Holyrood/Shallow water site trial, while (b) shows the flight patterns recorded during the Conception Bay (Deep Water) site trial. Each column displays a set of three plots, providing a comprehensive overview of the glider's internal mechanisms at both trials.

in contrast to a more subdued 3 °C variation observed in deeper waters.

Panel (a1) of Figure 4.13 delineates these temperature shifts, capturing the thermal dynamics of different marine zones. In terms of salinity, Conception Bay's deeper waters exhibit higher salinity levels, around 33, which gradually decrease to 31 near the seafloor, as indicated in Panel (a2). Conversely, Holyrood Bay demonstrates a relatively stable salinity profile, with variations less than 1 between the surface and the seafloor, as evidenced in Panels (b1 and b2).

These observed changes in temperature and salinity are not merely numerical

values; they significantly impact the sound speed profile, influencing the sound propagation in water.

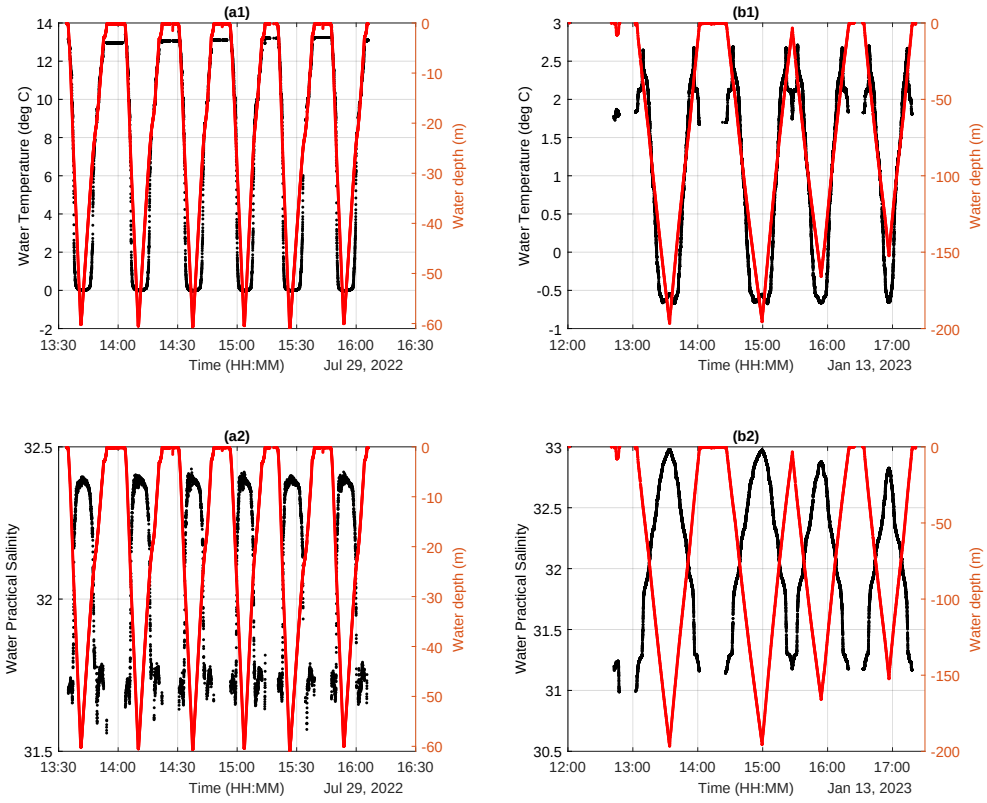

Figure 4.13: Temperature and salinity collected by the glider in (a) Holyrood Bay and (b) Conception Bay trials as a function of mission depth.

Holyrood Bay

The glider's buoyancy engine operated during the sea trials, resulting in a steady 26-second period of pumping for approximately 300 to -200 cc at both the top and bottom of each dive. The distinctive behavior of the pump occurred when the glider began to descend or climb, with the engine remaining inactive for the remainder of the dive. However, at a depth of approximately 22 metres, while the glider was heading toward the surface, the engine was restarted briefly for less than three seconds to pump another 50 cc to the bladder. This process was repeated similarly for all six flight trials.

Furthermore, the battery pack shifting motor was also in use during the sea trials. The motor moved the mass by 1 inch while returning to surface. The mass position varied multiple times between 0.1 and -0.3 inches when the glider was about to reach its maximum depth, and it continued at the beginning of the climb. The glider performed this process almost identically throughout the six dives.

On the other hand, the motor controller that manages the glider's fin to maintain heading also observed notable changes throughout the water trials. The peak of steering input was reached at the mid-dive and mid-climb. The fin adjustments ranged from -12 degrees to -25 degrees, and a predictable pattern was consistently observed to maintain heading as a result of currents and density gradients.

Conception Bay

The oil pump of the glider was limited to operating at the top and bottom of the dives, making no adjustments during the process of ascending or descending. The pump performed an apparent trend comparable to a square wave with uniform amplitude and duration. The duration of buoyancy adjustment was estimated to be 28 seconds, during which the oil was filled and pumped out, resulting in a volume change equivalent to that observed during the shallow water trial.

The glider maintained a fixed position of the center of mass, which was identified as the battery pack, at -0.15 inches and 0.45 inches during its second and third dives, respectively. In contrast, the first and fourth dives involved an adjustment of the mass position by roughly 0.15 inches at the midpoint of the ascent and descent. The data is illustrated in the supplementary materials.

The glider's heading went through multiple adjustments throughout its vertical trajectory, with short operational intervals. During the initial stages of the dives, the rudder angle underwent a transition from 20 degrees to -25 degrees. Subsequently, the alterations made during the process of ascending or descending were observed to be within the range of 15 to -10 degrees. The rudder exhibited a response time of fewer than 0.2 seconds per alteration.

Slocum gliders, with the total buoyancy drive available, can typically achieve maximum forward speeds of 0.25 m/s or 22 km/day in still water. In the deep water site, ocean currents were negligible, and the glider achieved average forward speeds of 0.23

m/s. Using uncertainty estimates in Claus and Bachmayer [2015], the glider position accuracy in the trials was accurate to within 50 m since the average dive interval was less than 40 min and currents were less than 5 cm/s.

In shallow water, the glider stayed on the surface for a long period of time after diving. Thus, Figure 3.4 shows a drift before each dive. While this drift could be a concern in some scenarios, it didn't compromise our study. We focused on evaluating the glider's self-noise on a dive-by-dive basis.

4.2.2 Glider self-noise assessment

Applying the time-frequency analysis to the glider acoustic data, revealed that the brushless DC motor of the oil pump is the dominant source of self-noise for the glider, with its levels notably higher than those of the rudder and background noise across the measured frequency spectrum. In the shallow water trial, it emitted a tonal peak at 16 Hz (960 rpm) along with harmonics up to 1 kHz (Figures 4.14a & 4.14b). The pitch motor noise was included in the oil pump analysis as both occurred at the same time, see Figure 4.12 plots of the glider's internal mechanisms operation with respect to the glider depth. The comparison between port (Figure 4.14a) and starboard (Figure 4.14b) indicates a slightly higher intensity of noise on the starboard, especially in the low-frequency range, hinting at possible asymmetries in glider noise emissions between the two sides. The starboard hydrophone recorded a peak noise level of 135 dB at 48 Hz, while the port hydrophone recorded 125 dB. According to Table 4.6, the broadband noise levels differed by about 9 dB, with the starboard side being noisier. The Slocum glider's 350 m HD pump pumps oil faster than its 1000 m HD pump. This may cause random noise fluctuations changing port vs. starboard when the glider pump is activated. There is no one-sided spinning mechanical component that causes this effect. Since this is only a feature while the pump is on, it does not affect the rest of the findings and only changes the uncertainty in self-noise when comparing hydrophones.

The time-frequency analysis and the flight data were applied to the recorded acoustic data. In the shallow water trial, the analysis revealed that the brushless DC motor of the oil pump is the dominant source of self-noise for the glider, with its levels notably higher than those of the rudder and background noise across the measured

frequency spectrum. It emitted a tonal peak at 16 Hz (960 rpm), along with harmonics up to 1 kHz (Figures 4.14a & 4.14b). The pitch motor noise was included in the oil pump analysis as both occurred at the same time; see Figure 4.12. The comparison between port (Figure 4.14a) and starboard (Figure 4.14b) indicates a slightly higher intensity of noise on the starboard, especially in the low-frequency range, hinting at possible asymmetries in glider noise emissions between the two sides. The starboard hydrophone recorded a peak noise level of 135 dB at 48 Hz, while the port hydrophone recorded 125 dB. According to Table 4.6, there was a difference in broadband noise levels of about 9 dB, with the starboard side being noisier.

In contrast, the rudder noise is evenly distributed across frequencies, with moderate peaks, and consistently goes above the background noise level, which remains steady across frequencies. The rudder's noise added 6 to 13 dB over the ambient noise across a wide frequency range from 25 Hz to 10 kHz. This is consistent with [Jiang et al., 2019] findings. The noise levels recorded by both hydrophones were found to be comparable during the rudder motion, as the difference is less than 1 dB, as shown in Table 4.6.

During the deep water trial, background noise levels were 8 dB higher compared to shallow water (see Table 4.6). The oil pump noise profile exhibits decreased sound levels compared to the shallow water trial. The oil pump's noise signature was characterized by a tonal peak at 14 Hz (840 rpm), with a maximum level of approximately 127 dB at 44 Hz (Figures 4.14c & 4.14d). Starboard hydrophone noise levels exceeded the port side by approximately 4 dB. The rudder noise was observed several times during the glider's descent and ascent phases. The rudder produced more frequent movement, resulting in a wide-band noise generating a broad-spectrum signal with amplified harmonic energy between 100 Hz and 10 kHz, consistent with [Liu et al., 2018] and [Haxel et al., 2019] findings. Its noise remains recognizable from the background noise, with fewer peaks and a smoother distribution across the frequency spectrum. The noise output on the starboard side (Figure 4.14d) was slightly higher than on the port (Figure 4.14c), which could indicate consistent side-dependent self-noise characteristics, and the self-noise is characterized as directional noise.

According to the final analysis, the oil pump performed at a higher operational speed in the shallow water experiment of 960 rpm compared to 840 rpm in deep water, leading to an increased level of self-noise, as shown in Table 4.6. This observation

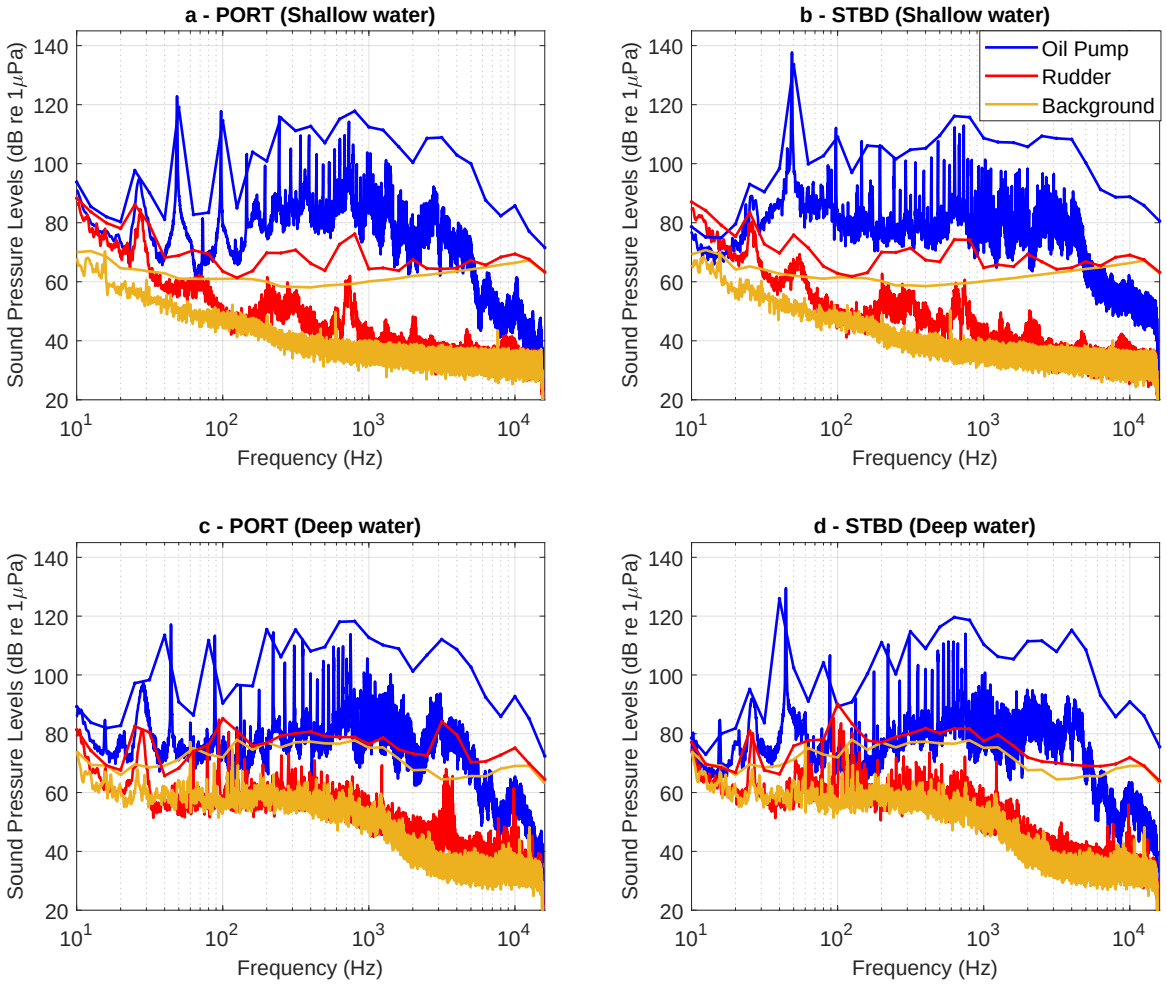

Figure 4.14: Glider self-noise is presented in a narrowband of 1 Hz resolution. The figure shows the oil pump and rudder noise compared to the recorded background noise during the trials. The straight dotted lines represent the one-third octave band analysis for each source of noise. (a) The self-noise was observed during the Holyrood sea trial in shallow water, and (b) during the Conception Bay trial in deep water.

suggests that the glider's propulsion system operates differently at different water depths. Furthermore, the rudder showed greater variability in its movements in deep water compared to the consistent and predictable patterns observed in shallow water. These inconsistencies in deep water led to shorter, less detectable rudder noise durations compared to the longer, more apparent durations seen in shallow water trials. This suggests that the glider's self-noise emissions were affected by the ocean environment in which the rudder tried to keep the glider heading on track.

Table 4.6: Broadband self-noise levels of sources of noise in the glider are up to 10,000 Hz [dB $re\ 1\mu Pa$]. The results are compared to the ocean background noise.

Direction	**Oil pump**		**Rudder**		**BNL**
	Shallow	**Deep**	**Shallow**	**Deep**	
Port	125.25	125.18	92.45	93.40	80.00
Starboard	134.70	129.00	91.32	94.40	88.15

4.2.3 Underwater radiated noise

This section presents the results of the vessel noise signature campaign that was conducted in Conception Bay. The glider, array of three hydrophones, and bottom-moored hydrophone were deployed simultaneously at a certain distance from the vessel under test.

The background noise levels measured by the three platforms are presented in Figure 4.15. The RNL of the vessel showed disagreement between the platforms due to the variation in the CPA between the vessel and each observer in each trial. The BNL was below the sound received by the hydrophones, making the measurement reliable and comparable.

Using the spherical spreading loss method from the literature, it was clear that the 1/3 octave band URN measured by the three PAM observers are generally similar across wide bands but with some variations at specific frequencies in the 1500 rpm trial. Figure 4.16a shows that at 2000 rpm engine speed, the UNR levels from all platforms displayed prominent peaks in the lower frequency range, followed by a gradual decrease as the frequency increased. In contrast, Figure 4.16b illustrates the 1500 rpm engine speed trial, which exhibits a less noticeable peak in the low-frequency range and a gradual decrease in the noise levels. The peaks below 100 Hz represent the fundamental frequencies of the propeller and the engine of the vessel.

Comparing the two experiments, the total vessel noise signature across most frequencies from all observer platforms was higher in the 2000 rpm experiment than in the 1500 rpm trial. Furthermore, the 2000 rpm trial typically has a more significant standard error. The URN changed from 157 to 165 dB as an overall noise by increasing the engine speed. The noise results were aligned with the findings of small vessels

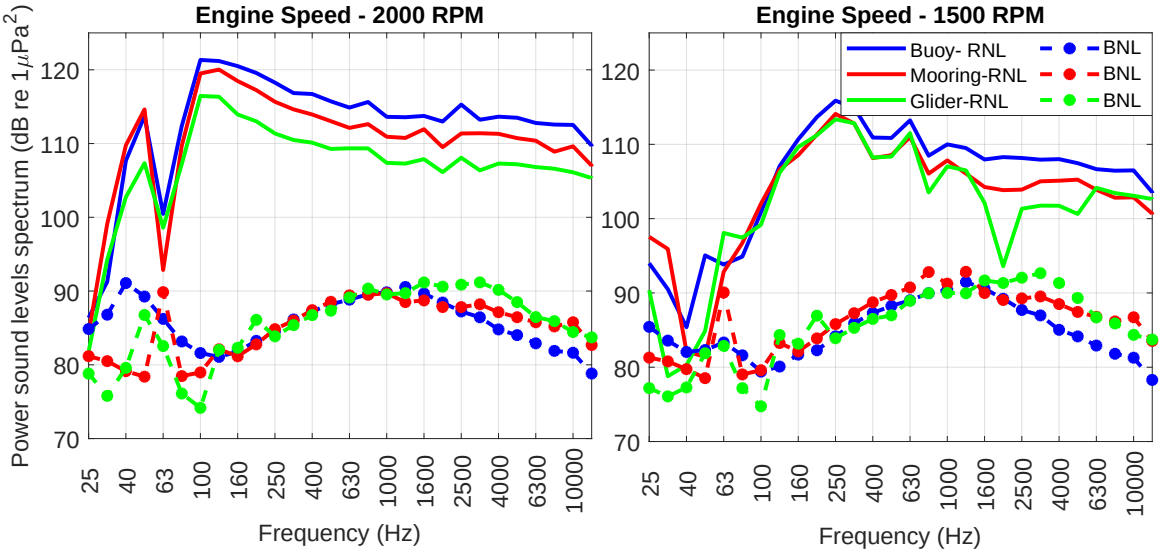

Figure 4.15: Received sound levels (RNL) and background noise level (BNL) measured by the three platforms.

studied by [Wladichuk, 2019]. The buoy and the glider measured similar URN levels across the frequency range except at the 2 kHz band, where the noise levels tended to lower during the 1500 rpm experiment. The moored hydrophone was almost located in the deep sound channel. The deep sound channel acts as a waveguide for sound waves, which means that sound waves travel from long distances captured by the moored hydrophone [Gassmann et al., 2017]. Therefore, the URN levels were the highest over the glider and the drifting buoy.

The glider exhibited remarkable performance by producing comparable uncertainty values in the URN measurements, reaching $\pm$ 2 dB at frequencies between 250 and 630 Hz. The glider demonstrated reduced uncertainty levels in all frequency bands, except for the 125 Hz band, compared to the single-moored hydrophone platform and competitive uncertainties with the drifting buoy. The absence of long cables and floats in the glider system reduces uncertainties, while the glider's rudder and hydrodynamic flow may introduce some uncertainties. The rudder noise was centered in the 100 and 125 Hz bands, as discussed in the previous section, and that was reflected at the URN, as seen in Figure 4.16a.

At 1500 rpm vessel engine speed, the glider depth was 18 m below the water's

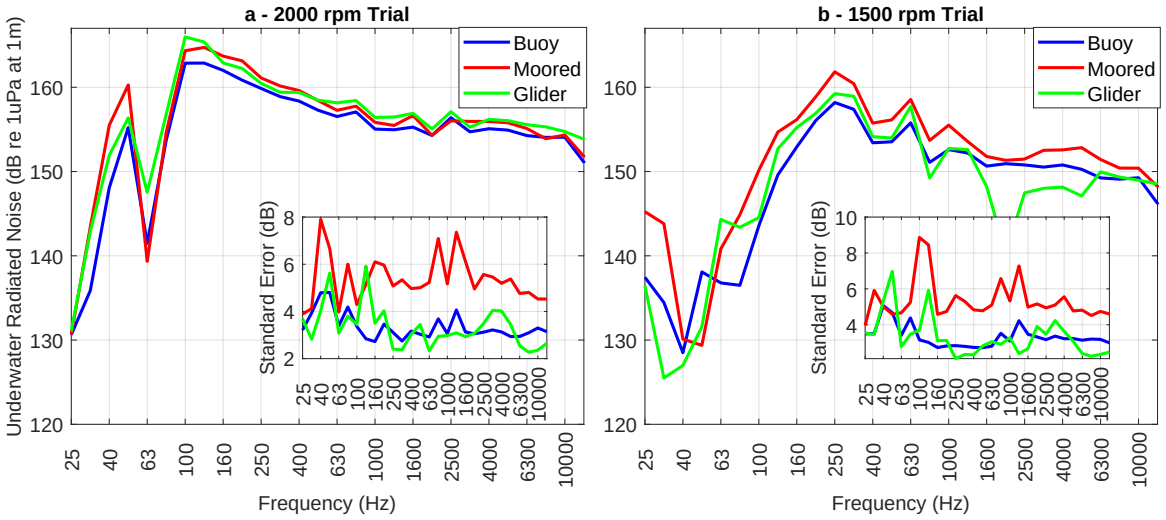

Figure 4.16: Underwater radiated noise levels of the vessel under testing by the three platforms at two engine speeds. The panels show the estimated standard error of the URN by each platform.

surface and above the mixed layers. A notable URN discrepancy was observed, particularly at frequencies above 2 kHz compared to the other two platforms Figure 4.16b. At that depth, the propagation of the high frequencies near the surface attenuates significantly due to the positive gradient of the sound speed profile, which can cause the sound waves to propagate away from the hydrophone [Garrett, 2020]. Thus, above 2 kHz, the recorded sound integrity where the glider is about to reach the surface needs to be investigated. The drifting buoy showed promising uncertainty values that match ISO 17208-1 [ISO-17208/1, 2016]. Due to the random motion of the rudder, the glider exhibited favorable uncertainty values, except for the 125 Hz band. The results emphasize the glider's potential as a dependable instrument for reliable underwater radiated noise evaluation for vessels.

It will be important to further assess and validate these results against longer deployments under different ocean conditions. The absence of long cables and floats, compared to the mooring and drifting buoy contributed to the reduced sound measurement uncertainties of the glider. In contrast, previous research showed that bottom-moored systems generally have lower levels of uncertainty. I acknowledge that some circumstances may have contributed to the glider's impressive performance: (1) Depth Variability: The glider's ability to change depth enabled sampling of various places within the water column, potentially mitigating noise fluctuations that depend on

Table 4.7: Broadband levels of the underwater radiated noise level (URN) (dB re 1 μPa at 1m) of the fishing vessel were measured by the three platforms during Conception Bay trials. The data are represented in some of the interested frequency bands. The levels in the table are measured at an engine speed of 1500 and 2000 rpm.

Band [Hz]	**1500 rpm**			**2000 rpm**		
	Glider[1]	**Buoy[2]**	**Mooring[3]**	**Gider[1]**	**Buoy[2]**	**Mooring[3]**
63	144	138	141	147	141	140
125	153	150	155	165	163	165
250	160	158	162	160	160	161
500 - 1k	154	154	156	158	157	158
2k - 8k	148	150	152	156	155	155
10 - 10k	153	152	155	160	158	159

[1] Slocum glider with two mounted-wing hydrophones
[2] Array of three hydrophones attached to a surface buoy
[3] Bottom-mounted hydrophone

depth. (2) Location of the moored system: the hydrophone, which is anchored at a single location near the deep sound channel, recorded distant sources of noise during trials, with a particular impact on low frequencies. (3) Cable-Induced Noise: The vibrations and chafing caused by the cables created low-frequency self-noise that was unique to the particular configuration. Although cable-induced noise is not present in all moored systems, it helped the glider perform with less uncertainty across most frequency bands than the single-moored hydrophone platform.

4.2.4 Propagation loss of sound

Using the methodology described in Section 3.7, I involved six propagation loss models to determine PL values at distances of 100 and 500 metres from the sound source in both shallow and deep water environments. The Holyrood trial (shallow water) showed that the simplified models ECHO, SCA, and M-A produced similar estimations of PL at a distance of 100 metres from the sound source. However, as traveling deeper into the ocean, the differences between these models became increasingly apparent. The PE model showed a significant deviation from the other models below 200 Hz, leading to higher PL values, as shown in Figure 4.17. When considering the seafloor bathymetry profile that the glider passed over during the mission into the PE model, PL values increased, particularly in frequency bands below 100 Hz. The 250 Hz band

was where all the models almost matched; as shown, the gray envelope thickness decreased until half the water depth. This highlights the important role of bathymetry in shallow-water situations. When the sound wavelength is much larger than the ocean depth, the ocean acts as a high-pass filter for sound waves.

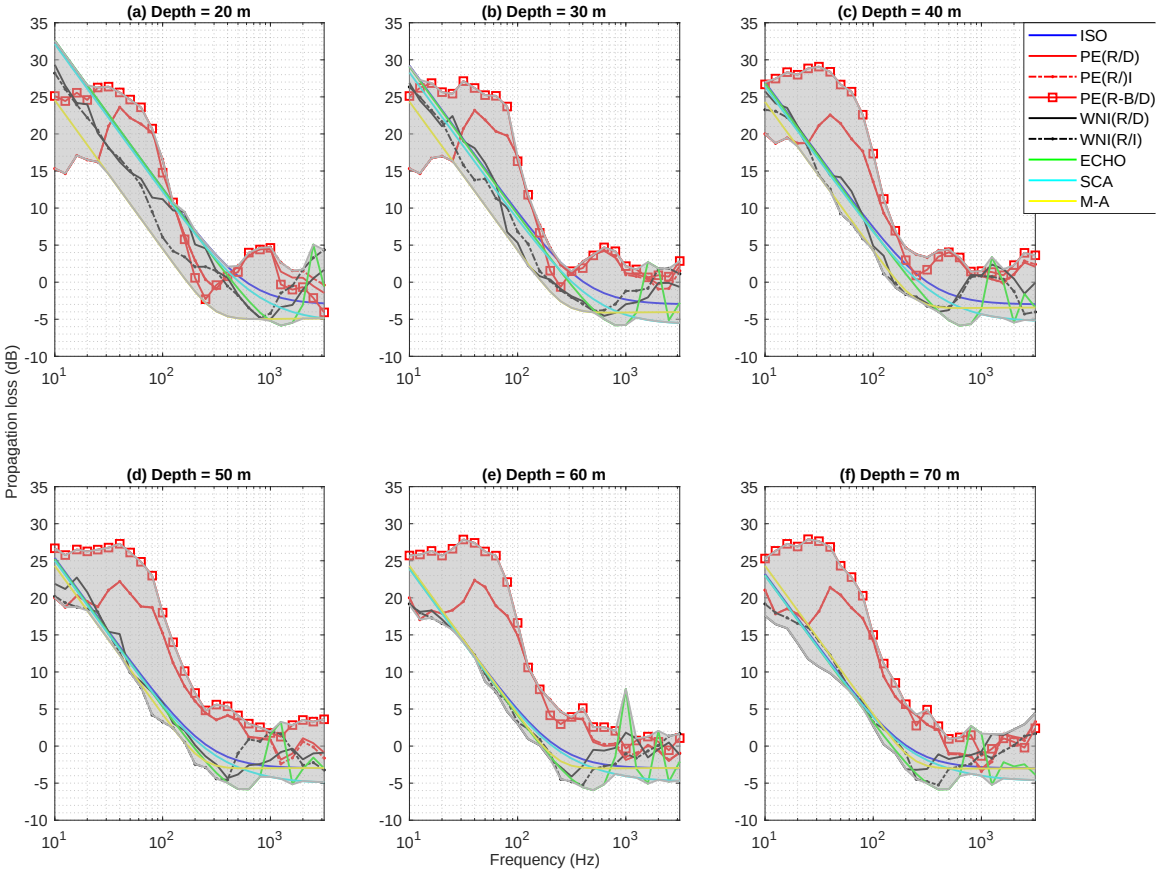

Figure 4.17: PL models were measured at six points through the water column 100 m apart from the source at the Holyrood site (shallow water). (R/D) range-dependent SSP. (R/I) range-independent SSP. (R-B/D) range-dependent SSP and bathymetry

Increasing the horizontal distance between the measurement point and the sound source to 500 meters revealed expected behavior within the simplified models due to the more interactions between the sound and the environment boundaries. The gray envelope's width increased, resulting in an unpromising representation of the PL using the simplified models. The convergence of the ISO 17208-2 and ECHO models with the PE model can be seen in Figure 4.18, regardless of whether the bathymetry is flat

or not, significantly below 100 Hz. However, the models differed significantly as the depth of the water increased for frequencies above 250 Hz. Figure B.1 visually shows the inconsistencies or absolute errors between ISO standard 17208-2 and the other models. The significant deviation of the numerical PE model at frequencies below 250 Hz, compared to other models, is obvious. The error increased as the model approached the seafloor. The other models showed good agreement at low frequencies with ISO standard 17208-2, indicating their difficulty in predicting PL values in this frequency range. This could potentially lead to an underestimation of the vessel noise signature at low frequencies. Overall, discrepancies between PE (R/D) and (R/I), assuming flat bottom, and PE (R-B/D), actual bathymetry, in Figure 4.19 suggested that the bathymetry is critical for predicting PL at the shallow water site, which implies the importance of the seabed geoacoustic properties to the PL prediction.

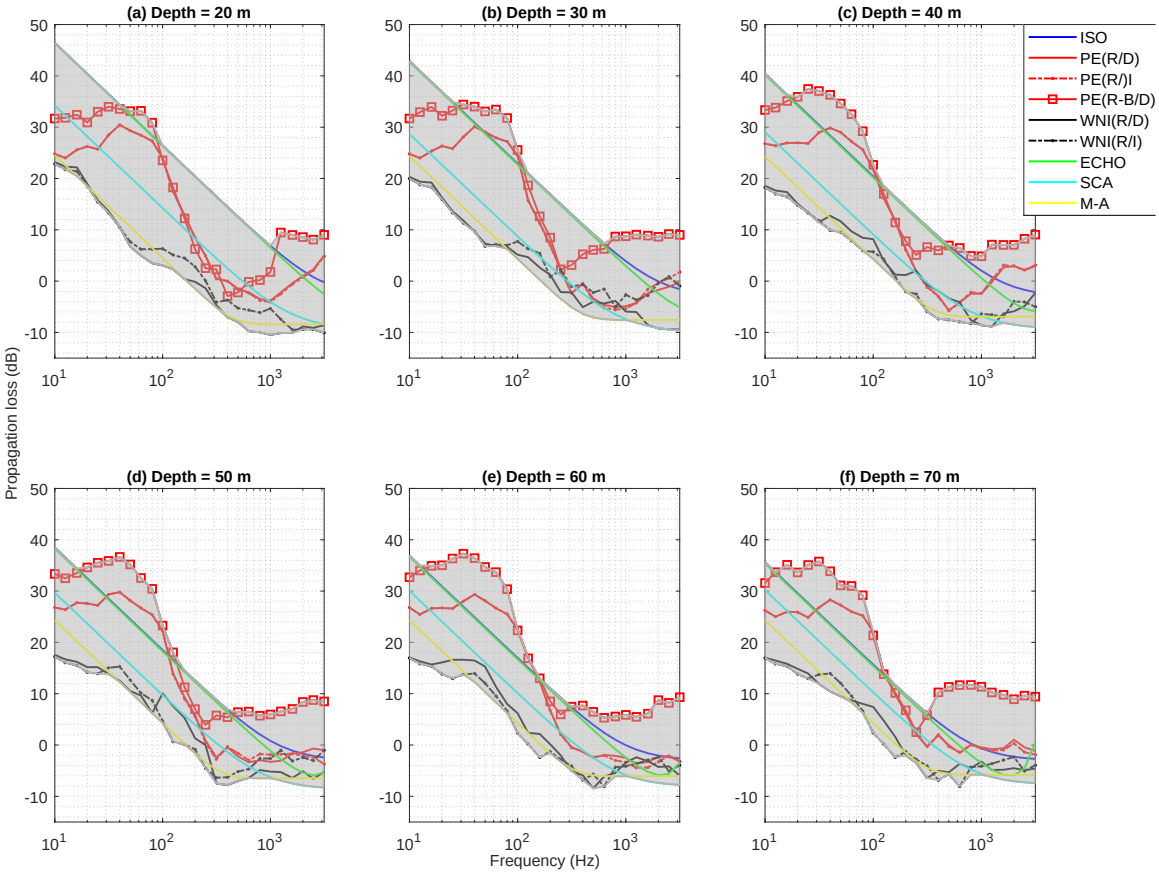

Figure 4.18: PL models were measured at six points through the water column 500 m apart from the source at the Holyrood site (shallow water). (R/D) range-dependent SSP. (R/I) range-independent SSP. (R-B/D) range-dependent SSP and bathymetery

In the deep water trial, a significant deviation with the M-A model was observed, especially above 200 Hz. Therefore, I chose not to include the M-A model in the gray envelope to represent the critical frequency bands while estimating the PL values. The PE model showed a similar pattern, particularly in representing high PL values between 30 and 150 Hz. Actual bathymetry data had a more minor effect on the PE model than the flat assumption, as shown in Figure 4.19. At 250 Hz, the grey envelope narrowed near the water's surface and shifted towards the 200 Hz band closer to the seafloor. In Figures B.1 and B.2 from rows 4 to 8, all simplified models, including the WNI model, showed significant alignment below 500 Hz at the 100 m range.

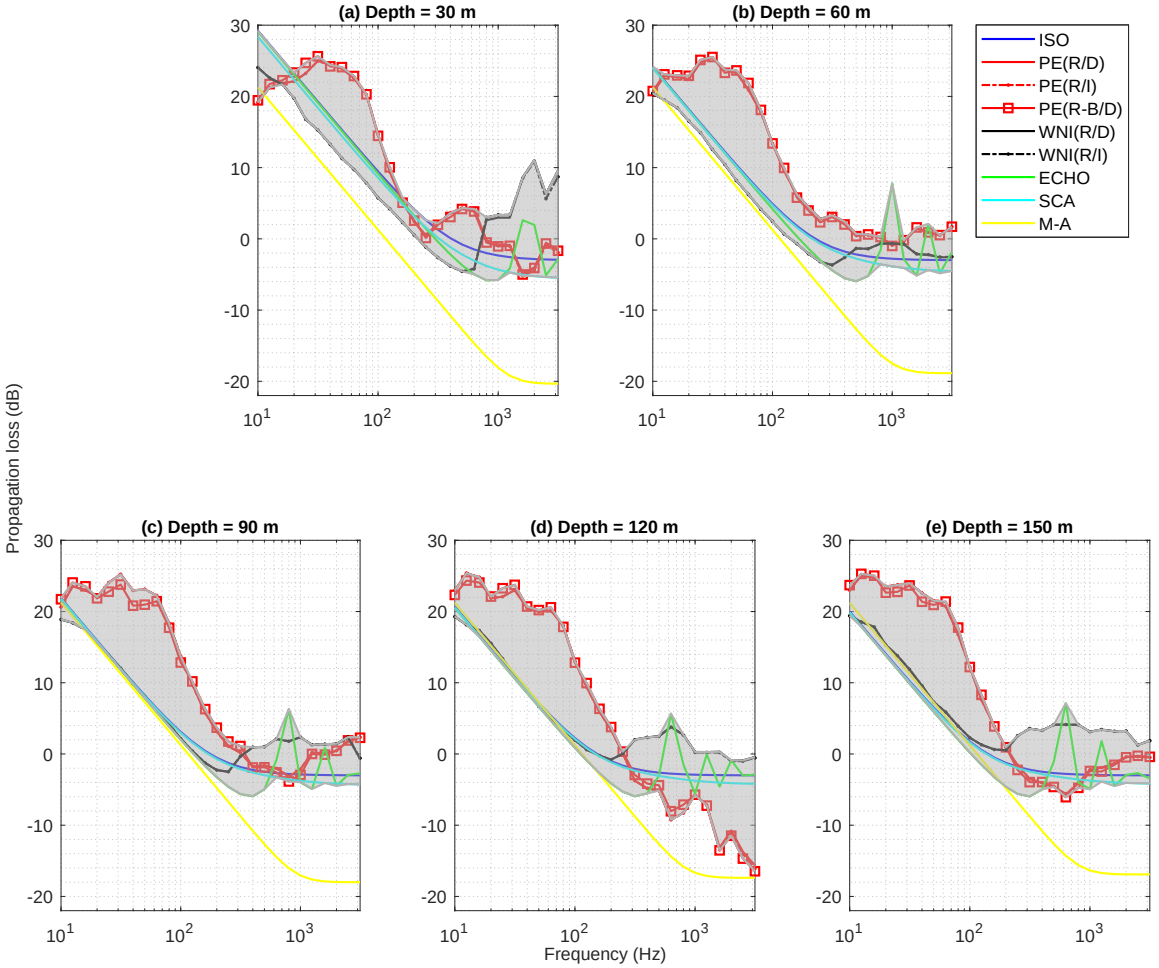

Figure 4.19: PL models were measured at six points through the water column 100 m apart from the source in the Brigus site (Deepwater). (R/D) range-dependent SSP. (R/I) range-independent SSP. (R-B/D) range-dependent SSP and bathymetry

At 500 meters from the sound source, simplified models showed more noticeable differences in estimating the PL values near the water surface (30 m) and all agreed when going deeper (120 m), as shown in Figure 4.20. However, the PE model consistently agreed with the simplified models in estimating the PL values throughout the water column except for between 30 and 100 Hz, where high PL values were observed. The WNI model demonstrates strong agreement with simpler models at frequencies above 250 Hz, in both shallow and deep water, for short ranges. Figure 1 highlights the notable difference between the PE model and ISO 17208-2 in estimating PL values at low frequencies. The grey envelope in Figure 4.20 showed that the simplified equations (e.g., ISO 17208-2) accurately estimated the PL values in deep water, as it had small thicknesses across most frequency bands. However, the envelope thickness near the surface suggests that predicting the PL values near the water surface using simplified equations is complex. These findings provide valuable insight into the complexities of underwater sound propagation by highlighting the intricate variances in model behavior and their sensitivity to water depth.

These findings reveal the complex relationship between model choice, sound speed profile, and bathymetry in shaping the understanding of underwater sound propagation. The study found that simplified models such as ECHO, SCA, and M-A show close agreement in predicting propagation loss values at a 100-meter range in shallow water. However, as the depth increases, the deviations between the models become more noticeable. The inclusion of bathymetry data in the PE model results in higher PL values below 200 Hz, highlighting the importance of bathymetry in the filtration of sound waves by shallow waters. At a distance of 500 metres, the accuracy of the simplified models is compromised across a wide frequency range in deeper waters. The variability observed in the grey envelope suggests that using simplified models for estimating PL may be challenging due to underlying environmental complexities. Therefore, the numerical PE model with the range-dependent SSP and the bathymetry profile is crucial to determining PL values. In deep water, the simplified models are acceptable for representing the PL values. Consequently, the glider added more understanding about how a source of noise contributes to the ocean ambient noise by accurately estimating the sound propagation loss value using the range-dependent sound speed profile. The apparent agreement among the vessel's URN obtained from the three platforms shown in Figure 4.16 indicates that the geometrical spreading model law is acceptable for deep-water conditions due to the minimal interaction of

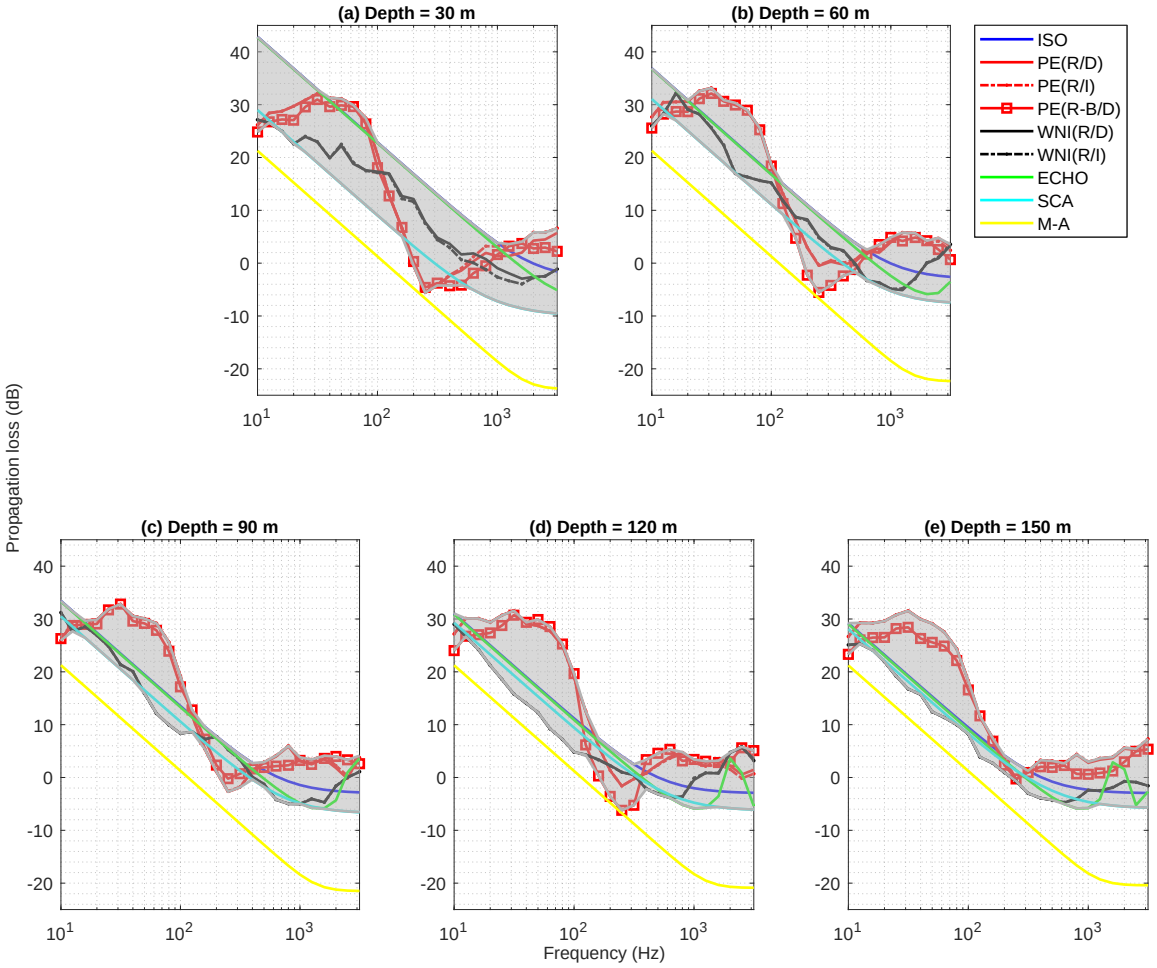

Figure 4.20: PL models were measured at six points through the water column 100 m apart from the source in the Brigus site (Deepwater). (R/D) range-dependent SSP. (R/I) range-independent SSP. (R-B/D) range-dependent SSP and bathymetry

the seabed.

The experimental data from this study showed that no single PL metric performed best in all water depths, array geometries, CPA distances, and frequency ranges. However, a robust metric should perform well over a wide range of measurement conditions and not just over a narrow range of conditions. This is particularly true when uncertainty in seabed geoacoustic properties is concerned, as these are difficult to measure reliably without considerable effort. Robustness across CPA ranges is also desirable in shallow water because the bathymetry profile restricts the distances at which hydrophones can be positioned to measure specific receiver angles. Generally,

standards, such as ISO-17208/1, ensure reproducibility by limiting allowable CPA distances to an optimal range during URN measurements.

4.2.5 Monopole source level

The MSL represents the vessel in the 1500 and 2000 rpm trials, and the URN is presented in Figure 4.21. The MSL below 100 Hz that was picked up by all three platforms went up after the environmental-driven PL correction that was found using the PE (R-B/D) model at each CPA point was applied. Ideally, this correction would result in the same MSL being recorded on the different recording platforms. This close alignment suggests that the model accurately compensates for environmental factors, confirming the PL model reliability and overall good performance Figure 4.16.

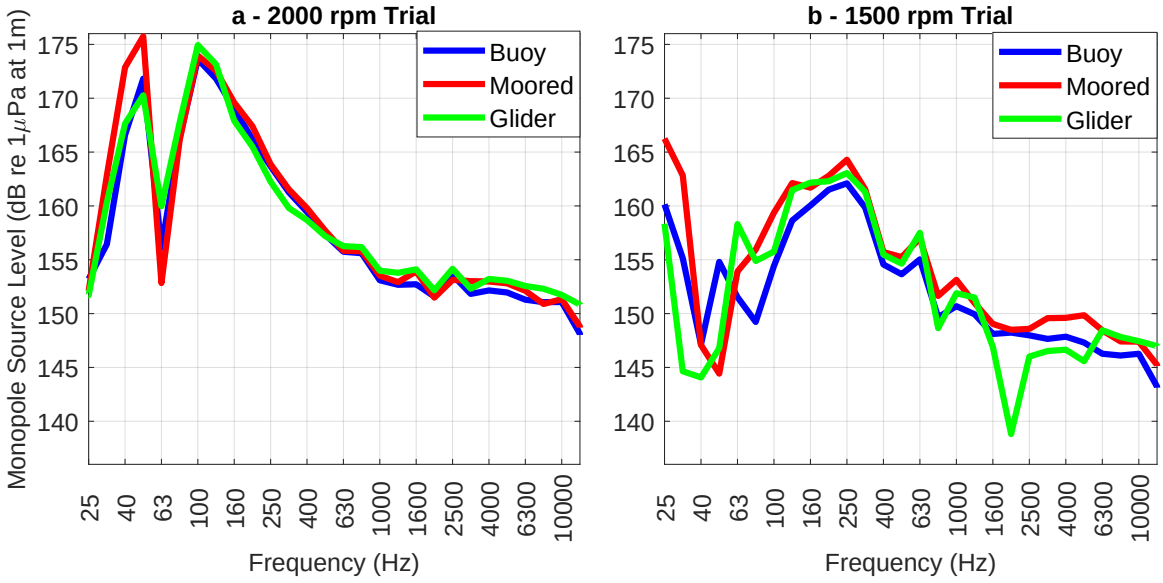

Figure 4.21: Monopole source levels of the vessel under testing by the three platforms at two engine speeds. The PL model used is PE (R-B/I).

4.3 Measurement uncertainty

Table 4.8 presents the parameters involved in the process of estimating the uncertainty in measuring the vessel noise signature. The study found that GPS-induced distance

uncertainty was 0.12 dB for an average CPA of 180 m, which was slightly lower than previous research by Keizer et al. in 2022. The study determined that the uncertainty in the distance between the vessel and the hydrophone was 0.2 dB at a 66% confidence level, without mentioning the specific methodology used [Keizer et al., 2022]. In summary, the accuracy of the CPA calculation is dependent on the precision of the measuring equipment. GPS technology plays a crucial role in enhancing this accuracy by reducing uncertainty in the measurement of CPA distance; consequently, reporting the CPA uncertainty is not common in research articles.

Table 4.8: The uncertainty value of each selected factor

Source of uncertainty	**Value ±**	**Probability distribution**	**Divisor**	**Standard uncertainty [dB]**
GPS[1,2,3]	4.9 m	Normal	2	0.12
Tilt angle[2]	13°	Rectangular	$\sqrt{3}$	0.36
Tilt angle[3]	9°	Rectangular	$\sqrt{3}$	0.22
Background noise	1.2, 0.3, 0.81 [dB] [1] 1.3, 0.8, 0.84 [dB] [2] 0.5, 1.5, 1 [dB] [3]	Normal	2	OTOB
Vessel directivity	0.7, 0.6, 0.5 [dB] [1] 1.2, 0.7, 0.4 [dB] [2] 1.6, 1.2, 0.8 [dB] [3]	Normal	1	OTOB
Frequency response	0.37, 0.30, 0.48 [dB] [1] 0.4, 0.3, 1.1 [dB] [2,3]	Normal	2	0.18, 0.15, 0.24 0.2, 0.15, 0.55
Source depth[1,2,3]	0.4 [m]	Rectangular	$\sqrt{3}$	0.2

[1] Ocean glider.
[2] Drifting buoy with an array of three hydrophones.
[3] Bottom-mounted hydrophone platform.

The built-in sensors inside the hydrophones recorded the tilt angles to be an average of 13° and 9.5° for the drifting buoy hydrophones and the seabed-mounted hydrophone, respectively. The inclination of the hydrophones led to a change in the slant range between the hydrophone and the vessel under testing to 0.36 dB and 0.22 dB of uncertainty in the assessed noise levels. According to ANSI/ASA, if the hydrophone orientation angle is greater than 5°, it will have a significant impact on the slant range. The ISO-17208/1 report also mentioned that the uncertainty of the GPS-induced distance and the movement of the hydrophone was 0.5 dB for all OTOB bands with a 66% confidence level, which matched the results.

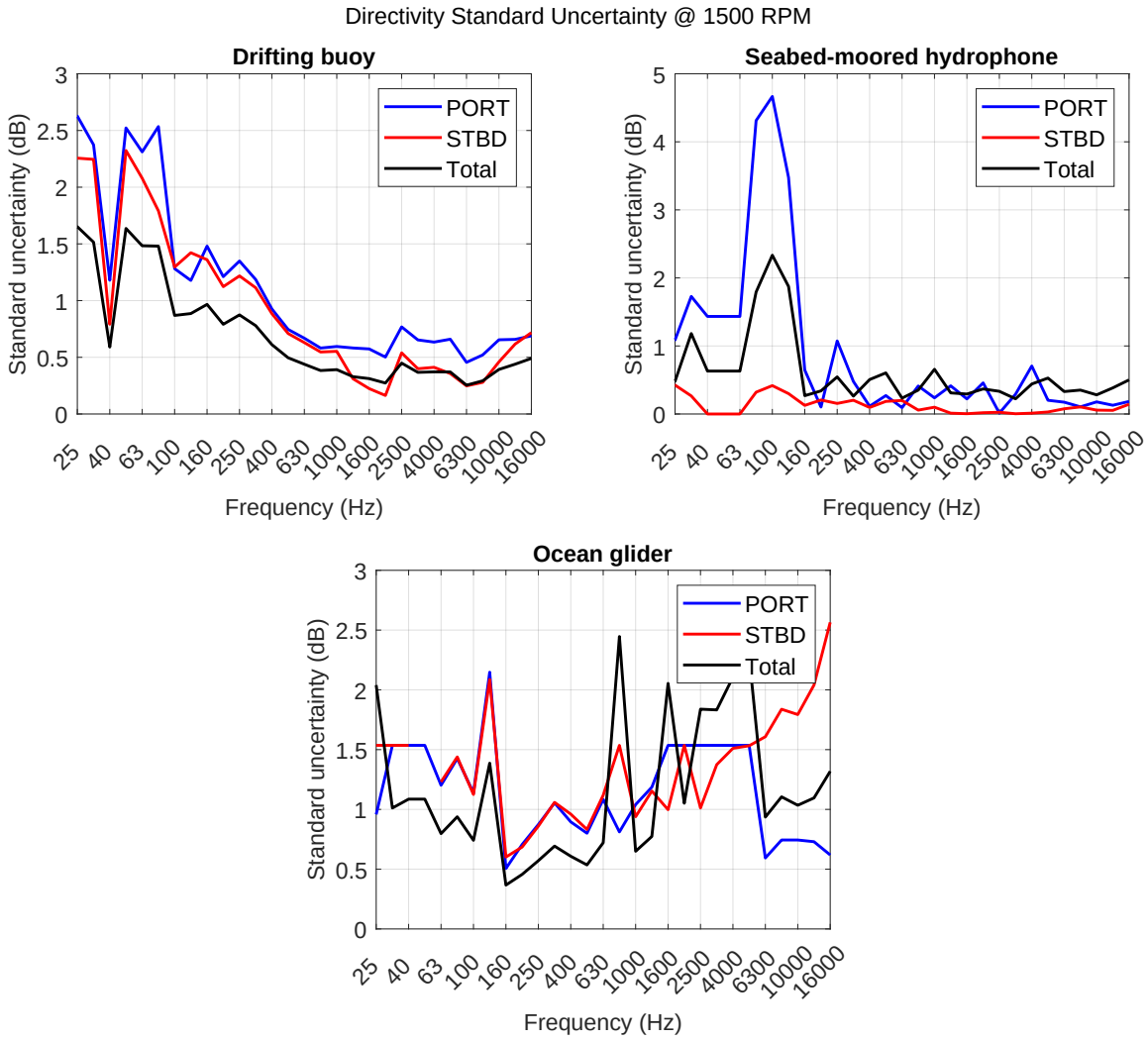

Figure 4.22: Standard uncertainty of vessel directivity at engine speed = 1500 rpm. The repeated runs represent the uncertainty on the port, starboard sides, and total. Three panels are for the three observer platforms in Conception Bay

Figures 4.22 and 4.23 provide crucial information regarding the standard uncertainty of vessel noise measurement at 1500 RPM and 2000 RPM engine speeds, respectively. The level of uncertainty is more significant at lower frequencies (specifically below 125 Hz), peaking at around 5 dB from the port side while the engine is running at 1500 RPM and 5.5 dB at 2000 RPM. The seabed-moored hydrophone had a noticeable discrepancy in the measured noise pattern between the port and starboard sides below 160 Hz, in comparison with the drifting buoy and ocean glider. This discrepancy leads to a significant standard uncertainty difference of 4 dB at 1500 RPM. The standard uncertainty, at 2000 rpm, is more closely matched between the port and starboard sides, except for a distinct 2.5 dB variation below 100 Hz that is recorded by the seabed-moored hydrophone. The total standard uncertainty of the directivity showed a noticeable pattern that is high at low frequencies and gradually decreases at high frequencies. Generally, as the engine speed is increased, there is a slight increase in the standard uncertainty by 0.5 dB, especially in the frequency band below 125 Hz.

In the comparative analysis illustrated in Figure 4.24, the three platforms have distinct capabilities in assessing underwater vessel noise, each with its own unique directivity standard uncertainty profile. The drifting buoy and seabed-moored hydrophone displayed similar patterns of uncertainty but with distinct variations across the spectrum. At 2000 RPM, the seabed-moored hydrophone showed greater standard uncertainty above 125 Hz than the drifting buoy, while their performance is comparable at 1500 RPM. The ocean glider had an interesting standard uncertainty pattern, specifically at frequencies exceeding 500 Hz in the 1500 RPM trials. Increased uncertainty results from surface noise contamination in the measurements when the glider approaches the water's surface during 1500 RPM trials. In contrast, when the glider reached a depth of approximately 85 m at 2000 RPM trials, it exhibited reduced uncertainty at lower frequencies compared to both the drifting buoy and seabed-moored hydrophone, aligning closely with the drifting buoy at higher frequencies.

Figure 4.25 illustrates notable fluctuations in background noise across various time intervals throughout the trials. The observations from the three platforms—the ocean glider, the drifting buoy, and the seabed-moored hydrophone—showed multiple patterns of standard uncertainty. The drifting buoy and glider presented comparable uncertainty throughout most of the spectrum, with a deviation of approximately 1 dB occurring only above 1 kHz. In contrast, the seabed-moored hydrophone had a lower uncertainty of 0.5 dB below 100 Hz but increased significantly to 3.3 dB at

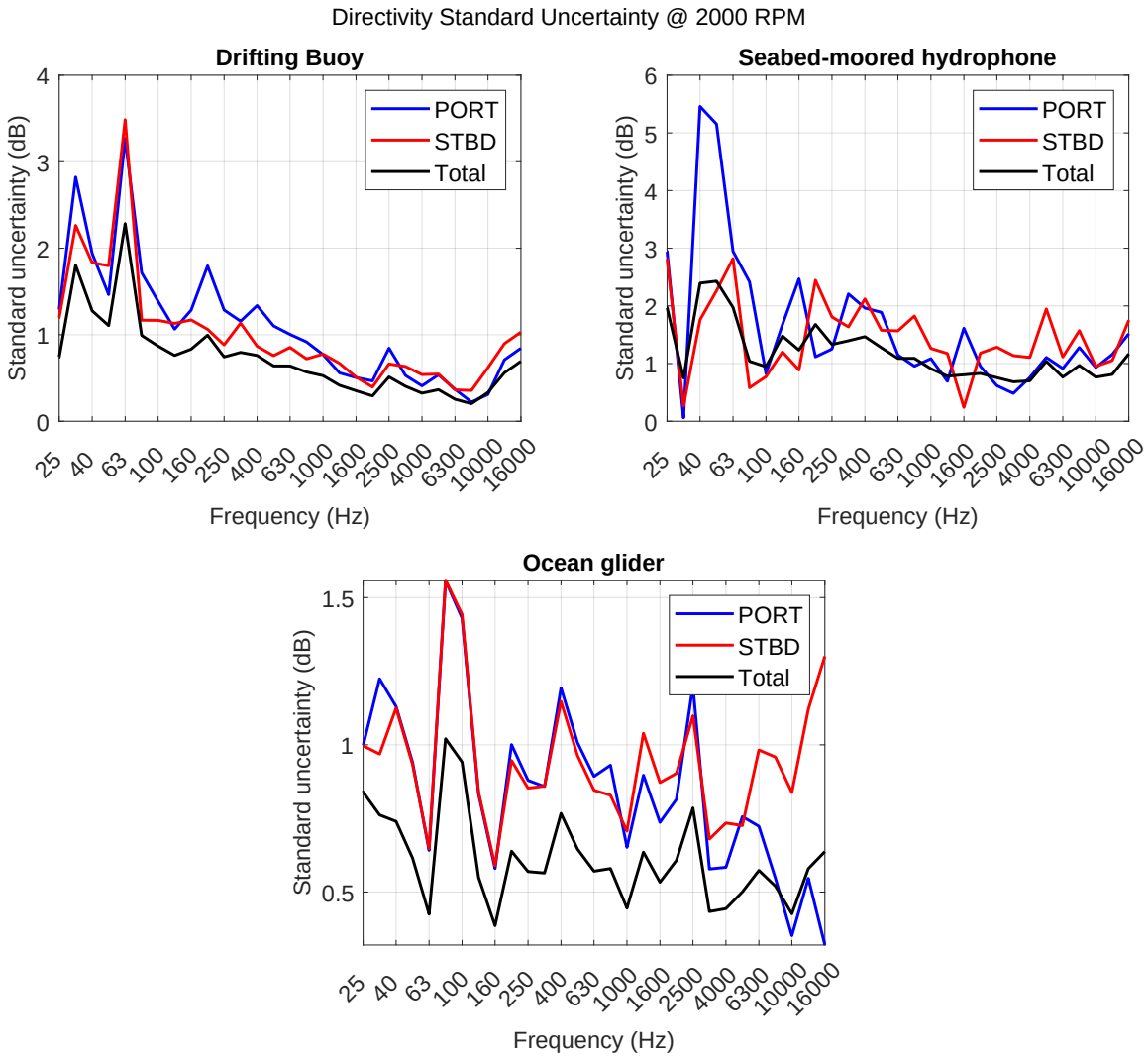

Figure 4.23: Standard uncertainty of vessel directivity at engine speed = 2000 rpm. The repeated runs depict the uncertainty on the port, starboard, and total sides of the vessel. Three panels are for the three observer platforms in Conception Bay

higher frequencies. The similarity in standard uncertainty between the drifting buoy and ocean glider can be attributed to their similar methods of averaging for background noise measurement. Both platforms conduct averaging at different depths in the water column, both prior to and following the experiments, in contrast to the seabed-moored hydrophone, which involved averaging at a fixed received point over the two same time periods.

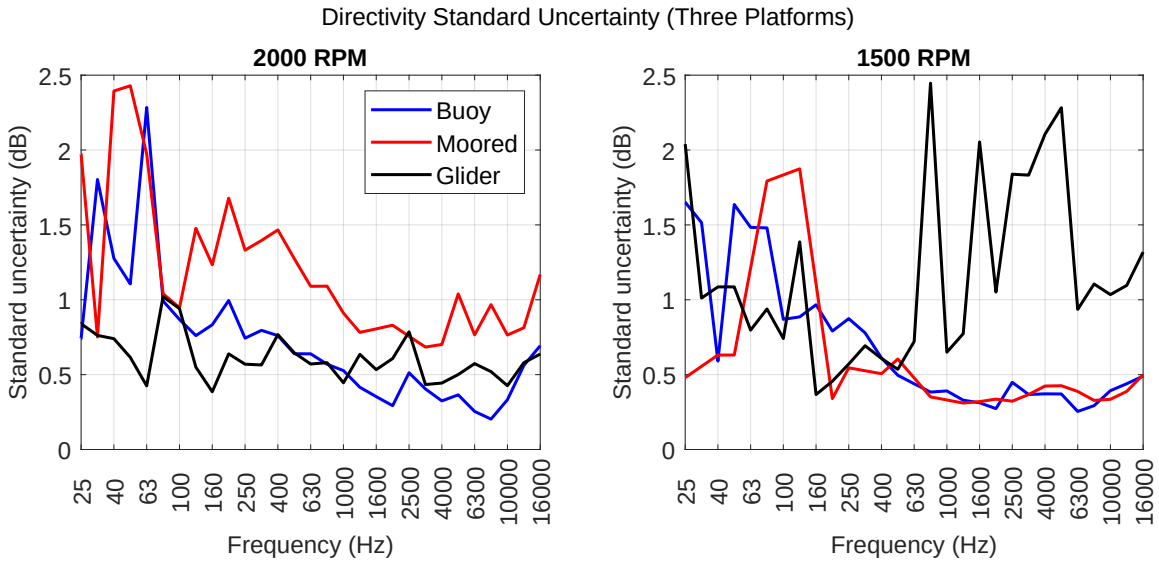

Figure 4.24: Comparison between the total vessel directivity calculated for the drifting buoy, seabed-moored, and the glider for the two engine speeds 1500 and 2000 rpm

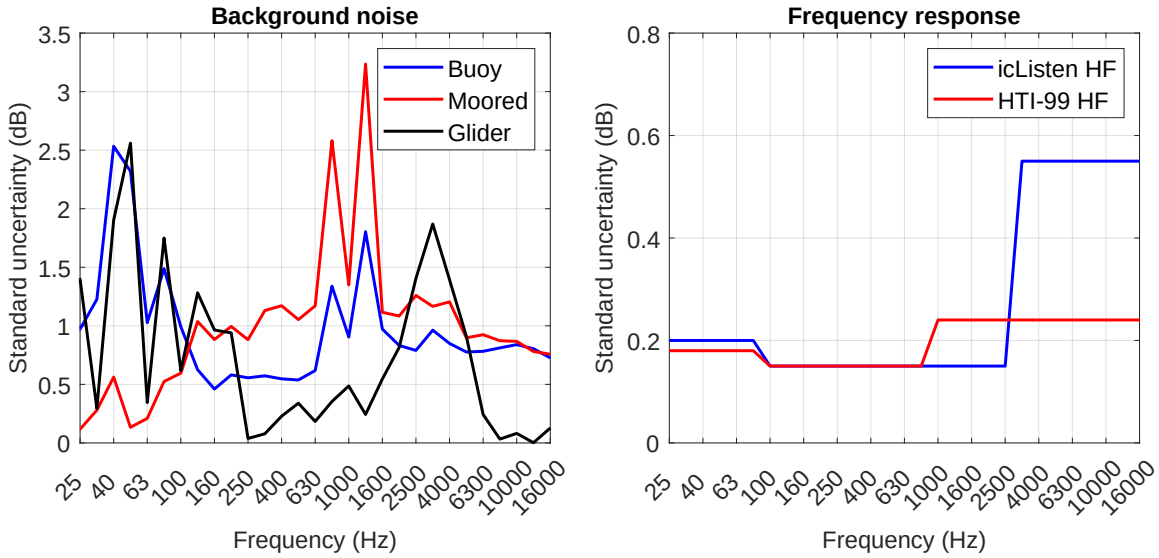

Figure 4.25: Background noise and frequency response standard uncertainty of the three PAM platforms

4.4 Conclusion

This study has yielded extensive insights into the characterization and measurement techniques of underwater vessel noise. The study investigated the URN of a fishing vessel through sea trials carried out in Petty Harbour-Maddox Cove and Conception

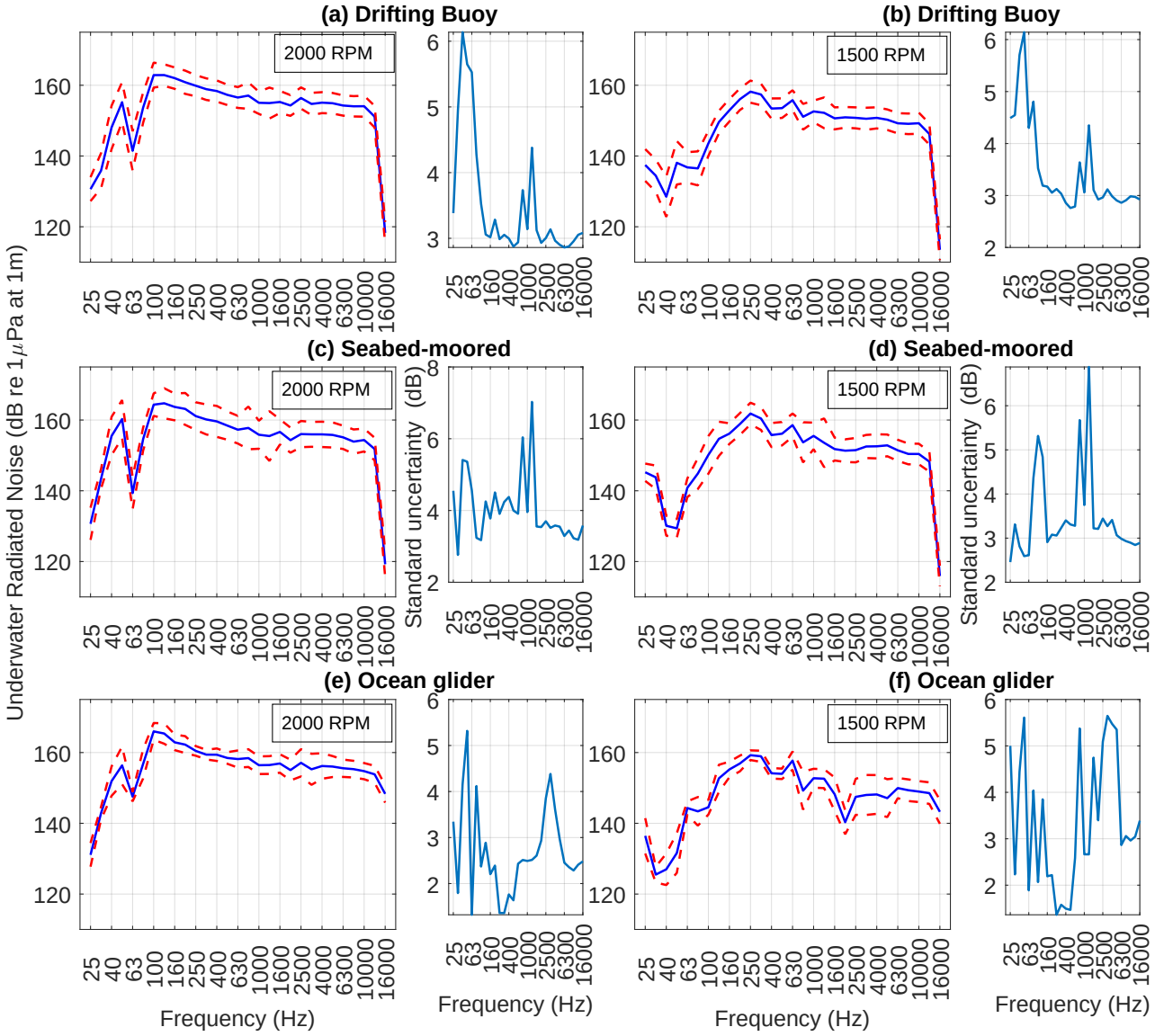

Figure 4.26: URN of the vessel under testing with the uncertainty limits. Two speeds are observed using the drifting buoy (a and b), seabed-moored (c and d), and ocean glider (e and f). The total uncertainty is represented in a small panel associated with each URN.

Bay, utilizing various platforms such as a glider, an array of hydrophones, and a bottom-mounted hydrophone.

The study assessed the effectiveness of an ocean glider as a platform for passive acoustic monitoring. The glider showed performance that was either comparable to or exceeded that of traditional platforms in assessing vessel noise, while also achieving

lower measurement uncertainties across the majority of frequency bands. The investigation highlighted the significance of taking into account environmental elements, including sound speed profiles and bathymetry, for precise estimation of monopole source levels.

The experimental data from this study showed that no single SL metric performed best over all of the water depths, array geometries, CPA distances, and frequency ranges. However, a robust metric should perform well over a wide range of measurement conditions and not just over a narrow range of conditions. This is particularly true when uncertainty in seabed geoacoustic properties is concerned, as these are difficult to measure reliably without considerable effort. Robustness across CPA ranges is also desirable in shallow water because bathymetry restricts the distances at which hydrophones can be positioned to measure specific receiver angles. Generally, standards, such as ISO-17208/1, ensure reproducibility by limiting allowable CPA distances to an optimal range during URN measurements.

The investigation demonstrated that the engine plays a substantial role in the vessel's noise profile, especially at frequencies under 500 Hz, whereas the contribution of the propeller becomes more pronounced at elevated frequencies as a result of cavitation phenomena.

Though marine vessels have various sources that contribute to their overall noise signature, they can be assumed to be a single sound source point. This assumption is a loose approximation because of the contribution to the underwater noise signature of multiple complex sources. The methodology in this chapter is valid only for far-field measurements (when the directivity of the source is not significant) or in the assessment of retrofit-induced changes and noise reduction studies.

Chapter 5

Discussion: Direction of arrival using a glider

This chapter is based on the published article:

- *Advancing Glider-based Measurements of Underwater-Radiated Ship Noise*, which is under review in *The Journal of the Acoustical Society of America*, *Vol.*: 156(4) and *ISSN*: 0001-4966 [Helal et al., 2024c].

5.1 Overview

One key motivation for PAM-type glider missions is not only to measure sound amplitudes or identify the source, but also to localize them [Jiang et al., 2019; Kowarski et al., 2020; Stinco et al., 2021; Wang and Yuan, 2021a]. In general, locating a sound source requires information on the time delay of receiving a signal between at least three hydrophones required to identify an omnidirectional sound source. Processing these time delays can be used to calculate the relative angle of the sound source to the receiver (hydrophones), referred to in the literature as Direction of Arrival (DOA) [Zhang and Rao, 2009; Yang et al., 2017; Li et al., 2019; Tokgöz et al., 2020]. For the case of only two hydrophones, the time-delay information produced a mirror result, allowing two possible sets of angles where the source (vessel) could be on the port or starboard side of the glider. There has been some work with sound data to compute DOA from a set of only two hydrophones to a moving sound target [Yang et al., 2017;

Li et al., 2019]. Here, I attempted a different approach, utilizing the directional sensitivity of the glider's HTI hydrophones and showing an accurate estimation of DOA to a moving sound source relative to the glider in two cases: (i) the vessel and glider have the same heading; (ii) the glider and vessel have the opposite heading. This approach is simple and can be used on platforms where both hydrophones are pointed in the same direction. In addition, the limitations of this approach have been discussed.

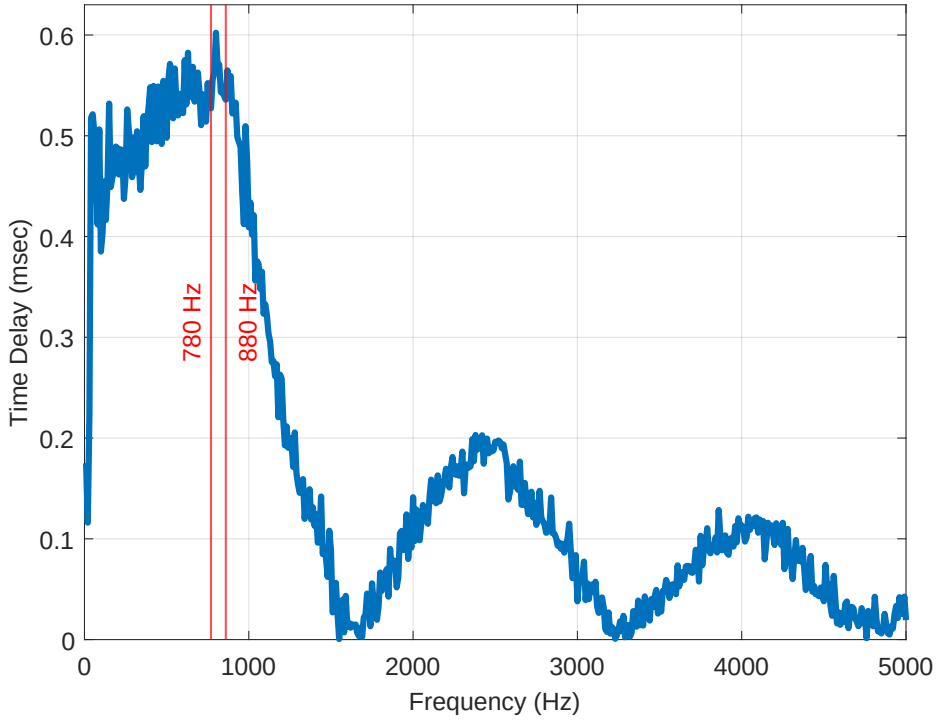

Figure 5.1: Time delay estimation at different frequency 1/3 octave bands

5.2 Time delay

The ocean glider was equipped with only two hydrophones, placed at a fixed distance of 0.9 metres on the port and starboard wings. Orienting the hydrophones pointing to the glider's aft resulted in significant directional sensitivity to sound waves coming from the glider's back. The signal-to-noise ratio (SNR), the distance between the two hydrophones (d_H), and the characteristics of the sound source influence the frequency range of the DOA estimate [Tokgöz et al., 2020; Stinco et al., 2021]. Time delay was plotted against frequency, and the effective frequency range of DOA estimation

in the study was between 790 and 820 Hz (see Figure 5.1), where the sound wavelength is precisely twice the hydrophone separation distance [Zhang and Rao, 2009; Chen et al., 2023]. The DOA depends mainly on the time delay (τ) between the two signals received by the hydrophones. The zero time delay means that the source is located precisely at 0° in the north direction. The time delay is calculated using the cross-spectrum method [Tachioka et al., 2012; Chen et al., 2023]. The maximum possible time delay can be approximately 0.6 milliseconds, calculated as the relationship between d_H and the average sound speed (c_w). Figure 5.1 illustrates an extended analysis of the received sound levels that represents the change in time delay in the frequency domain and reveals the distinct effective frequency range to estimate DOA. The time delay was about to hit 0.6 ms at a frequency range between 780 and 880 Hz, which aligns with the theoretical estimation using the half-wavelength principle.

$$DOA = \sin^{-1}(\frac{\tau.c_w}{d_H}) \tag{5.1}$$

5.3 Source heading relative to the glider

The glider's pitch angle had a minimal variation during diving and climbing, less than ±1.2°, which had negligible impact on sound arrival to the hydrophones. A 360-degree view around the glider was considered to determine the vessel's position relative to the glider. The time delay sign was critical in determining the vessel's position within a semicircle. That analysis showed a negative sign indicating that the vessel was located on the port side of the glider in both trials, and this is consistent with the actual recorded geographic data during the sea trials. After identifying the semicircle, the direction angle was reduced from 360 degrees to a range of 180 degrees. An essential question at this point pertained to the vessel's movement, precisely whether it was aligned with or opposed to the glider's heading direction. The received sound pressure level was utilized to address the question. As a result, the received sound level increased when the vessel was positioned behind the glider but lowered once the vessel had passed the glider, as shown in Figure 5.2 a and b. This comparison is feasible when the selected points are equidistant from the CPA.

Therefore, six points were selected prior to and after the CPA between the vessel and the glider. The points shown in Figure 5.2 were approximately equal distances

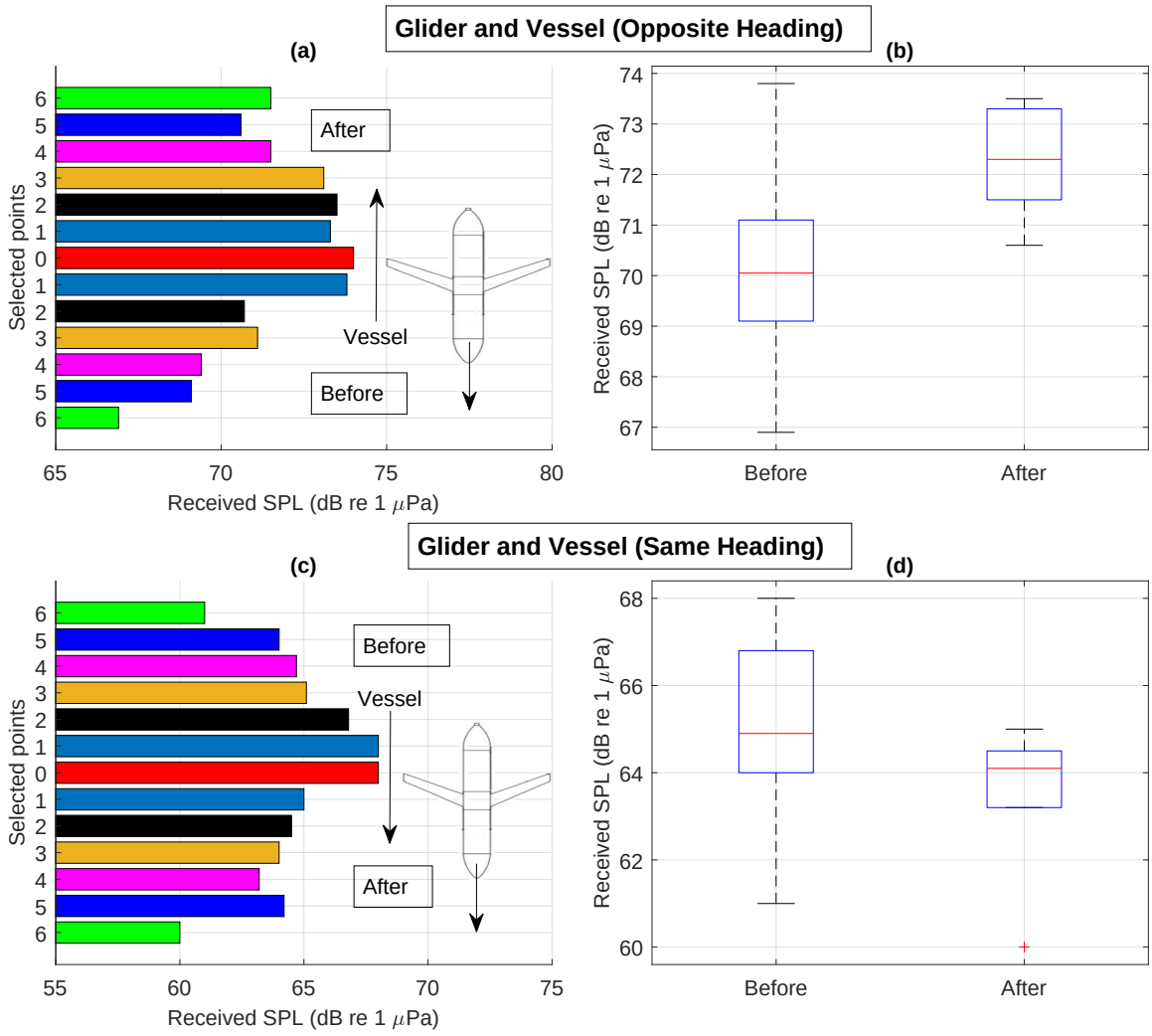

Figure 5.2: The received sound levels by the glider for six vessel locations before and after passing the glider. The zero point is at the CPA. (a) The vessel and glider have the opposite heading. (c) Show the received sound levels when both have the same heading. (b & d) illustrate the mean and standard deviation of the received sound levels at six locations before and after passing the glider

from the CPA (point ”0”). The received sound levels were measured at all 12 locations of the vessel. The direction of the ship was determined by comparing the sound levels received before and after the ship passed the glider at the corresponding points. An increase in the average mean of received sound after the vessel passes the glider suggests that the vessel is likely following a similar heading angle as the glider. In contrast, a decrease in the average mean after passing the glider indicates that the vessel is moving in the opposite direction of the glider. This allowed for precise

identification of the vessel's movement in relation to the glider's trajectory.

The HTI hydrophones have consistent sensitivity from 50 to 10,000 Hz, with a minimal uncertainty of $\pm 0.1 dB$. Figure 5.2(b and d) display the mean and standard deviation values for the received sound levels measured at six equidistant points before and after the vessel passage of the glider. The standard deviation was evaluated to represent the uncertainty in DOA, as it is a simple metric of variance in sound levels received during the vessel's approach and departure from the glider. This variation is caused by the changing distance between the sound source and the receiver, as the sound transmission is significantly affected by this distance.

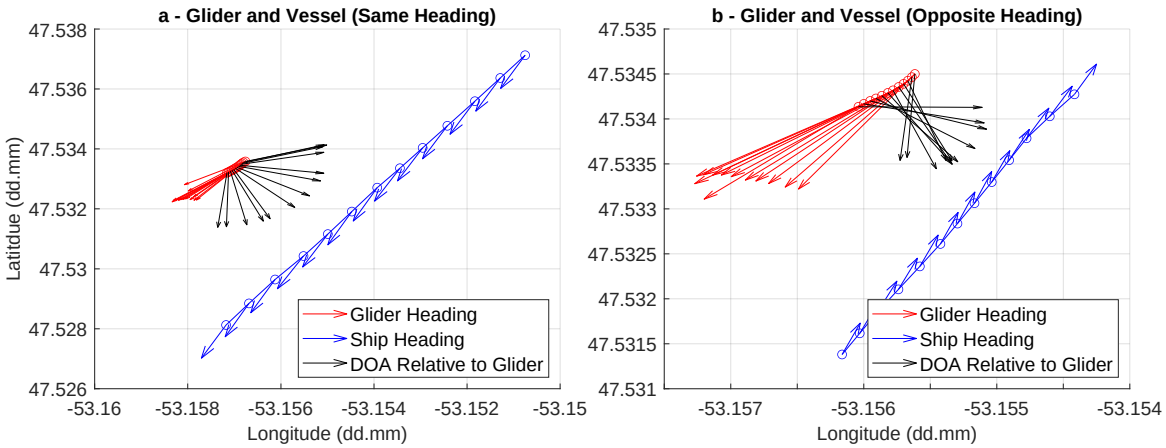

Figure 5.3: The DOA of the vessel relative to the glider is represented in black arrows. Two trials represent the same and opposite headings between the vessel and the glider.

5.4 Angle correction

The DOA values were corrected after determining the vessel's relative movement direction to the glider. Figure 5.3(a) represents a trial in which the glider and the vessel (9 knots) had the same heading, and the estimated DOA obviously pointed towards the direction of the vessel at each point of motion. Figure 5.3(b) shows the opposite heading between the glider and the vessel. The vessel was sailing at a lower speed of 6 knots. Thus, the glider with two hydrophones successfully estimated the angle of any sound source emitting a frequency above 800 Hz. However, the system is not sufficient in getting the elevation angle because of one-dimensional spatial information

using only two hydrophones. Additional experiments are necessary to improve the understanding of the glider's ability to detect DOA under different operating conditions and in lower signal-to-noise ratio (SNR) scenarios, such as sea trials during sea-state 3 or more. These experiments will provide insights into the glider's reliability in practical scenarios. It is essential to acknowledge that the glider's ability to determine the distance of the source was limited by the number of hydrophones used. A third hydrophone would need to be attached to estimate the distance from the glider to the source. This would also enhance and verify the method used to estimate DOA. In future trials with this glider, I intend to equip it with an additional hydrophone to further evaluate this method.

Chapter 6

Conclusion

This research has successfully addressed the main research questions concerning the performance of autonomous underwater gliders in monitoring and assessing vessels' noise signature levels. The research questions were answered by studying the underwater noise of a fishing vessel in Newfoundland and Labrador, Canada.

6.1 Sources of noise in a fishing vessel

Firstly, the overall results of underwater radiated noise have shed light on the significant role of fishing vessels in contributing to the overall spectrum of oceanic ambient noise, either while sailing or stationary. Specifically, the study highlights the substantial impact of fishing vessel engines on acoustic energy emissions, particularly at frequencies of 63 and 125 Hz. Furthermore, the rotation of propellers induces additional disturbances, notably at frequencies exceeding 250 Hz, primarily due to cavitation events. The engine contributed more than 60% at low frequencies (below 250 Hz) and in specific bands (63 Hz, 100 Hz, and 250 Hz), with values surpassing 70%. The propeller substantially contributed more to the URN at frequencies ranging from 16 Hz to 50 Hz and at mid-frequencies between 400 Hz and 4000 Hz.

These findings underscore the importance of comprehending and mitigating the noise emissions of fishing vessels to safeguard marine ecosystems and minimize potential adverse effects on aquatic life. To conclude, the first study was important for

identifying the sources of noise on the fishing vessel being measured and determining its noise signature levels. This information was essential for involving the AUG in conducting a similar investigation and investigating its performance in PAM missions.

6.2 Glider self-noise

The first topic of investigation was the gliders' self-noise. This is a significant limitation in their use for PAM missions. The self-noise was assessed through several dives in shallow (< 70 m) and deep (< 210 m) water. The sources of self-noise were found to be the actuated motors of the glider buoyancy engine, pitch battery-pack, and fin, and the hydrodynamic noise was negligible due to its slow speed (< 0.4 m/sec). The buoyancy pump created broadband noise between 10 Hz and 12.5 kHz for 26 seconds during the first part of the dive. Before the glider reached the maximum depth, the fin noise could be eliminated by averaging the sound level along the water column due to its intermittent small intervals (< 0.5 sec). Thus, the gliders are capable of acquiring acoustic data with a high signal-to-noise ratio during their descent and ascent while simultaneously discarding data that has been contaminated by the noise emitted from the oil pump.

In conclusion, the AUG is a quiet platform, and its use in passive acoustic monitoring missions presents numerous advantages and promising prospects for advancing the understanding of the ocean environment. AUGs are versatile tools capable of conducting various passive acoustic monitoring missions, including the measurement of underwater noise generated by vessels and improved post-processing of source level estimation. AUGs also allow us to collect extensive, autonomous data on temporal and spatial variations across vast ocean areas, enhancing our grasp of oceanographic characteristics and underwater noise levels.

6.3 Glider performance in PAM

Acoustic AUGs are versatile tools that can conduct various PAM missions, including monitoring ocean soundscapes, detecting and characterizing marine species, and measuring underwater noise from vessels. The understanding of oceanographic characteristics and underwater noise levels can also be expanded by deploying AUGs,

which allows us to collect helpful information autonomously on temporal and spatial changes in large areas of the ocean.

In Conception Bay, the autonomous underwater glider was utilized to assess the underwater noise signature of a fishing vessel similar to the one used in the early trial in Petty Harbour-Maddox Cove with only the array of three hydrophones. A simultaneous comparison with two other fixed platforms was conducted. The findings show that the glider's data closely matches the data from other platforms, with an approximate error range of 1 to 2 dB. The glider has a lower standard deviation between repetitions than the hydrophone array at mid-frequencies (200–2000 Hz), indicating its effectiveness in collecting acoustic data. The observations suggest that the glider's operating depth significantly impacts data quality. In one trial at 1500 RPM engine speed, the glider almost reached the seafloor, causing increased uncertainty at low frequencies due to the effect of long-distance low-frequency noise. I suggest conducting multiple vessel runs (at least 5 or 6) at the same engine speed when measuring with an AUG to minimize potential disturbances caused by the seafloor or water surface.

Moreover, due to the increase in glider position uncertainty in rough environmental situations, acoustic gliders are unsuitable for quantifying the source level of ship noise in harsh environmental conditions, despite their potential for URN monitoring and identification.

6.4 Sound propagation loss

The second goal of this study is to investigate the ability of AUGs to improve sound propagation loss models by using the oceanographic samples collected across the water column. The advantage of this data holds the potential to shed light on sound speed variations across horizontal distances and throughout the water column. By integrating range- and depth-dependent oceanography data with seafloor acoustic characteristics and its bathymetry profile, a more comprehensive understanding of sound propagation behavior can be achieved in remote areas. This integrated approach is particularly valuable in shallow water environments, where reflections from the sea surface and seafloor can significantly impact sound propagation. The combination of oceanography and PAM data collected by the glider promises to improve the

understanding of sound propagation in a remote area without significant discrepancies in the reported noise levels and the influence of diminishing over long distances, particularly the low frequencies emitted from marine vessels.

The study used six propagation loss models to determine PL values at distances of 100 and 500 metres from the sound source in shallow and deep water environments. The Holyrood trial showed that the simplified models ECHO, SCA, and M-A produced similar estimates of PL at 100 metres. However, as the distance increased, the differences between models became more apparent. The PE model showed a significant deviation from the other models below 200 Hz, leading to higher PL values. The M-A model showed a significant deviation in the deep water trial, significantly above 200 Hz. The PE model showed a similar pattern, particularly in representing high PL values between 30 and 150 Hz. Actual bathymetry data had a more minor effect on the PE model than the flat assumption. These findings reveal the complex relationship between model choice, sound speed profile, and bathymetry in shaping the understanding of underwater sound propagation. The agreement between PE models below 250 Hz and the accurate representation of PL values above 250 Hz by the WNI or simplified models with range-dependent SSP is significant.

6.5 Overall comments and recommendations

Despite these significant achievements, it is important to acknowledge certain limitations in this research. The scope of this study focused primarily on fishing vessels and their underwater noise emissions, with the potential for broader applications to other vessel types. Methodological considerations regarding the estimation of measurement uncertainties in passive acoustic monitoring data, particularly when comparing data from different platforms, water depths, and environmental conditions, remain an ongoing challenge. A comprehensive methodology for estimating and reporting uncertainties in passive acoustic monitoring of underwater noise is still under development and requires further investigation.

In the Petty Harbour-Maddox Cove trials, the study employed a propagation loss model that assumed a flat seafloor topology, as precise bathymetry data for the area was unavailable. The previously mentioned assumption has the potential to introduce a few uncertainties in the evaluation of sound propagation, which may impact the

precision of the outcomes. Acquiring bathymetry data with greater precision for the study area might improve the accuracy of the propagation loss model, as explained by the Conception Bay trials where the seabed profile was available. Additionally, it is crucial to validate the numerical PL models experimentally. A calibrated underwater sound source and receiver should be deployed in the area of the sea trials, ensuring the distance between them is aligned with the CPA values between the vessel and the PAM system.

In conclusion, this study has provided valuable insights into glider self-noise and sound propagation loss in shallow water environments. These insights hold considerable importance for researchers and marine scientists engaged in passive acoustic monitoring and underwater acoustics, facilitating more accurate interpretation of acoustic data and improved assessment of noise source impacts on marine ecosystems. Furthermore, the quest to establish a comprehensive methodology for estimating uncertainties in passive acoustic monitoring remains an ongoing pursuit with the potential to enhance the reliability and comparability of PAM data in various oceanic conditions.

The use of AUGs for PAM missions leverages their mobility, endurance, and ability to collect comprehensive acoustic data, making them a valuable tool for improving the knowledge of marine ecosystems and informing conservation and management efforts.

6.6 Future work

Improvements to the study could expand our understanding of acoustic measurements using gliders.

Increasing the number of hydrophones on the glider's wings from two to three would yield more extensive data. Relocating hydrophones to the glider's hull may influence results because of the glider's self-noise and requires careful consideration.

Additional measurements in shallow waters (less than 150 m deep) are necessary for a more accurate assessment of glider performance. Incorporating more categories of vessel types operating under various conditions would produce more generic data.

To ensure accuracy, it is essential to experimentally validate the PL model using a known sound source, especially in shallow water environments. That would help to understand the impact of parameters on developing numerical PL models.

Bibliography

United Nations Conference on Trade and Development (UNCTAD). Review of Marine Transport). Technical report, United Nations, Geneva, 2023.

Susanna B. Blackwell, Charles R. Greene, and W. John Richardson. Drilling and operational sounds from an oil production island in the ice-covered Beaufort Sea. *The Journal of the Acoustical Society of America*, 2004. doi: 10.1121/1.1806147.

Patrick Miller, Petter Kvadsheim, Frans-Peter Lam, Paul Wensveen, Ricardo Antunes, Ana Alves, Fleur Visser, Lars Kleivane, Peter Tyack, and L. Silve. The severity of behavioral changes observed during experimental exposures of killer (orcinus orca), long-finned pilot (globicephala melas), and sperm (physeter macrocephalus) whales to naval sonar. *Aquatic Mammals*, 2012. doi: 10.1578/AM.38.4.2012.362.

George V. Frisk. Noiseonomics: The relationship between ambient noise levels in the sea and global economic trends. *Scientific Reports*, 2012. doi: 10.1038/srep00437.

R.K. Andrew, B.M. Howe, J.A. Mercer, and M.A. Dzieciuch. Ocean ambient sound: Comparing the 1960s with the 1990s for a receiver off the California coast. *Acoustic Research Letters Online*, 2002. doi: 10.1121/1.1461915.

Mark A. McDonald, John A. Hildebrand, and Sean M. Wiggins. Increases in deep ocean ambient noise in the Northeast Pacific west of San Nicolas Island, California. *The Journal of the Acoustical Society of America*, 2006. doi: 10.1121/1.2216565.

N. Ross Chapman and Andrea Price. Low frequency deep ocean ambient noise trend in the Northeast Pacific Ocean. *The Journal of the Acoustical Society of America*, 2011. doi: 10.1121/1.3567084.

Rex K. Andrew, Bruce M. Howe, and James A. Mercer. Long-time trends in ship traffic noise for four sites off the North American West Coast. *The Journal of the Acoustical Society of America*, 2011. doi: 10.1121/1.3518770.

R. Williams, A. J. Wright, E. Ashe, L. K. Blight, R. Bruintjes, R. Canessa, C. W. Clark, S. Cullis-Suzuki, D. T. Dakin, C. Erbe, P. S. Hammond, N. D. Merchant, P. D. O'Hara, J. Purser, A. N. Radford, S. D. Simpson, L. Thomas, and M. A. Wale. Impacts of anthropogenic noise on marine life: Publication patterns, new discoveries, and future directions in research and management. *Ocean and Coastal Management*, 2015. doi: 10.1016/j.ocecoaman.2015.05.021.

Lauren McWhinnie, Leh Smallshaw, Norma Serra-Sogas, Patrick D. O'Hara, and Rosaline Canessa. The grand challenges in researching marine noise pollution from vessels: A horizon scan for 2017. *Frontiers in Marine Science*, 2017. doi: 10.3389/FMARS.2017.00031.

Scott D. Kraus, Moira W. Brown, Hal Caswell, Christopher W. Clark, Masami Fujiwara, Philip K. Hamilton, Robert D. Kenney, Amy R. Knowlton, Scott Landry, Charles A. Mayo, William A. McLellan, Michael J. Moore, Douglas P. Nowacek, D. Ann Pabst, Andrew J. Read, and Rosalind M. Rolland. North atlantic right whales in crisis. *Science*, 2005. doi: 10.1126/science.1111200.

Rosalind M. Rolland, Susan E. Parks, Kathleen E. Hunt, Manuel Castellote, Peter J. Corkeron, Douglas P. Nowacek, Samuel K. Wasser, and Scott D. Kraus. Evidence that ship noise increases stress in right whales. *Proceedings of the Royal Society B: Biological Sciences*, 2012. doi: 10.1098/rspb.2011.2429.

Natacha Aguilar de Soto, Natali Delorme, John Atkins, Sunkita Howard, James Williams, and Mark Johnson. Anthropogenic noise causes body malformations and delays development in marine larvae. *Scientific Reports*, 2013. doi: 10.1038/srep02831.

Scott D. Kraus, Robert D. Kenney, Charles A. Mayo, William A. McLellan, Michael J. Moore, and Douglas P. Nowacek. Recent scientific publications cast doubt on north atlantic right whale future. *Frontiers in Marine Science*, 3:137, 2016. ISSN 2296-7745. doi: 10.3389/fmars.2016.00137.

Christine Erbe, Sarah A. Marley, Renée P. Schoeman, Joshua N. Smith, Leah E. Trigg, and Clare Beth Embling. The Effects of Ship Noise on Marine Mammals—A Review. *Frontiers in Marine Science*, 2019. doi: 10.3389/fmars.2019.00606.

Steven Benjamins, Wayne Ledwell, Julie Huntington, and Anthony Raphael Davidson. Assessing changes in numbers and distribution of large whale entanglements in newfoundland and labrador, canada. *Marine Mammal Science*, 2012. doi: 10.1111/j.1748-7692.2011.00511.x.

Anthony D. Hawkins and Arthur N. Popper. A sound approach to assessing the impact of underwater noise on marine fishes and invertebrates. *ICES Journal of Marine Science*, 2016. doi: 10.1093/icesjms/fsw205.

Transport Canada. Quiet Vessel Initiative (QVI). https://tc.canada.ca/en/programs/quiet-vessel-initiative, 2020.

North Atlantic Treaty Organization (NATO). Undersea Research Centre Human Diver and Marine Mammal Risk Mitigation Rules and Procedures. Technical report, NATO Undersea Research Centre, 2008.

European Union Commission Decision 2017. laying down criteria and methodological standards on good environmental status of marine waters and specifications and standardised methods for monitoring and assessment, and repealing Decision 2010/477/EU. Technical report, New York, 2017.

United Nations. Nineteenth Meeting of the United Nations Open-Ended Informal Consultative Process on Oceans and the Law of the Sea: Anthropogenic Underwater Noise. Technical report, New York, June 2018.

Protection of the Arctic Marine Environment (PAME). Underwater Noise in the Arctic: A State of Knowledge Report. Protection of the Arctic Marine Environment (PAME) Secretariat, Akureyri. Technical report, New York, 2019.

Simone Cominelli, Rodolphe Devillers, Harald Yurk, Alexander MacGillivray, Lauren McWhinnie, and Rosaline Canessa. Noise exposure from commercial shipping for the southern resident killer whale population. *Marine Pollution Bulletin*, 2018. doi: 10.1016/j.marpolbul.2018.08.050.

Laura Recuero Virto, Hervé Dumez, Carlos Romero, and Denis Bailly. How can ports act to reduce underwater noise from shipping? Identifying effective management frameworks. *Marine Pollution Bulletin*, 2022. doi: 10.1016/j.marpolbul.2021.113136.

American Bureau of Shipping. Guide for the Classification Notation Underwater Noise and External Airborne Noise. Technical report, TX, USA, 2022. URL `https://ww2.eagle.org/content/dam/eagle/rules-and-guides/current/other/295-guide-notation-underwater-noise-and-external-airborne-noise-2022/uwn-airn-guide-july22.pdf`.

DNV GL. Part 6 Additional class notations, Chapter 7 Environmental protection and pollution control, Section 6 Underwater noise emission - silent. Technical report, Rules for the Classification of Ships, 2017.

Lloyd's Register Group Limited. ShipRight Design and Construction, Additional Design Procedures, Additional Design and Construction Procedure for the Determination of a Vessel's Underwater Radiated Noise. Technical report, ShipRight Design and Construction, 2018.

Bureau Veritas. Underwater Radiated Noise (URN). Technical report, Rule Note NR 614 DT R00 E, 2014.

Leila S. Lemos, Joseph H. Haxel, Amy Olsen, Jonathan D. Burnett, Angela Smith, Todd E. Chandler, Sharon L. Nieukirk, Shawn E. Larson, Kathleen E. Hunt, and Leigh G. Torres. Effects of vessel traffic and ocean noise on gray whale stress hormones. *Scientific Reports*, 12, 2022. doi: 10.1038/s41598-022-14510-5.

Brian G. Ferguson, Kam W. Lo, and Joshua D. Rodgers. Sensing the underwater acoustic environment with a single hydrophone onboard an undersea glider. In *OCEANS'10 IEEE Sydney, OCEANSSYD 2010*, 2010. doi: 10.1109/OCEANSSYD.2010.5603889.

Joseph H. Haxel, Haru Matsumoto, Christian Meinig, Gabriella Kalbach, T. K. Lau, Robert P. Dziak, and Scott Stalin. Ocean sound levels in the northeast Pacific recorded from an autonomous underwater glider. *PLoS ONE*, 2019. doi: 10.1371/journal.pone.0225325.

Pierre Testor, Brad DeYoung, Daniel L. Rudnick, Scott Glenn, Daniel Hayes, et al. OceanGliders: A component of the integrated GOOS. *Frontiers in Marine Science*, 2019. doi: 10.3389/fmars.2019.00422.

Mark F. Baumgartner, Julianne Bonnell, Peter J. Corkeron, Sofie M. Van Parijs, Cara Hotchkin, Ben A. Hodges, Jacqueline Bort Thornton, Bryan L. Mensi, and Scott M. Bruner. Slocum Gliders Provide Accurate Near Real-Time Estimates of Baleen Whale Presence From Human-Reviewed Passive Acoustic Detection Information. *Frontiers in Marine Science*, 2020. doi: 10.3389/fmars.2020.00100.

Fabiano Marcos de Lima, Carlos Correa, William Soares Filho, Catia Galottas, José Antonio Moreira Lima, and Thiago Pires de Paula. An underwater acoustic modelling framework for Santos Basin, Brazil. *Proceedings of Meetings on Acoustics*, 2020. doi: 10.1121/2.0001347.

Cheng Jiang, Jian Long Li, and Wen Xu. The use of underwater gliders as acoustic sensing platforms. *Applied Sciences (Switzerland)*, 2019. doi: 10.3390/app9224839.

Rob Williams, Christine Erbe, I Made Iwan Dewantama, and I Gede Hendrawan. Effect on ocean noise: Nyepi, a balinese day of silence. *Oceanography*, June 2018.

Haru Matsumoto, Joseph H. Haxel, Robert P. Dziak, Delwayne R. Bohnenstiehl, and Robert W. Embley. Mapping the sound field of an erupting submarine volcano using an acoustic glider. *The Journal of the Acoustical Society of America*, 2011. doi: 10.1121/1.3547720.

Nicolai von Oppeln-Bronikowski, Mingxi Zhou, Taimaz Bahadory, and Brad de Young. Overview of a new ocean glider navigation system: Oceangns. *Frontiers in Marine Science*, 8, 2021. doi: 10.3389/fmars.2021.671103.

Donald Ross and W. A. Kuperman. Mechanics of underwater noise. *The Journal of the Acoustical Society of America*, 1989. doi: 10.1121/1.398685.

Pengfei Jiang, Jianheng Lin, Junping Sun, Xuejuan Yi, and Yuanchun Shan. Source spectrum model for merchant ship radiated noise in the Yellow Sea of China. *Ocean Engineering*, 2020. doi: 10.1016/j.oceaneng.2020.107607.

AQUO. Task 3.1 Development of an European URN Standard Measurement Method. Technical report, Achieve Quieter Oceans by Shipping Noise Footprint Reduction - European Commission, 2014.

ISO-17208/1. Underwater acoustics — Quantities and procedures for description and measurement of underwater sound from ships — Part 1: Requirements for precision measurements in deep water used for comparison purposes, 2016.

Tomaso Gaggero, Mike Schaar, Raul Salinas, Publio Palomo, Enrico Rizzuto, and Michel André. Uncertainties in measurements of ship underwater noise emissions. In *11th European Conference on Underwater Acoustics 2012, ECUA 2012*, volume 34, 2012.

Tom A. Smith and Jake Rigby. Underwater radiated noise from marine vessels: A review of noise reduction methods and technology. *Ocean Engineering*, 2022. doi: 10.1016/j.oceaneng.2022.112863.

Guosong Zhang, Tonje Nesse Forland, Espen Johnsen, Geir Pedersen, and Hefeng Dong. Measurements of underwater noise radiated by commercial ships at a cabled ocean observatory. *Marine Pollution Bulletin*, 2020. doi: 10.1016/j.marpolbul.2020.110948.

Megan F. McKenna, Donald Ross, Sean M. Wiggins, and John A. Hildebrand. Underwater radiated noise from modern commercial ships. *The Journal of the Acoustical Society of America*, 2012. doi: 10.1121/1.3664100.

Nathan D. Merchant, Matthew J. Witt, Philippe Blondel, Brendan J. Godley, and George H. Smith. Assessing sound exposure from shipping in coastal waters using a single hydrophone and Automatic Identification System (AIS) data. *Marine Pollution Bulletin*, 2012. doi: 10.1016/j.marpolbul.2012.05.004.

Samara M. Haver, Jeffrey D. Adams, Leila T. Hatch, Sofie M. Van Parijs, Robert P. Dziak, Joseph Haxel, Scott A. Heppell, Megan F. McKenna, David K. Mellinger, and Jason Gedamke. Large Vessel Activity and Low-Frequency Underwater Sound Benchmarks in United States Waters. *Frontiers in Marine Science*, 8, 2021. doi: 10.3389/fmars.2021.669528.

ANSI/ASA S12.64-2009/Part 1. Quantities and Procedures for Description and Measurement of Underwater Sound from Ships – Part 1 :General Requirements. American National Standards Institute Inc., 2009. URL `https://webstore.ansi.org/standards/asa/ansiasas12642009partr2014`.

Daniel P. Zitterbart, Alessandro Bocconcelli, Miles Ochs, and Julien Bonnel. Tossit: A low-cost, hand deployable, rope-less and acoustically silent mooring for underwater passive acoustic monitoring. *HardwareX*, 2022. doi: 10.1016/j.ohx.2022.e00304.

Yvan Simard, Nathalie Roy, Cédric Gervaise, and Samuel Giard. Analysis and modeling of 255 source levels of merchant ships from an acoustic observatory along St. Lawrence Seaway. *The Journal of the Acoustical Society of America*, 2016. doi: 10.1121/1.4962557.

Tzu-Hao Lin, Chong Chen, Hiromi Kayama Watanabe, Shinsuke Kawagucci, Hiroyuki Yamamoto, and Tomonari Akamatsu. Using soundscapes to assess deep-sea benthic ecosystems. *Trends in Ecology and Evolution*, 2019. doi: https://doi.org/10.1016/j.tree.2019.09.006.

Katie A. Kowarski, Briand J. Gaudet, Arthur J. Cole, Emily E Maxner, Stephen P Turner, S. Bruce Martin, Hansen D. Johnson, and John E. Moloney. Near real-time marine mammal monitoring from gliders: Practical challenges, system development, and management implications. *The Journal of the Acoustical Society of America*, 2020. doi: 10.1121/10.0001811.

ISO-17208/2. Underwater acoustics — Quantities and procedures for description and measurement of underwater sound from ships — Part 2: Determination of source levels from deep water measurements, 2019.

Alexander O. MacGillivray, S. Bruce Martin, Michael A. Ainslie, Joshua N. Dolman, Zizheng Li, and Graham A. Warner. Measuring vessel underwater radiated noise in shallow water. *The Journal of the Acoustical Society of America*, 2023. doi: 10.1121/10.0017433.

Michael A. Ainslie, S. Bruce Martin, Krista B. Trounce, David E. Hannay, Justin M. Eickmeier, Terry J. Deveau, Klaus Lucke, Alexander O. MacGillivray, Veronique Nolet, and Pablo Borys. International harmonization of procedures for measuring

and analyzing of vessel underwater radiated noise. *Marine Pollution Bulletin*, 2022. doi: 10.1016/j.marpolbul.2021.113124.

Ziyang Li, Shengchun Piao, Minghui Zhang, and Lijia Gong. Influence of range-dependent sound speed profile on position of convergence zones. *Remote Sensing*, 2022. doi: 10.3390/rs14246314.

Tiago C. A. Oliveira, Ying-Tsong Lin, and Michael B. Porter. Underwater sound propagation modeling in a complex shallow water environment. *Frontiers in Marine Science*, 2021. doi: 10.3389/fmars.2021.751327.

DFO. Fisheries licensing policy newfoundland and labrador region, 2022. URL `https://www.dfo-mpo.gc.ca/reports-rapports/regs/licences-permis/nfld-Labrador-tn-labrador-eng.htm`. Accessed on June 06, 2022.

Giorgio Burella, Lorenzo Moro, and Bruce Colbourne. Noise sources and hazardous noise levels on fishing vessels: The case of Newfoundland and Labrador's fleet. *Ocean Engineering*, 2019. doi: 10.1016/j.oceaneng.2018.12.062.

Line Hermannsen, Kristian Beedholm, Jakob Tougaard, and Peter T. Madsen. High frequency components of ship noise in shallow water with a discussion of implications for harbor porpoises (Phocoena phocoena). *The Journal of the Acoustical Society of America*, 136(4):1640–1653, 2014. ISSN 0001-4966. doi: 10.1121/1.4893908.

Scott Veirs, Val Veirs, and Jason D. Wood. Ship noise extends to frequencies used for echolocation by endangered killer whales. *PeerJ*, 2016. doi: 10.7717/peerj.1657.

Marta Picciulin, Enrico Armelloni, Raffaela Falkner, Nikolina Rako-Gospić, Marko Radulović, Grgur Pleslić, Stipe Muslim, Hrvoje Mihanović, and Tomaso Gaggero. Characterization of the underwater noise produced by recreational and small fishing boats (¡14 m) in the shallow-water of the Cres-Lošinj Natura 2000 SCI. *Marine Pollution Bulletin*, 2022. doi: 10.1016/j.marpolbul.2022.114050.

Tomaso Gaggero, Enrico Armelloni, Antonio Codarin, Carola Chicco, Maurizio Spoto, Carlo Franzosini, Saul Ciriaco, and Marta Picciulin. Electric boat underwater radiated noise and its potential impact on species of conservation interest. *Marine Pollution Bulletin*, 2024. doi: https://doi.org/10.1016/j.marpolbul.2023.115937.

Giorgio Burella, Lorenzo Moro, and Barbara Neis. Is on-board noise putting fish harvesters' hearing at risk? A study of noise exposures in small-scale fisheries in Newfoundland and Labrador. *Safety Science*, 2021. doi: 10.1016/j.ssci.2021.105325.

Clément Chion, Dominic Lagrois, and Jérôme Dupras. A Meta-Analysis to Understand the Variability in Reported Source Levels of Noise Radiated by Ships From Opportunistic Studies. *Frontiers in Marine Science*, 2019. doi: 10.3389/fmars.2019.00714.

Miles J.G. Parsons, Christine Erbe, Mark G. Meekan, and Sylvia K. Parsons. A review and meta-analysis of underwater noise radiated by small (¡25 m length) vessels. *Journal of Marine Science and Engineering*, 2021. doi: 10.3390/jmse9080827.

Alexander O. MacGillivray, Zizheng Li, David E. Hannay, Krista B. Trounce, and Orla M. Robinson. Slowing deep-sea commercial vessels reduces underwater radiated noise. *The Journal of the Acoustical Society of America*, 2019. doi: 10.1121/1.5116140.

Oscar Schofield, Josh Kohut, David Aragon, Liz Creed, Josh Graver, Chip Haldeman, John Kerfoot, Hugh Roarty, Clayton Jones, Doug Webb, and Scott Glenn. Slocum Gliders: Robust and ready. *Journal of Field Robotics*, 2007. doi: 10.1002/rob.20200.

Pierre Cauchy, Karen J Heywood, Nathan D Merchant, Denise Risch, Bastien Y Queste, and Pierre Testor. Gliders for passive acoustic monitoring of the oceanic environment. *Frontiers in Remote Sensing*, 2023. doi: 10.3389/frsen.2023.1106533.

Nicolai von Oppeln-Bronikowski, Brad de Young, Melany Belzile, Adam Comeau, Frédéric Cyr, Richard Davis, Pamela Emery, Clark Richards, David Hebert, and Jude Van Der Meer. Best practices for operating underwater gliders in Atlantic Canada. *Frontiers in Marine Science*, 2023. doi: 10.3389/fmars.2023.1108326.

Nathan D. Merchant, Kurt M. Fristrup, Mark P. Johnson, Peter L. Tyack, Matthew J. Witt, Philippe Blondel, and Susan E. Parks. Measuring acoustic habitats. *Methods in Ecology and Evolution*, 2014a. doi: 10.1111/2041-210X.12330.

Alex Brooker and Victor Humphrey. Measurement of radiated underwater noise from a small research vessel in shallow water. *Ocean Engineering*, 2016. doi: 10.1016/j.oceaneng.2015.09.048.

Finn Jensen, William Kuperman, Michael Porter, and Henrik Schmidt. *Computational Ocean Acoustics*. Springer, 01 2011. doi: 10.1063/1.2808704.

J. Shaw and D.P. Potter. Surficial geology, coastal waters, island of Newfoundland, Newfound and Labrador. Technical report, Geological Survey of Canada Bulletin 605, Canada, 2015.

Megan S Ballard and Kevin M Lee. The Acoustics of Marine Sediments. *Acoustics Today*, 2017.

J B R Eamer, J Shaw, E L King, and K Mackillop. Seabed conditions on the inner shelves of Atlantic Canada. Technical report, Geological Survey of Canada, 2020.

Valentin Meyer and Christian Audoly. Accounting for sea floor properties in the assessment of underwater noise radiated from ships in shallow water. *Proceedings of Meetings on Acoustics*, 2020. doi: 10.1121/2.0001307.

Alec Duncan and Amos Maggi. Underwater acoustic propagation modeling software-AcTUP v2.2L. *Centre for Marine Science and Technology (Curtin University, Australia)*, 2005. URL `https://cmst.curtin.edu.au/products/underwater/`.

Khaled Helal and Lorenzo Moro. Assessment of the underwater noise levels from a fishing vessel using passive acoustic monitoring and structure hull vibration. *Canadian Acoustics*, 50(3):110–111, Aug. 2022. URL `https://jcaa.caa-aca.ca/index.php/jcaa/article/view/3876`.

Khaled Mohsen Helal, Jacopo Fragasso, and Lorenzo Moro. Effectiveness of ocean gliders in monitoring ocean acoustics and anthropogenic noise from ships: A systematic review. *Ocean Engineering*, 295:116993, 2024a. ISSN 0029-8018. doi: https://doi.org/10.1016/j.oceaneng.2024.116993. URL `https://www.sciencedirect.com/science/article/pii/S0029801824003305`.

Khaled Mohsen Helal, Jacopo Fragasso, and Lorenzo Moro. Underwater noise characterization of a typical fishing vessel from Atlantic Canada. *Ocean Engineering*, 299:117310, 2024b. ISSN 0029-8018. doi: https://doi.org/10.1016/j.oceaneng.2024.117310. URL `https://www.sciencedirect.com/science/article/pii/S0029801824006474`.

Khaled Helal, Nicolai von Oppeln-Bronikowski, and Lorenzo Moro. Advancing Glider-based Measurements and Applications of Underwater-Radiated Noise. *The Journal of the Acoustical Society of America*, 2024c. doi: Submitted.

N.D. Merchant, E. Pirotta, T.R. Barton, and P.M. Thompson. Monitoring ship noise to assess the impact of coastal developments on marine mammals. *Marine Pollution Bulletin*, 2014b. doi: 10.1016/j.marpolbul.2013.10.058.

David K. Mellinger, Kathleen M. Stafford, Sue E. Moore, Robert P. Dziak, and Haru Matsumoto. An overview of fixed passive acoustic observation methods for cetaceans. *Oceanography*, 2007. doi: 10.5670/oceanog.2007.03.

Tyler A. Helble, Gerald L. D'Spain, John A. Hildebrand, Gregory S. Campbell, Richard L. Campbell, and Kevin D. Heaney. Site specific probability of passive acoustic detection of humpback whale calls from single fixed hydrophones. *The Journal of the Acoustical Society of America*, 2013. doi: 10.1121/1.4816581.

Russell A. Charif, Yu Shiu, Charles A. Muirhead, Christopher W. Clark, Susan E. Parks, and Aaron N. Rice. Phenological changes in north atlantic right whale habitat use in massachusetts bay. *Global Change Biology*, 2020. doi: https://doi.org/10.1111/gcb.14867.

I. Sánchez-Gendriz and L. R. Padovese. Underwater soundscape of marine protected areas in the south Brazilian coast. *Marine Pollution Bulletin*, 2016. doi: 10.1016/j.marpolbul.2016.02.055.

R.L. Putland, M.K. Brey, and A.F. Mensinger. Exploring how vessel activity influences the soundscape at a navigation lock on the Mississippi River. *Journal of Environmental Management*, 2021. doi: 10.1016/j.jenvman.2021.112720. URL `https://linkinghub.elsevier.com/retrieve/pii/S0301479721007829`.

Holger Klinck, David K. Mellinger, Karolin Klinck, Neil M. Bogue, James C. Luby, William A. Jump, Geoffrey B. Shilling, Trina Litchendorf, Angela S. Wood, Gregory S. Schorr, and Robin W. Baird. Near-real-time acoustic monitoring of beaked whales and other cetaceans using a Seaglider™. *PLoS ONE*, 2012. doi: 10.1371/journal.pone.0036128.

Lu Liu and Ling Xiao. Extraction and analysis of line spectrum characteristics of underwater glider self-noise. In *2017 IEEE International Conference on Signal*

Processing, Communications and Computing, ICSPCC 2017, 2017. doi: 10.1109/ICSPCC.2017.8242479.

Carrie C Wall, David A Mann, Chad Lembke, Chris Taylor, Ruoying He, and Todd Kellison. Mapping the soundscape off the southeastern USA by using passive acoustic glider technology. *Marine and Coastal Fisheries*, 2017. doi: 10.1080/19425120.2016.1255685.

Elizabeth T. Küsel, Tessa Munoz, Martin Siderius, David K. Mellinger, and Sara Heimlich. Marine mammal tracks from two-hydrophone acoustic recordings made with a glider. *Ocean Science*, 2017. doi: 10.5194/os-13-273-2017.

Cédric Gervaise, Yvan Simard, Florian Aulanier, and Nathalie Roy. Optimizing passive acoustic systems for marine mammal detection and localization: Application to real-time monitoring north Atlantic right whales in Gulf of St. Lawrence. *Applied Acoustics*, 2021. doi: 10.1016/j.apacoust.2021.107949.

Chao Wang and Meng Yuan. Research on the Ambient Noise Observation Technology Based on the Underwater Glider. *Acoustics Australia*, 2021a. doi: 10.1007/s40857-021-00243-4.

Donatas Bagočius and Aleksas Narščius. Simplistic underwater ambient noise modelling for shallow coastal areas: Lithuanian area of the baltic sea. *Ocean Engineering*, 2018. doi: 10.1016/j.oceaneng.2018.06.055.

Alexander Macgillivray and Christ de Jong. A reference spectrum model for estimating source levels of marine shipping based on automated identification system data. *Journal of Marine Science and Engineering*, 2021. doi: 10.3390/jmse9040369.

Lu Liu, Ling Xiao, Shi Quan Lan, Ting Ting Liu, and Guo Li Song. Using Petrel II Glider to Analyze Underwater Noise Spectrogram in the South China Sea. *Acoustics Australia*, 2018. doi: 10.1007/s40857-018-0126-y.

Chao Wang and Meng Yuan. Application study of a new underwater glider with single vector hydrophone for target direction finding. *IEEE Access*, 2021b. doi: 10.1109/ACCESS.2021.3061669.

Pablo Vicente Torres-Carrión, Carina Soledad González-González, Silvana Aciar, and Germania Rodríguez-Morales. Methodology for systematic literature review applied to engineering and education. In *2018 IEEE Global Engineering Education Conference (EDUCON)*, 2018. doi: 10.1109/EDUCON.2018.8363388.

Barbara Kitchenham and Pearl Brereton. A systematic review of systematic review process research in software engineering. *Information and Software Technology*, 2013. doi: 10.1016/j.infsof.2013.07.010.

Kai Petersen, Sairam Vakkalanka, and Ludwik Kuzniarz. Guidelines for conducting systematic mapping studies in software engineering: An update. *Information and Software Technology*, 2015. doi: 10.1016/j.infsof.2015.03.007.

Mojtaba Shahin, Muhammad Ali Babar, and Liming Zhu. Continuous Integration, Delivery and Deployment: A Systematic Review on Approaches, Tools, Challenges and Practices. *IEEE Access*, 2017. doi: 10.1109/ACCESS.2017.2685629.

Valentina Lenarduzzi, Terese Besker, Davide Taibi, Antonio Martini, and Francesca Arcelli Fontana. A systematic literature review on Technical Debt prioritization: Strategies, processes, factors, and tools. *Journal of Systems and Software*, 2021. doi: 10.1016/j.jss.2020.110827.

Barbara Kitchenham and Stuart Charters. Guidelines for performing systematic literature reviews in software engineering. Technical report, School of Computer Science and Mathematics, Keele University, UK, 2007. URL `https://www.researchgate.net/publication/302924724_Guidelines_for_performing_Systematic_Literature_Reviews_in_Software_Engineering`.

John A. Hildebrand. Anthropogenic and natural sources of ambient noise in the ocean. *Marine Ecology Progress Series*, 2009. doi: 10.3354/meps08353.

Craig Radford, Andrew Jeffs, Chris Tindle, and John Montgomery. Resonating sea urchin skeletons create coastal choruses. *Marine Ecology-progress Series*, 2008. doi: 10.3354/meps07444.

R. L. Putland, R. Constantine, and C. A. Radford. Exploring spatial and temporal trends in the soundscape of an ecologically significant embayment. *Scientific Reports*, 2017. doi: 10.1038/s41598-017-06347-0.

Valentina Cafaro, Daniele Piazzolla, TCristiano Melchiorri, Calogero Burgio, Giorgio Fersini, Francesca Conversano, Viviana Piermattei, and Marco Marcelli. Underwater noise assessment outside harbor areas: The case of Port of Civitavecchia, Northern Tyrrhenian Sea, Italy. *Marine Pollution Bulletin*, 2018. doi: 10.1016/j.marpolbul.2018.06.058.

C. Soares, A. Pacheco, F. Zabel, E. González-Goberña, and C. Sequeira. Baseline assessment of underwater noise in the Ria Formosa. *Marine Pollution Bulletin*, 2020. doi: 10.1016/j.marpolbul.2019.110731.

Laurence H. De Clippele and Denise Risch. Measuring Sound at a Cold-Water Coral Reef to Assess the Impact of COVID-19 on Noise Pollution. *Frontiers in Marine Science*, 2021. doi: 10.3389/fmars.2021.674702.

Chenyang Zhu, Tomaso Gaggero, Nicholas C. Makris, and Purnima Ratilal. Underwater Sound Characteristics of a Ship with Controllable Pitch Propeller. *Journal of Marine Science and Engineering*, 2022. doi: 10.3390/jmse10030328.

Vanessa M. ZoBell, Kaitlin E. Frasier, Jessica A. Morten, Sean P. Hastings, Lindsey E. Peavey Reeves, Sean M. Wiggins, and John A. Hildebrand. Underwater noise mitigation in the Santa Barbara Channel through incentive-based vessel speed reduction. *Scientific Reports*, 2021. doi: 10.1038/s41598-021-96506-1.

Caroline Magnier and Cédric Gervaise. Acoustic and photographic monitoring of coastal maritime traffic: Influence on the soundscape. *The Journal of the Acoustical Society of America*, 2020. doi: 10.1121/10.0001321.

Gordon M. Wenz. Acoustic ambient noise in the ocean: Spectra and sources. *The Journal of the Acoustical Society of America*, 1962. doi: 10.1121/1.1909155.

Mehdi Farrokhrooz, Kathleen E. Wage, Matthew A. Dzieciuch, and Peter F. Worcester. Vertical line array measurements of ambient noise in the North Pacific. *The Journal of the Acoustical Society of America*, 2017. doi: 10.1121/1.4976706.

G. Bazile Kinda, Florent Le Courtois, and Yann Stéphan. Ambient noise dynamics in a heavy shipping area. *Marine Pollution Bulletin*, 2017. doi: 10.1016/j.marpolbul.2017.07.031.

Teledyne Webb Research. Slocum G3 Glider Operators Manual. Technical report, Teledyne Marine Technologies Incorporated, 2017. URL `https://www.teledynemarine.com/brands/webb-research/slocum-glider`.

Jung Han Lee, Sung Hyub Ko, Seom Kyu Jung, and Jong Wu Hyeon. Tertiary waves measured during 2017 pohang earthquake using an underwater glider. *Applied Sciences (Switzerland)*, 2019. doi: 10.3390/app9183860.

Ana Sofia Aniceto, Geir Pedersen, Raul Primicerio, Martin Biuw, Ulf Lindstrøm, and Lionel Camus. Arctic Marine Data Collection Using Oceanic Gliders: Providing Ecological Context to Cetacean Vocalizations. *Frontiers in Marine Science*, 2020. doi: 10.3389/fmars.2020.585754.

Conor Ryan, Frederick Wenzel, Pedro López-Suárez, and Simon Berrow. An abundance estimate for humpback whales Megaptera novaeangliae breeding around Boa Vista, Cape Verde Islands. *Zoologia Caboverdiana*, 2014. doi: https://research.thea.ie/handle/20.500.12065/234.

Selene Fregosi, Danielle V. Harris, Haruyoshi Matsumoto, David K. Mellinger, Christina Negretti, David J. Moretti, Stephen W. Martin, Brian Matsuyama, Peter J. Dugan, and Holger Klinck. Comparison of fin whale 20 hz call detections by deep-water mobile autonomous and stationary recorders. *The Journal of the Acoustical Society of America*, 2020. doi: 10.1121/10.0000617.

Susan M. Jarvis, Ronald P. Morrissey, David J. Moretti, Nancy A. DiMarzio, and Jessica A. Shaffer. Marine mammal monitoring on navy ranges (m3r): A toolset for automated detection, localization, and monitoring of marine mammals in open ocean environments. *Marine Technology Society Journal*, 2014. doi: 10.4031/MTSJ.48.1.1.

R.E. Burnham, D.A. Duffus, and X. Mouy. The presence of large whale species in Clayoquot Sound and its offshore waters. *Continental Shelf Research*, 2019. doi: 10.1016/j.csr.2019.03.004.

Clausius D.G. Reis, Linilson Rodrigues Padovese, and Maria C.F. de Oliveira. Automatic detection of vessel signatures in audio recordings with spectral amplitude variation signature. *Methods in Ecology and Evolution*, 10(9):1501–1516, 2019. ISSN 2041210X. doi: 10.1111/2041-210X.13245.

Carrie Wall, Peter Simard, Chad Lembke, and David Mann. Large-scale passive acoustic monitoring of fish sound production on the West Florida Shelf. *Marine Ecology Progress Series*, 2013. doi: 10.3354/meps10268.

Antonio Silva, Anibal Matos, Cristiano Soares, Jose Carlos Alves, Jose Valente, Frederich Zabel, Henrique Cabral, Nuno Abreu, Nuno Cruz, Rui Almeida, Rui Nunes Ferreira, Salman Ijaz, and Victor Lobo. Measuring underwater noise with high endurance surface and underwater autonomous vehicles. In *OCEANS 2013 MTS/IEEE - San Diego: An Ocean in Common*. IEEE, 2013. doi: 10.23919/OCEANS.2013.6741313. URL `https://ieeexplore.ieee.org/document/6741313`.

Zilong Peng, Bin Wang, and Jun Fan. Assessment on source levels of merchant ships observed in the East China Sea. *Ocean Engineering*, 2018. doi: 10.1016/j.oceaneng.2018.02.035.

Duncan McIntyre, Waltfred Lee, Héloïse Frouin-Mouy, David Hannay, and Peter Oshkai. Influence of propellers and operating conditions on underwater radiated noise from coastal ferry vessels. *Ocean Engineering*, 2021. doi: 10.1016/j.oceaneng.2021.109075.

National Research Council. *Ocean Noise and Marine Mammals*. The National Academies Press, Washington, DC, 2003. ISBN 978-0-309-08536-6. doi: 10.17226/10564.

Line Hermannsen, Lonnie Mikkelsen, Jakob Tougaard, Kristian Beedholm, Mark Johnson, and Peter T. Madsen. Recreational vessels without Automatic Identification System (AIS) dominate anthropogenic noise contributions to a shallow water soundscape. *Scientific Reports*, 2019.

Vanessa M. ZoBell, Martin Gassmann, Lee B. Kindberg, Sean M. Wiggins, John A. Hildebrand, and Kaitlin E. Frasier. Retrofit-induced changes in the radiated noise and monopole source levels of container ships. *PLOS ONE*, 2023. doi: 10.1371/journal.pone.0282677.

Johan Bosschers. The Specialist Committee on Hydrodynamic Noise – Final Report and Recommendations to the 28th ITTC. In *Proceedings of 28th ITTC, Wuxi, China*, volume II, pages 503–578. IEEE, 2017.

Victor Humphrey, Alex Brooker, Ruggero Dambra, and Erica Firenze. Variability of underwater radiated ship noise measured using two hydrophone arrays. In *OCEANS 2015 - Genova*, 2015. doi: 10.1109/OCEANS-Genova.2015.7271383.

R.J. Urick. *Principles of Underwater Sound*. McGraw-Hill Co, New York, 1983.

A. Dassatti, M. van der Schaar, P. Guerrini, S. Zaugg, L. Houégnigan, A. Maguer, and M. André. On-board underwater glider real-time acoustic environment sensing. In *OCEANS 2011 IEEE - Spain*, 2011. doi: 10.1109/Oceans-Spain.2011.6003482.

James S. Bennett, Frederick R. Stahr, Charles C. Eriksen, Martin C. Renken, Wendy E. Snyder, and Lora J. Van Uffelen. Assessing seaglider model-based position accuracy on an acoustic tracking range. *Journal of Atmospheric and Oceanic Technology*, 2021. doi: 10.1175/JTECH-D-20-0091.1.

The Fisheries and Marine Institute of Memorial University of Newfoundland's Centre for Applied Ocean Technology (CTec) and the Centre for Ocean Ventures and Entrepreneurship (COVE) of Halifax. SmartAtlantic Alliance, 2021. URL `https://www.smartatlantic.ca/station_alt.html?id=stjohns`.

Ocean Sonics. Radio drifting buoy. `https://oceansonics.com/products/drifting-buoy/`, 2021a.

Ocean Sonics. icListen HF Hydrophone. `https://oceansonics.com/products/iclisten-rb9/`, 2021b.

M Baird. Ballasting Slocum electric gliders. Technical report, NRC-IOT, 2007.

High Tech, INC. HTI-99-HF Hydrophone, Accessed: 2021. URL `https://www.hightechincusa.com/products/hydrophones/hti99hf.html`.

JASCO Applied Science. OceanObserver. `https://www.jasco.com/oceanobserver`, 2021.

Alessandra Tesei, Pietro Stinco, Michele Micheli, Bartolome Garau, Stefano Biagini, Luigi Troiano, and Piero Guerrini. A buoyancy glider equipped with a tridimensional acoustic vector sensor for real-time underwater passive acoustic monitoring at low frequency. In *OCEANS 2019 - Marseille, OCEANS Marseille 2019*, volume 2019-June. IEEE, 2019. doi: 10.1109/OCEANSE.2019.8867391.

Kunde Yang, Liya Xu, Qiulong Yang, and Ganxian Li. Two-step inversion of geoacoustic parameters with bottom reverberation and transmission loss in the deep ocean - acoustics australia, 2018.

Wei Liu, Lilun Zhang, Yongxian Wang, Xinghua Cheng, and Wenbin Xiao. A vector wavenumber integration model of underwater acoustic propagation based on the matched interface and boundary method. *Journal of Marine Science and Engineering*, 9, 2021. doi: 10.3390/jmse9101134.

F. R. DiNapoli and R. L. Deavenport. Theoretical and numerical Green's function field solution in a plane multilayered medium. *The Journal of the Acoustical Society of America*, 67:92–105, 1980. ISSN 0001-4966. doi: 10.1121/1.383794.

David R. Dall'Osto and Dajun Tang. Acoustic resonances within the surficial layer of a muddy seabed. *The Journal of the Acoustical Society of America*, 2022. doi: 10.1121/10.0011472.

Ying-Tsong Lin. Three-dimensional boundary fitted parabolic-equation model of underwater sound propagation. *The Journal of the Acoustical Society of America*, 146, 2019. doi: 10.1121/1.5126011.

Michael D. Collins. A split-step Padé solution for the parabolic equation method. *The Journal of the Acoustical Society of America*, 93, 1993. doi: 10.1121/1.406739.

Christine Erbe, Alec Duncan, and Kathleen J. Vigness-Raposa. *Introduction to Sound Propagation Under Water*, pages 185–216. Springer International Publishing, 2022. doi: 10.1007/978-3-030-97540-1_6.

Xiao-Tong Gong, Hong-Tao Zhou, Shao-Cong Zhang, Yan-Feng Wang, and Yue-Sheng Wang. Tunable sound transmission through water–air interface by membrane-sealed bubble metasurface. *Applied Physics Letters*, 123, 2023. ISSN 0003-6951. doi: 10.1063/5.0171461.

Singiresu Rao. *Mechanical Vibrations*. Pearson, 2016.

Esen Cintosun and Layton Gilroy. Estimating ship underwater radiated noise from onboard vibrations. In *SNAME Maritime Convention 2021, 27-29 October, Providence RI*. SNAME, 2021.

Tjakko Keizer, Renaud Gaudel, Lean Macleane, David Tolman, Bruce Paterson, and Chanwoo Bae. Estimation of uncertainties in underwater sound measurements of ships. *Proceedings of Meetings on Acoustics*, 47:070002, 2022. ISSN 1939-800X. doi: 10.1121/2.0001571.

Korean register. Guidances for Underwater Radiated Noise. Technical report, Busan, Korea, 2021. URL https://www.krs.co.kr/KRRules/KRRules2022/data/data_other/ENGLISH/gc37e000.pdf.

Ian Farrance and Robert Frenkel. A Review of the Rules for Calculating Uncertainty Components through Functional Relationships. *Clin Biochem Rev*, 2012. doi: PMC3387884.

Taylor, Barray N. and Kuyatt, Chris E. Guidelines for Evaluating and Expressing the Uncertainty of NIST Measurement Results. Technical report, NIST Technical Note 1297, National Institute of Standards and Technology, 1994. URL https://www.nist.gov/pml/nist-technical-note-1297.

ISO/IEC Guide 98-3. Uncertainty of measurement, Guide to the expression of uncertainty in measurement (GUM:1995), 2008.

Alan Oxley. Chapter 8 - sources of inaccuracy. In Alan Oxley, editor, *Uncertainties in GPS Positioning*, pages 99–114. Academic Press, 2017. ISBN 978-0-12-809594-2. doi: https://doi.org/10.1016/B978-0-12-809594-2.00008-3. URL https://www.sciencedirect.com/science/article/pii/B9780128095942000083.

Frank van Diggelen and Per Enge. The World's first GPS MOOC and Worldwide Laboratory using Smartphones. In *Proceedings of the 28th International Technical Meeting of the Satellite Division of The Institute of Navigation (ION GNSS+ 2015)*, pages 361–369. The Institute of Navigation, September 2015. URL https://www.ion.org/publications/abstract.cfm?articleID=13079.

Gary Hayman, Yuebing Wang, and Stephen Robinson. A comparison of two methods for phase response calibration of hydrophones in the frequency range 10–400 kHz. *The Journal of the Acoustical Society of America*, 133(2):750–759, 01 2013. doi: 10.1121/1.4774272. URL https://doi.org/10.1121/1.4774272.

Emma Cotter, Paul Murphy, Christopher Bassett, Benjamin Williamson, and Brian Polagye. Acoustic characterization of sensors used for marine environmental monitoring. *Marine Pollution Bulletin*, 144:205–215, 2019. ISSN 0025-326X. doi: https://doi.org/10.1016/j.marpolbul.2019.04.079. URL `https://www.sciencedirect.com/science/article/pii/S0025326X19303583`.

Megan F. McKenna, Sean M. Wiggins, and John A. Hildebrand. Relationship between container ship underwater noise levels and ship design, operational and oceanographic conditions. *Scientific Reports*, 2013. doi: 10.1038/srep01760.

Amy Deeb and Mae L Seto. A methodology to define underwater acoustic radiated noise norms for small commercial vessel classes using neural networks. In *Proceedings of Meetings on Acoustics*, volume 47. AIP Publishing, 2022.

Giorgio Burella and Lorenzo Moro. Design solutions to mitigate high noise levels on small fishing vessels. *Applied Acoustics*, 2021. doi: 10.1016/j.apacoust.2020.107632.

Brian Claus and Ralf Bachmayer. Terrain-aided navigation for an underwater glider. *Journal of Field Robotics*, 32(7):935–951, 2015.

Jennifer Wladichuk. Systematic source level measurements of whale watching vessels and other small boats. *The Journal of Ocean Technology*, 14, 2019.

Martin Gassmann, Sean M. Wiggins, and John A. Hildebrand. Deep-water measurements of container ship radiated noise signatures and directionality. *The Journal of the Acoustical Society of America*, 2017. doi: 10.1121/1.5001063.

Steven L. Garrett. *Attenuation of Sound*, pages 673–698. Springer Cham, 2020. doi: 10.1007/978-3-030-44787-8_14.

Pietro Stinco, Alessandra Tesei, Richard Dreo, and Michele Micheli. Detection of envelope modulation and direction of arrival estimation of multiple noise sources with an acoustic vector sensor. *The Journal of the Acoustical Society of America*, 149, 2021. doi: 10.1121/10.0003628.

Wenyi Zhang and Bhaskar D. Rao. Two microphone based direction of arrival estimation for multiple speech sources using spectral properties of speech. In *2009 IEEE International Conference on Acoustics, Speech and Signal Processing*, 2009. doi: 10.1109/ICASSP.2009.4960053.

Kunde Yang, Yanyang Lu, Zhixiong Lei, and Huijun Xia. Passive localization based on multipath time-delay difference with two hydrophones in deep ocean. *Acoustics Australia*, 2017. doi: 10.1007/s40857-017-0084-9.

Peng Li, Xinhua Zhang, and Wenlong Zhang. Direction of arrival estimation using two hydrophones: Frequency diversity technique for passive sonar. *Sensors*, 2019. doi: 10.3390/s19092001.

Serkan Tokgöz, Anton Kovalyov, and Issa Panahi. Real-time estimation of direction of arrival of speech source using three microphones. In *2020 IEEE Workshop on Signal Processing Systems (SiPS)*, pages 1–5, 2020. doi: 10.1109/SiPS50750.2020.9195217.

Xiao Chen, Hao Zhang, Yong Gao, and Zhen Wang. Doa estimation of underwater acoustic co-frequency sources for the coprime vector sensor array. *Frontiers in Marine Science*, 10, 2023. ISSN 2296-7745. doi: 10.3389/fmars.2023.1211234. URL `https://www.frontiersin.org/articles/10.3389/fmars.2023.1211234`.

Yuuki Tachioka, Tomohiro Narita, and Tomohiro Iwasaki. Direction of arrival estimation by cross-power spectrum phase analysis using prior distributions and voice activity detection information. *Acoustical Science and Technology*, 33(1):68–71, 2012. doi: 10.1250/ast.33.68.

Appendix A

Appendix A: Supplementary information related to the systematic literature review

The information extracted from the papers includes the scope and findings of the presented research, the equipment used, the post-processing technique, and how the study relates to the previous research. Table A.1 summarizes the key points of the 29 articles selected. A final screening was performed using the criteria presented in Table 2.1. Eight articles were removed for the reasons explained in Table A.1.

Table A.1: The selected articles in the systematic literature review

#	Author-Date	Title	State	Reason
	RQ_1: Ocean source sound and/or Ship noise monitoring and assessment using ocean glider			
1	Stinco et al., (2021)	Detection of envelope modulation and direction of arrival estimation of multiple noise sources with an acoustic vector sensor	Included	• Autonomous underwater glider used as passive acoustic monitoring • Self-noise of the glider was investigated • The glider detected the underwater radiated noise of two types of a vessel using cavitation-induced noise
2	Wang and Yuan, (2021)	Research on the ambient noise observation technology based on the underwater glider	Included	• Autonomous underwater glider used as passive acoustic monitoring • Self-noise of the glider was investigated • Ocean ambient noise was monitored by the glider • The glider measured a passing vessel noise

#	Author-Date	Title	State	Reason
3	Gervaise et al., (2021)	Optimizing passive acoustic systems for marine mammal detection and localization: Application to real-time monitoring North Atlantic right whales in the Gulf of St. Lawrence	Excluded	• Focus on determining the optimal design of passive acoustic monitoring systems • Self-noise of the glider was not investigated
4	Tesei et al., (2020)	Tracking of multiple surface vessels based on passive acoustic underwater arrays	Excluded	• Used wave-glider in measuring and tracking radiated boat noise • There is no presentation to the URN of the boats, e.g., spectrogram or power spectrum
5	Aniceto et al., (2020)	Arctic marine data collection using oceanic gliders: providing ecological context to cetacean vocalizations	Included	• Comprehensive study of oceanographic variables and background noise together with marine mammals detection • Connection marine mammals-ecosystem

#	Author-Date	Title	State	Reason
6	Fregosi et al., (2020)	Detections of whale vocalizations by simultaneously deployed bottom-moored and deep-water mobile autonomous hydrophones	Included	• Glider was used as passive acoustic monitoring in detecting whales • Representation of detecting data by both the glider and a mooring system • Self-noise of the glider was investigated, especially the flow-induced noise
7	Baumgartner et al., (2020)	Slocum gliders provide accurate near real-time estimates of baleen whale presence from human-reviewed passive acoustic detection information	Included	• Glider was used as passive acoustic monitoring in detecting whales • Self-noise of the glider was investigated
8	Fregosi et al., (2020)	Comparison of fin whale 20 Hz call detections by deep-water mobile autonomous and stationary recorders	Included	• Glider was used as passive acoustic monitoring in detecting fin whales • Representation of detecting data by both the glider and a mooring system
9	Cauchy et al., (2020)	Sperm whale presence observed using passive acoustic monitoring from gliders of opportunity	Excluded	• Free ranging marine mammals

#	Author-Date	Title	State	Reason
10	Jiang et al., (2019)	The use of underwater gliders as acoustic sensing platforms	Included	• Petrel II glider used as passive acoustic monitoring • Self-noise of the glider was investigated • The glider used to detect underwater noise sound sources • Discussed the factors that affect the measurement uncertainty using the glider
11	Haxel et al., (2019)	Ocean sound levels in the northeast Pacific recorded from an autonomous underwater glider	Included	• Slocum glider G2 used as passive acoustic monitoring • Self-noise of the glider was investigated • Representation of ocean ambient noise levels collected by both the glider and a long-term mooring data • The glider detected vessel noise, and Automatic Identification System (AIS) data is used

#	Author-Date	Title	State	Reason
12	Burnham et al., (2019)	The presence of large whale species in Clayoquot Sound and its offshore waters	Included	• Glider was used as passive acoustic monitoring in detecting large whales • Representation of detecting data by both the glider and a mooring system
13	Silva et al., (2019)	Temporal and spatial distributions of delphinid species in Massachusetts Bay (USA) using passive acoustics from ocean gliders	Excluded	• Self-noise of the glider was not investigated • Free ranging marine mammals
14	Liu et al., (2018)	Using Petrel II Glider to analyze underwater noise spectrogram in the South China Sea	Included	• Petrel II glider used as passive acoustic monitoring • Self-noise of the glider was investigated • Glider used to assess ocean ambient noise as a function of the water column and different location
15	Bittencourt et al., (2018)	Mapping cetacean sounds using a passive acoustic monitoring system towed by an autonomous Wave Glider in the Southwestern Atlantic Ocean	Excluded	• Using surface glider instead of autonomous underwater glider

#	Author-Date	Title	State	Reason
16	Wall et al., (2017)	Mapping the soundscape of the South-eastern USA by using passive acoustic glider technology	Included	• Slocum glider G2 was used as passive acoustic monitoring • Monitoring underwater ambient noise for 29 days of recordings • Marine fauna and vessels' noise were detected and classified by frequencies
17	Cazau et al., (2017)	Measuring the marine soundscape of the Indian Ocean with southern elephant seals used as acoustic gliders of opportunity	Excluded	• Using animals as an acoustic glider to map the soundscape
18	Wall et al., (2017)	Mapping the soundscape of the south-eastern USA by using passive acoustic glider technology	Excluded	• Mapping soundscape • Free ranging marine mammals
19	Suberg.et al., (2014)	Assessing the potential of autonomous submarine gliders for ecosystem monitoring across multiple trophic levels (plankton to cetaceans) and pollutants in shallow shelf seas	Excluded	• Ecosystem monitoring and pollutant • Free ranging marine mammals

#	Author-Date	Title	State	Reason
20	Matsumoto et al., (2011)	Mapping the sound field of an erupting submarine volcano using an acoustic glider	Included	• Slocum glider G2 was used as passive acoustic monitoring • Oceangraphy data collected by the glider and aided to estimated propagation loss model • Representation of volcano noise levels collected by both the glider and a mooring system
		RQ_2: Underwater ship noise measurement uncertainties in general		
1	ZoBell et al., (2021)	Underwater noise mitigation in the Santa Barbara Channel through incentive-based vessel speed reduction	Included	• Investigated the effect of reducing vessel speed on its underwater radiated noise • Discussed several factors that affect the URN uncertainty, e.g., Lloyd's mirror, hydrophone depths, and power averaging
2	Haver et al., (2021)	Large vessel activity and low-frequency underwater sound benchmarks in United States waters	Included	• Investigated the seasonal changes that impact the measured ship noise levels • Variability in measured ship noise categorized by vessel types

#	Author-Date	Title	State	Reason
3	Macgillivray and Jong - (2021)	A reference spectrum model for estimating source levels of marine shipping based on automated identification system data	Excluded	• No discussion for the uncertainties of estimating source levels
4	Jiang et al., (2020)	Source spectrum model for merchant ship radiated noise in the Yellow Sea of China	Included	• Shallow water measurement of merchant ships • Discussed the effect of the background noise levels on certainty • Discussed the effect of range on uncertainty • Discussed the variability in ship noise levels by vessel category
5	Magnier and Gervaise, (2020)	Acoustic and photographic monitoring of coastal maritime traffic: Influence on the soundscape	Included	• Monitored small boats in shallow water using a moored hydrophone • Discussed some the factor that impacts the boat noise uncertainties

#	Author-Date	Title	State	Reason
6	Peng et al., (2018)	Assessment on source levels of merchant ships observed in the East China Sea	Included	• Shallow water measurements conducted using moored hydrophones • Presented the factors impact the underwater radiated noise uncertainty in shallow water • Illustrated the significant parameters that affect the numerical propagation loss model
7	Simard et al., (2016)	Analysis and modeling of 255 source levels of merchant ships from an acoustic observatory along St. Lawrence Seaway	Included	• Investigated the ship source level uncertainty for different vessel type • Discussed the effect of the vessel's speed on radiated noise levels in low frequencies ($\leq$ 100Hz) • Showed the importance of having an accurate propagation loss model in case of using only a single hydrophone instead of three
8	Merchant et al., (2012)	Assessing sound exposure from shipping in coastal waters using a single hydrophone and AIS data	Included	• Investigated the propagation loss model uncertainty • The effect of the untraceable small vessels in mapping underwater radiated noise was discussed

#	Author-Date	Title	State	Reason
9	McKenna et al., (2012)	Underwater radiated noise from modern commercial ships	Included	• Discussed the uncertainty of underwater radiated noise measurement of large vessels • Investigated the effect of the propagation loss model in estimating ship noise levels • Recommended to categorize the vessel by their type while processing and reporting the underwater radiated noise

Table A.2: Summary to the selected articles related to the use of the AUG with ocean ambient noise assessment

Author (Year)	**Mobile Platform**	**Fixed Platform**	**Study Aim**	**Mission Duration/Covered Distance**	**Propagation Loss Model**	**Data Representation**
Wang and Yuan (2021)	• Petrel-II Glider • Dive Depth: 1200 m • Water Depth: 1600m	Not specified	• Underwater Ambient Noise assessment • One vessel detected	7 h of recording/5.2 km (Straight line operation)	Not Mentioned	• 1/3 octave power spectrum density (PSD) vs. depth and time • Frequency range: 63 Hz-3.15 kHz
Jiang et al. (2019)	• Petrel-II Glider • First Dive Depth: 800 m • Second Dive Depth: 1 Km • Water Depth: 1400m	Not specified	• Underwater Ambient Noise assessment • Target Detection (azimuth angle)	• First Dive: 55 h • Second Dive: 92 h	• Used a known sound source and Sonar equation. • Compared to the cylindrical and spherical spreading.	• 1/3 octave p vs. Depth • Spectrogram and PSD for the glider self-noise • PL Estimation vs. Range

Author (Year)	**Mobile Platform**	**Fixed Platform**	**Study Aim**	**Mission Duration/Covered Distance**	**Propagation Loss Model**	**Data Representation**
Haxel et al. (2019)	• Slocum Glider (G2 - 1000 m) • Dive Depth: Avg 625 m • Water Depth: <1000m	Yes	• Underwater Ambient Noise assessment • Comparison with a fixed hydrophone	18-days/458 km (Straight line mission)	• Cylindrical Propagation Loss: $PL = 15\log(r)$ • Range dependent Acoustic Model (RAM) propagation model using measured sound speed profile	• Frequency range: 10 Hz-4.4 kHz • PSD and Spectrogram of the whole mission • Spectral Probability Distributions vs. Depth (1st, 50th and 99th percentile) • 2-D scatter maps for ambient noise (Depth vs. Distance) in two frequency ranges (1-1.05 kHz and 50 - 100 Hz) • Spectrogram of Bioacoustic signals
Liu et al. (2018)	• Petrel-II Glider • Dive depth: <1036 m • Water Depth: 1100 m	Not specified	Analyzing and monitoring underwater noise spectrogram in the South China Sea.	26 km in 3 h (Straight line mission)	Not Mentioned	• Frequency range: 10 Hz-3.15 kHz • Frequency-Depth plot • Spectrogram and Spectrum level of the glider's self-noise

Author (Year)	**Mobile Platform**	**Fixed Platform**	**Study Aim**	**Mission Duration/Covered Distance**	**Propagation Loss Model**	**Data Representation**
Matsumoto et al. (2011)	• Slocum Glider (G2-1000 m) • Dive Depth: <950 m • Water Depth: 1500 m-2500 m	Yes	• Investigate the ability of the glider in volcano-acoustic monitoring. • Comparison with a moored autonomous hydrophone.	40 km in 2 days (Straight line mission)	RAM-propagation model	• Frequency range: 10-860 Hz • Received sound levels map • propagation loss map • Source level map

Table A.3: Summary of measurement uncertainty by the selected articles

Authors	**Method of measurement**	**Vessels**	**Source levels representation**	**Uncertainties**
Mckenna et al. (2012)	• One hydrophone • Bottom-mounted system • Hydrophone depth: 580 m • water depth: 590 to 600 m	29 vessels	• Broadband source level (20-1000 Hz) • One and One-third octave bands • Versus ship speed	• Speed over ground adjustment • Source depth • Season • Closest point of approach
Merchant et al. (2012)	• One hydrophone • Bottom-mounted system • Water Depth: 30 m	46 vessels were uniquely identified by the AIS during the measurement	• Broadband sound pressure level (1 Hz-1kHz) • Sound exposure levels	• Background assessment • Ship density (non-AIS vessels) • Closet point of approach • Propagation loss in shallow water • Wind speed (variation up to 20 dB)

Authors	**Method of measurement**	**Vessels**	**Source levels representation**	**Uncertainties**
Simard et al. (2016)	• Three hydrophones (ANSI/S12.64) • Bottom-mounted system • Hydrophones' depths: 62, 161 and 288 m • Water depth: 350 m	255 ships	• OTOB source level • Broadband source level (20-500 Hz)	• Source of noise directivity • Tilt angle and its effect on CPA precision ($\pm 1dB$) • Interference with other sources of noise • propagation loss using spherical spreading
Peng et al. (2018)	• One hydrophone (ANSI/S12.64) • A bottom-mounted system with surface AIS buoy • Water depth: 24 m	57 vessels (Container and Bulk cargo ships)	• OTOB source sound level • Uncertainty statistical analysis with the parameters under investigation	• Background noise changes over time • Closest point of approach • Source depth • Receiver depth • Bathymetry type

Authors	**Method of measurement**	**Vessels**	**Source levels representation**	**Uncertainties**
Magnier and Gervaise (2020)	• One hydrophone • Bottom-mounted system • Water depth: 50 m	Non-AIS vessels (more than 550 boats)	• OTOB sound pressure level • Broadband (100 Hz-30 kHz) sound pressure level • Spearman correlation between sound pressure and both distance and vessel number	• Frequency range of interest (shallow water low-frequency attenuation) • Closest point of approach (¡ 1.2 dB) • vessel density (absence of AIS)
Jaing et al. (2020)	• one hydrophone • Bottom-mounted system • Water depth: 30 m	27 vessels (container, cargo, and tankers)	• 20-1000 Hz broadband noise	• Closest point of approach • Background noise assessment • Source depth

Table A.4: Standards and classification societies ship noise measurement requirements

Parameters	ANSI/ASA S12.64	ISO-17208/1/2	BV (2018)	ABS (2018)	LR	DNV GL
Source levels Measurement variability						
Uncertainty	• G-A: 1.5 dB • G-B: 3 dB • G-C: 4 dB	• -5 dB (10-100 Hz) • -3 dB (125 Hz-16 kHz) • -4 dB (>=20 kHz)	• ±4 dB for shallow water • ±3.5 dB for deep water	• ISO-17208/1/2	• ISO-17208/1/2	Not specified
Repeatability	• G-A: ± 1 dB • G-B: ± 2 dB • G-C: ± 3 dB	• -3 dB (10-100 Hz) • -1 dB (125 Hz-16 kHz) • -1 dB (>=20 kHz)	• ± 4 dB for shallow water • ± 3.5 dB for deep water	• ISO-17208/1/2	• ISO-17208/1/2	Not specified
Instruments Specification						
Frequency range	• G-A: 10 Hz-50 kHz • G-B: 20 Hz-25 kHz • G-C: 50 Hz-10 kHz	• 10 Hz-20 kHz ± 2 dB	• 10 Hz - 50 kHz	• Commercial vessels (10 Hz-50 kHz) • Research vessels (10 Hz-100 kHz)	• ISO-17208/1	• 10 Hz-50 kHz
Bandwidth	• OTOB • Narrowband for G-A and G-B	• OTOB	• OTOB	• OTOB • Narrowband • Broadband	• ISO-17208/1	• 1/3 octave band • Narrowband

Parameters	ANSI/ASA S12.64	ISO-17208/1/2	BV (2018)	ABS (2018)	LR	DNV GL
Range Error	• ±10%	• ±10 m	• ISO-17208/1	• ISO-17208/1	• ±5 m	Not specified
Tilt (floating devices)	Not specified	• Not exceed 5°	Not specified	• ISO-17208/1	• ISO-17208/1	Not specified
CPA	• Which is large between 100 m or 1 x overall ship length	• Which is large between 100 m or 1 x overall ship length (<10 %)	• 200 ±10 m or 1x ship length • 100 ±10 m or 1x ship length in the presence of anticipated background noise	• 100 ±10% m or 1x ship length	• ISO-17208/1	• 100 m to 200 m
Hydrophones Number	• G-A: Three • G-B: Three • G-C: One	• Three	• Three	• Three	• One	
Directivity	• Omnidirectional	• Omnidirectional	• ISO-17208/1	• ISO-17208/1	• ISO-17208/1	

Parameters	ANSI/ASA S12.64	ISO-17208/1/2	BV (2018)	ABS (2018)	LR	DNV GL
Hydrophones Depth	• 15, 30 and 45 depression angles between the water surface and source-receiver distance as function in CPA (Pythagorean Theorem) • 20 ±5 depression angle for Grade C	• 15, 30 and 45 depression angles between the water surface and source-receiver distance as function in CPA (Pythagorean Theorem)	• **Shallow**: Bottom-mounted (the distance between hydrophones is 15 m to 20 m, and the deepest one should be above the seafloor by 3m - 5m) • **Deep** :Floating line where the distance between hydrophones is >30 m, and the deepest one should be above the seafloor by (depth/2) m	• 15, 30 and 45 depression angles between the water surface and source-receiver distance as function in CPA (Pythagorean Theorem)	• **Shallow**: -H1: 1/10 water depth -H2: 1/2 water depth -H3: 5 m above the seabed • **Deep**: ISO-17208/1/2	• Hydrophone bottom-mounted 0.2 m above the seabed
Underwater Environment Factors						

Parameters	ANSI/ASA S12.64	ISO-17208/1/2	BV (2018)	ABS (2018)	LR	DNV GL
Water Depth	• G-A: 300 m or 3x overall ship length • G-B: 150 m or 1.5x overall ship length • G-C: 75 m or 1x overall ship length	• **Shallow**: Not specified • **Deep**: @ 150 m @ or 1.5x overall ship length	• **Shallow**: @ >= 60 m @ or 0.3x(vessel speed)^2 • **Deep**: @ > 200 m @ or 2x vessel's length @ or 1.5x vessel's length if ship >than 200 m	• **Shallow**: @ > 60 m @ or 0.3x(vessel speed) ^{2} • **Deep**: @ 150 m @ or 1.5x overall ship length	• **Shallow**: @ >= 60 m @ or 0.3x(vessel speed) ^{2} • **Deep**: @ ISO-17208/1/2	• Minimum water depth: 0.6x(vessel speed) ^{2}
Mirror effect correction	• Interference patterns are less in G-A and increased in G-B and G-C	• Smoothed by averaging over the time (Data window length) and the hydrophones • Linear correction for Monopole source level	• Low-frequency correction term • Smoothed by averaging over time the period and the hydrophones	• ISO-17208/1	• **Shallow water**: @ specify a correction for the Monopole source level • **Deep water**: @ ISO-17208/1/2	• Correction of (-5dB)

Parameters	ANSI/ASA S12.64	ISO-17208/1/2	BV (2018)	ABS (2018)	LR	DNV GL
Seabed correction	• Directly proportional with the distance to bottom-depth ratio	Not specified	• Seabed characteristics must be known for the propagation loss model	• 5 dB reduction in SPL, if the hydrophone is less than 0.2 m above the sea floor	• ISO-17208/1/2	• Not specified except the recommendation of sloping seabed
Wind/ Sea state	• <=20 knots and decent weather condition	• <=20 knots and decent weather condition	• Not during a rainy day • Beaufort 2, floating line hydrophone • Beaufort 3, bottom mounted hydrophone	• Sea State <=3 • Maximum wind speed <= 20 kt (Beaufort 4)	• Sea state 2 • Beaufort 4 • Sea state 3 can be accepted in condition cases	• Sea state 3 • Beaufort 4
Propagation loss model	• Spherical spreading propagation loss equation (Normalized distance)	• Spherical spreading propagation loss equation (Normalized distance)	• Numerical modeling (less uncertainty) • Simple equation based on water depth (high uncertainty)	• ISO-17208/1/2	• ISO-17208/1/2	• Distance correction: 18 log(Range)

Parameters	ANSI/ASA S12.64	ISO-17208/1/2	BV (2018)	ABS (2018)	LR	DNV GL
Background noise correction	• A window of 30 seconds • Recorded at 2 km apart from the PAM • Recorded at the beginning and the end	• A window of 30 seconds • At least 2 km apart from the PAM	• A window of 2 minutes • At least 2 miles apart from the PAM	• ISO-17208/1	• ISO-17208/1	• ISO-17208/1
Vessel Operating Conditions						
Speed	• Maximum 50 knots • Constant speed during the measurement window	• Constant speed during the measurement window • Straight line	• Constant speed during the measurement window • Straight line	• Constant speed without excessive rudder action • Straight line	• ISO-17208/1	• <= 5 knots • Straight line • Constant speed
Length	• All surface vessels, either manned or unmanned	• All surface vessels, either manned or unmanned	• Any self-propelled ships	• Self-propelled commercial and research vessels	• ISO-17208/1	• Any vessel classed

Parameters	ANSI/ASA S12.64	ISO-17208/1/2	BV (2018)	ABS (2018)	LR	DNV GL
Number of runs	• G-A: 3 port / 3 starboard • G-B: 2 port / 2 starboard • G-C: 1 port / 1 starboard	• **Four runs** in total @ 2 runs for Port @ 2 runs for Starboard	• **Six runs** in total @ 2 runs at CPA @ 2 runs at 1.5 CPA @ 2 runs at 2 CPA if ship GT>10000, 2 runs are accepted or one run in a condition of using two hydrophone lines	• **Four runs** in total @ 2 runs for Port @ 2 runs for Starboard	• ISO-17208/1	2 runs
Data window	• ± 30°	• ± 30°	• ± 45° (step of 5°)	• ISO-17208/1	• ISO-17208/1	Not specified

Appendix B

Appendix B: The error between the proposed numerical PL compared to the ISO Standard in Conception Bay trials

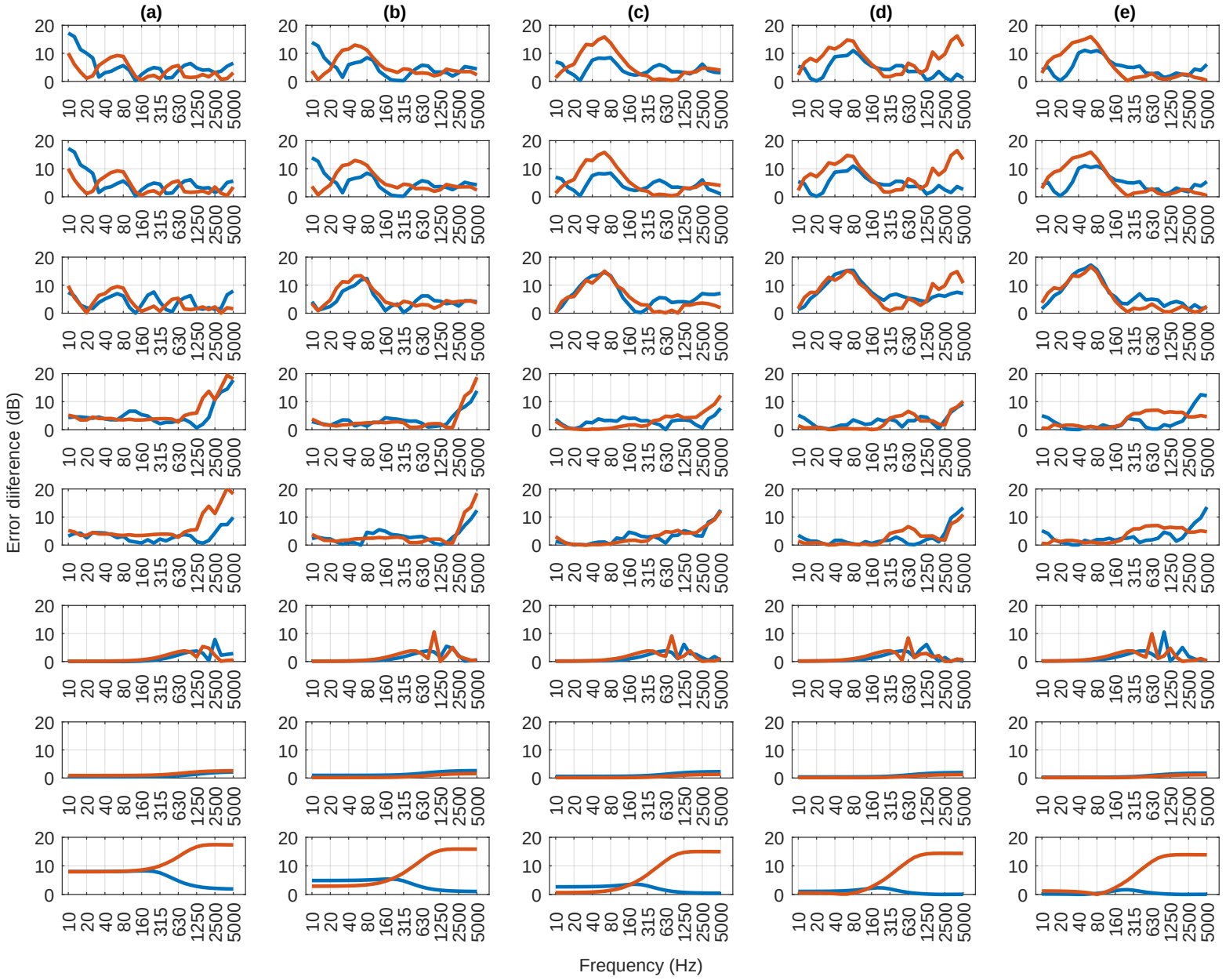

Figure B.1: Error between the ISO 17208-2 and the other models at 100 m. The rows are representing the models as follows: PE(R/I), PE(R/D), PE(R-B/D), WNI(R/I), WNI(R/D), ECHO, SCA, and M-A.

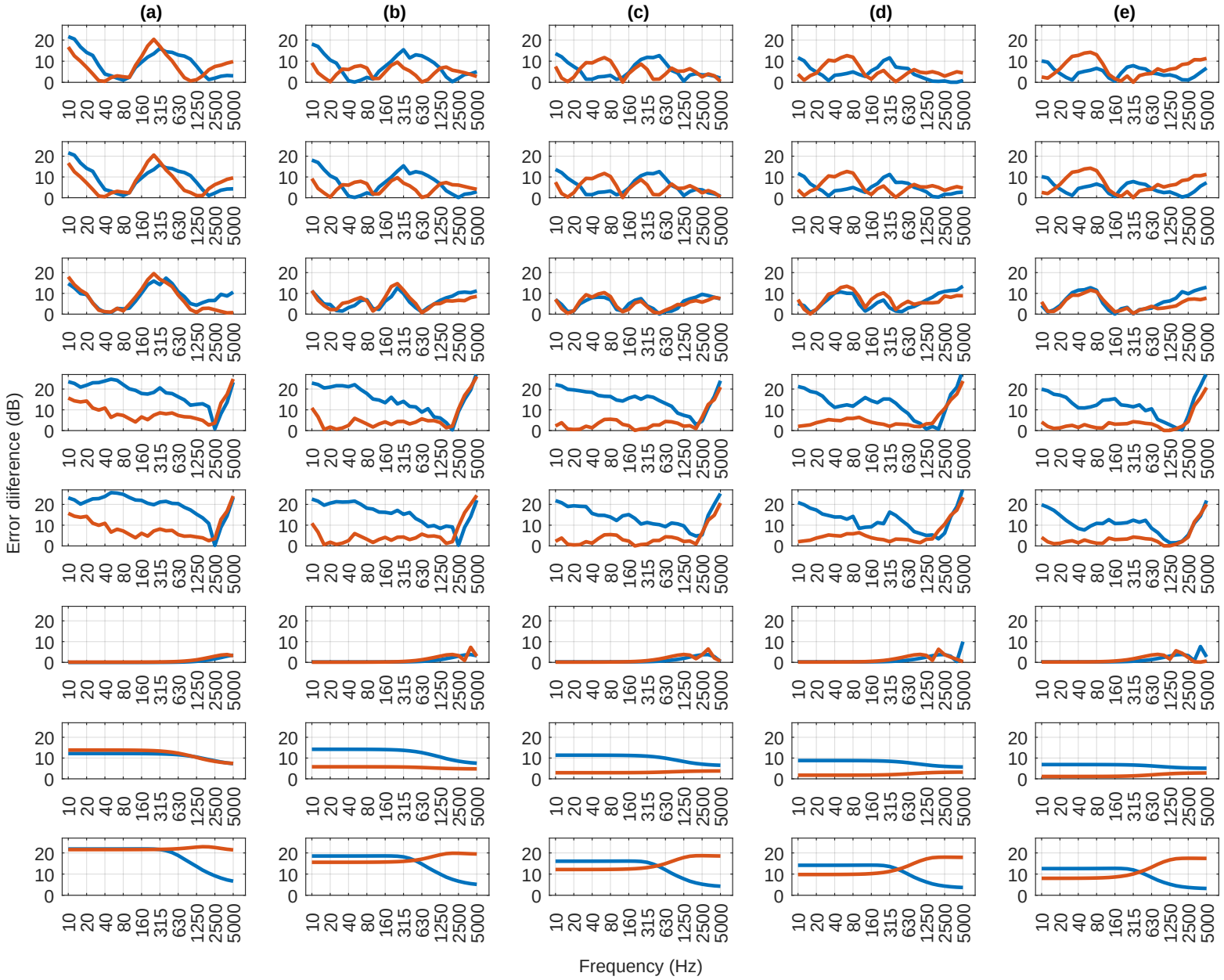

Figure B.2: Error between the ISO 17208-2 and the other models at 500 m. The rows are representing the models as follows: PE(R/I), PE(R/D), PE(R-B/D), WNI(R/I), WNI(R/D), ECHO, SCA, and M-A.